DETERMINATION OF JOJOBA OIL-BIODIESEL PSEUDO EUTECTIC PHASE DIAGRAM VIA COOLING CURVES OF BLENDS

A THESIS SUBMITTED TO THE GRADUATE
SCHOOL OF APPLIED SCIENCES
OF
NEAR EAST UNIVERSITY

By
MEKONNEN ASMARE FENTAHUN

In Partial Fulfillment of the Requirements for
the Degree of Master of Sciences
in
Mechanical Engineering

NICOSIA, 2019

MEKONNEN ASMARE DETERMINATION OF JOJOBA OIL-BIODIESEL PSEUDO NEU
FENTAHUN EUTECTIC PHASE DIAGRAM VIA COOLING CURVES OF BLENDS 2019

DETERMINATION OF JOJOBA OIL-BIODIESEL PSEUDO EUTECTIC PHASE DIAGRAM VIA COOLING CURVES OF BLENDS

A THESIS SUBMITTED TO THE GRADUATE
SCHOOL OF APPLIED SCIENCES
OF
NEAR EAST UNIVERSITY

By
MEKONNEN ASMARE FENTAHUN

In Partial Fulfillment of the Requirements for
the Degree of Master of Sciences
in
Mechanical Engineering

NICOSIA, 2019

Mekonnen Asmare FENTAHUN: DETERMINATION OF JOJOBA OIL-BIODIESEL PSEUDO EUTECTIC PHASE DIAGRAM VIA COOLING CURVES OF BLENDS

Approval of Director of Graduate School of
Applied Sciences

Prof. Dr. Nadire ÇAVUŞ

We certify this thesis is satisfactory for the award of the degree of Master of Sciences in Mechanical Engineering

Examining committee in charge:

Assist. Prof. Dr. Ali EVCİL	Supervisor, Department of Mechanical Engineering, NEU
Prof. Dr. Mahmut A. SAVAŞ	Co - Supervisor, Department of Mechanical Engineering, NEU
Assoc. Prof. Dr. Hüseyin ÇAMUR	Department of Mechanical Engineering, NEU
Assist. Prof. Dr. Youssef KASSEM	Department of Mechanical Engineering, NEU
Assoc. Prof. Dr. Kamil DİMİLİLER	Head, Department of Automotive Engineering, NEU

I hereby declare that all information in this document has been obtained and presented in accordance with academic rules and ethical conduct. I also declare that, as required by these rules and conduct, I have fully cited and referenced all material and results that are not original of this work.

Name, Last name: Mekonnen Asmare Fentahun
Signature:
Date: May 20, 2019

ACKNOWLEDGMENTS

I would like to express my deep gratitude to my thesis supervisors, Prof. Dr. Mahmut A. SAVAŞ and Assist. Prof. Dr. Ali EVCİL for their patient guidance, encouragement and helpful critiques of this thesis work. I am very thankful for all of their kind work which has started with selecting a thesis topic and went through valuable and constructive suggestions, beside offering me of courses, that helped me to reach on this stage from the very beginning. I am also very thankful to Metin BİLİN who provided me necessary materials for the study.

My grateful thanks are also extended to the staffs of the Mechanical Engineering Department of Near East University for the indispensable knowledge that they gave me.

To Near East University…

ABSTRACT

Biodiesel refers to an environmental friendly organic renewable fuel that is obtained from natural sources like animal fats, used cooking oils and plants. Biodiesel can be produced by a variety of techniques using simple technology. One of these methods is a supercritical transesterification also known as alcoholysis in which the fats or oils are reacted with alcohol at supercritical temperature and pressure to yield biodiesel. In this study, the eutectic behavior of a Biodiesel (BD)-Jojoba Oil (JO) blend sample was studied by a computer aided cooling curve analysis. Newtonian thermal analysis and cooling law were used. A total of 18 samples were studied and each of these samples were cooled down from an average temperature of 55°C to -18°C in an ethyl alcohol cooling bath. The samples were prepared based on a volume percentage. The freezing (liquidus) temperature was identified for the samples and it was observed that upon increment of volume percentage of JO in BD, the temperature drops toward the eutectic point. From the experiment, it was seen that 58%BD-42%JO is the eutectic composition (C_E) and the corresponding eutectic temperature (T_E) is 0.5°C. At the eutectic composition, cooling rate in the liquid region is from 0.0158 to 0.0491 °C/s and it ranges from 0.000833 to 0.00416 °C/s in the solid region. The temperature difference ranges from 74.7 to 27 °C in the liquid region and 16.6 to 4.1 °C in the solid region based on second order numerical differentiation approach. Based on the data collected, a binary pseudo eutectic BD-JO phase diagram was constructed.

Keywords: Temperature; eutectic; cooling curve analysis; Newton's law of cooling; phase diagram

ÖZET

Biyodizel hayvansal yağlar, kullanılmış kızartma yağları ve bitki tohumları gibi doğal kaynaklardan üretilen organik, çevre dostu ve yenilenebilir bir yakıttır. Birçok basit teknoloji kullanan üretim teknikleri mevcuttur. Transesterifikasyon en yaygın olanıdır. Süper kritik transesterifikasyon yönteminde hammadde olarak yararlanılan yağlar süperkritik sıcaklık ve basınçta alkol ile tepkimeye sokulur ve böylece biyodizel yakıtı elde edilir. Bu çalışmada biyodizel – jojoba yağı karışımlarının ötektik davranışları bilgisayar destekli soğuma eğrisi analizi yapılarak incelenmiştir. Newtonian termal analiz yöntemi ve katılaşma kuramları kullanılmıştır. Hacimsel oranlarla hazırlanan toplam 18 farklı numune test edilmiştir. Numuneler ortalama 55°C sıcaklıktan -18°C sıcaklığa kadar soğuk alkol banyosu içerisinde soğutulmuştur. Numunelerin katılaşma noktaları ve katılaşma aralıkları belirlenmiştir. Biyodizel içerisindeki jojoba yağı miktarı arttıkça katılaşma sıcaklığının ötektik sıcaklığa doğru düştüğü gözlenmiştir. %58 biyodizel - %42 jojoba yağı karışımının ötektik karışım olduğu ve ötektik sıcaklığın da 0.5°C olduğu belirlenmiştir. Ötektik karışımda, sıvı fazda soğuma oranı 0.0158 ile 0.0492 °C/s arasında, katı fazda ise 0.000833 ile 0300416 °C/s arasında değişmektedir. Sıcaklıklar ise sıvı fazda 74.7 ile 27 °C, katı fazda ise 16.6 ile 4.1 °C arasında değişmiştir. Toplanan veriler kullanılarak biyodizel - jojoba yağı karışımlarının psödo-ötektik faz diagramı elde edilmiştir.

Anahtar Kelimeler: Faz diyagramı, Newton termal analiz yöntemi; ötektik sistemi; soğuma eğrisi analizi

TABLE OF CONTENTS

CHAPTER 1: INTRODUCTION

CHAPTER 2: LITERATURE REVIEW

CHAPTER 3: **EXPERIMENTAL SET- UP AND METHODOLOGY**

CHAPTER 4: RESULTS AND DISCUSSION

CHAPTER 5: CONCLUSION AND RECOMMENDATION

LIST OF TABLES

LIST OF FIGURES

LIST OF ABBREVIATIONS

Å:	Angstrom
ASTM:	American Society for Testing and Materials
BD:	Biodiesel
B100:	Hundred percent biodiesel
B20:	Twenty percent biodiesel, Eighty percent petroleum diesel
CA-CCA:	Computer Aided –Cooling Curve Analysis
C_E**:**	Eutectic composition
CI:	Compression Ignition
EN:	European standard
FFA:	Free Fatty Acid
ISO:	International Organization for Standardization
JO:	Jojoba oil
JO-BD:	Jojoba oil- biodiesel blend
J100:	Hundred percent Jojoba oil
NLC:	Newton's law of cooling
NTA:	Newtonian Thermal Analysis
NZC:	Newtonian Zero Curve
SCMT:	Supercritical methanol transesterification
TAGs:	Triglycerides
T_E**:**	Eutectic temperature
VO:	Vegetable oil
Z_N**:**	Newtonian Zero Curve
A :	Area (m^2)
C**:**	Number of constituents
cc**:**	Cooling curve first derivative
C_p**:**	Specific heat (J/g°C)
E**:**	Energy (J)
F**:**	Degrees of freedom

$\boldsymbol{h}$:	Convective heat transfer coefficient (W/(m^{2}K))
$\boldsymbol{k}$:	Thermal conductivity (W/(m·K)).
$\boldsymbol{L}$:	Latent heat (J/kg)
$\boldsymbol{L_C}$:	Characteristics Length (M)
$\boldsymbol{N}$:	Non-compositional elements
$\boldsymbol{P}$:	Phase
$\boldsymbol{q}$:	Heat flux (W·m^{-2})
$\boldsymbol{t}$:	Time (S)
$\mathbf{t}_{\boldsymbol{s}}$:	Start time (S)
$\boldsymbol{U}$:	Overall heat transfer coefficient
$\boldsymbol{T_s}$:	Surface temperature (°C)
$\boldsymbol{T_\infty}$:	Ambient temperature (°C)
$\boldsymbol{zc}$:	Zero curve first derivative
$\boldsymbol{\rho}$:	Density (kg/m^3)
$\boldsymbol{\sigma}$:	Stephan-Boltzman constant ($wm^{-2}K^{-4}$)
$\boldsymbol{\epsilon}$:	Emissivity

CHAPTER 1
INTRODUCTION

Diesel fuels are primary and important input of energy in industry, manufacturing and transportation sectors. Most of worlds energy requirement is satisfied by petrochemical sources, i.e. natural gases, coals, hydroelectric power, nuclear energy and others (Murugesan et al., 2009). But all of these energy sources except hydropower are non-renewable and are about to vanish in a short period of time, therefore, it’s very necessary to look another way of getting fuel sources for consumption. This new and alternative source of energy should be easily available, eco-friendly, cost-effective and needs to be made with just ordinary technology. One of such fuels is triglycerides and their derivatives commonly known as biodiesel fuels which are produced from vegetable oils/waste cooking oils/animal fats reacted with long chain alcohols primary methanol or ethanol. Compared to petrochemical diesel and other energy sources biodiesel is considered as eco-friendly, non-toxic, renewable and have lower gas emission cause of its lower sulfur content (Demirbas, 2005b).

The term Biodiesel is coined from bio of Greek which implies to the diesel equivalent fuel derivatives of natural sources. American Society for Testing and Materials (ASTM) defines biodiesel chemically as a fuel of mono-alkyl esters of long chain fatty acids obtained from a renewable lipid feedstock like VOs, waste cooking oils and, fats. Biodiesel fuels can be used independently or as a blend with conventional petroleum-based diesel fuels without necessarily changing or modifying the engine operating system. Low-level blends (usually less than 20% blends) can be used in the majority of existing diesel engines and high-level blends (greater than 20% blends) in newest diesel engines. Biodiesel also can be a great potential for compression-ignition engines. Biodiesel fuels possess an advantage over regular gasoline that they are efficient as gasoline while emitting lower exhaust gases (carbon monoxide, particulate matter, and unburned hydrocarbons) (Demirbas, 2008). Biodiesels have a higher flash point (150^{o}C), which makes it safer, less volatile to handle and transport than petroleum diesel. It can also provide lubricating properties that can reduce engine wear and therefore extend engine life (Zhang, Dubé, McLean, & Kates, 2003).

Biodiesel is produced according to the given and specified standards. The requirement in the standards and properties leads to having a finer quality as well as competitive and accepted biodiesel fuel worldwide. It also enhances the produced fuel to provide better efficiency.

In early 1853 Duffy and Patrick conducted trans-esterification. The diesel engine that runs with VO was first designed by famous German engineer and inventor Dr. Rudolph Diesel in 1893. Many types of research have been conducted in the past decades on the biodiesel production and accordingly, there are four basic ways of producing biodiesel fuel from oil and fat as listed below (Antolın, Tinaut, & Briceno, 2002; Fukuda, Kond, & Noda, 2009; Han, Cao, & Zhang, 2005; Iso, Chen, Eguchi, Kudo, & Shrestha, 2001; Nelson, Foglia, & Marmer, 1996; Nie, Xie, Wang, & Tan, 2006; Shimada, 2002).

- Base-catalyzed trans-esterification,
- Direct acid catalyzed trans-esterification,
- Enzyme catalytic (oils to fatty acids and biodiesel)
- Trans-esterification with no catalyst using methanol or methanol/co-solvents.

Among these, the base-catalyzed trans-esterification is the most common and known method of production of biodiesel involving trans-esterification vegetable oil or animal fat with alcohol to give glycerin and methyl ester (biodiesel) from triglyceride (oil). On the other hand, non-catalytic trans-esterification of vegetable oils or animal fats in supercritical alcohols (methanol, ethanol…. etc.) are carried out without the addition or presence of any catalysts. The conversion in supercritical methanol trans-esterification method rises up to 95% (Demirbas, 2005a, 2006).

1.1. Background and Review

Biodiesel and its blends with conventional diesel fuels were in use for engine consumption in automotive and heavy-duty trucks. The study of eutectic and low-temperature behavior of its blends, especially the liquid to solid phase transition behavior around the cloud point is needed for the explanation of cold flow property and on the usability of the blends in the cold environment.

It's worth it to study the liquid-solid behavior of biodiesel and its blends at low temperature beginning from cloud point and understand the cold flow properties, because of the tendency to freeze at low temperature for biodiesel is faster than conventional diesel fuels due to the high concentration of saturated fatty acid esters in biodiesel.

Biodiesel and bioethanol are most promising biofuels becoming a point of interest in the contemporary world because they are extracted from plants and crops. Plant-based fuels come from renewable sources, can be grown easily and they are nontoxic, biodegradable, eco-friendly, lower emission of greenhouse gases and can be produced with less effort. Biofuels can be used independently as a substitute of diesel and petrodiesel fuel or it can be blended with gasoline, diesel, and petrodiesel for use in diesel engines. It also represents a sustainable solution to prevent the depletion of fossil resources. One of such fuel is biodiesel which is produced when the VOs or fats from animals reacts with an alcohol (usually ethanol & methanol) in the presence or without the presence of catalysts to yield biodiesel and glycerin (Demirbaş & Arin, 2002).

Biodiesel is a mono-alkyl ester obtained from renewable bio-lipids by a trans-esterification process, which adapts to ASTM D6751 specifications for use in diesel engines. Biodiesel possesses many advantages than that of petroleum and other nonrenewable fuels in terms of biocompatibility and production (Azam, Waris, & Nahar, 2005). The above-mentioned factors collectively initiate researchers to look into alternatives to find renewable energy which can supplement or replace fossil fuel and shapes a new way to focus on biodiesel energy. It is also a good challenge to utilize the local feedstock including waste frying oil, non-edible oils, etc.

1.2. Objectives (Aim) of The Study

The general objective of this study is to determine the phase diagram of Biodiesel-Jojoba oil blends of different compositions through the cooling curve analysis of blends. Construction of a binary eutectic type of phase diagram is the main aim of this study. Computer Aided – Cooling Curve Analysis (CA-CCA) is applied here in this study. An investigation and application of Newtonian Thermal Analysis (NTA) of the cooling curve, derivative curves, (rate curves), as well as Newtonian Zero Curve (NZC), are used to locate the start and end of phases in the blends. A representative eutectic temperature (T_E) and eutectic composition (C_E) can be also found. Numerical integration of the formulated theoretical equations are to be used in this study.

1.3. Thesis Layout

Chapter one introduces general information and overview of biodiesel and previous research works as well as the problem of statement and motivations, introductory definitions and general objectives. Chapter two discusses more on biodiesel and a detailed literature review including definitions, historical background, current status, application of biofuels and their feedstocks will be discussed. the production method, properties, and standards, merits and drawbacks are also expected in detail. Chapter three will give a brief summary of the methodology followed and experimental setups, as well as formulation, used to carry out this study. Chapter four discusses the result of the experiment, experiment results are interpreted and analyzed in this chapter. In the last, chapter five put the conclusion of the work and points out further work for the future.

CHAPTER 2
LITERATURE REVIEW

2.1. General Overview

Available petroleum sources are limited and will run out in the long run. Many types of research put the highest time for oil production between 1996 to that of 2035 (Demirbas, 2008). The possible substitute for petroleum gases are biofuels and biomasses with lower greenhouse gas emission than petroleum and fossil fuel sources, because of they are extracted from bio matters (plants) (Sheehan et al., 1998). One of such fuel is biodiesel fuel which has become a key source of energy mainly for transportation starting from early 1853 when Duffy and Patrick conducted trans-esterification (the process of a reaction of vegetable oil/fatty acid with alcohols to yield glycerol and mono-alkyl ester (biodiesel)) (Demirbas, 2008).

Numerous researches had pointed out the role of biofuels in the future energy supply. According to the estimations done, in the year 2050, a half of the oerall energy requirement is contributed by biomass energy in developing countries (IPCC, 1997). Consumption for transportation will replaced by a biomass fuel, leaving gasoline and diesel fuel. These fuel includes, biodiesel, bioethanol and non-biological hydrogen energy source. It is expected that fossil fuels are replaced by biodiesel while bioethanol replaces gasoline (Demirbas, 2008).

Biofuel refers to fluid fuels for the transportation purposes, mainly produced from biomass. Biofuels give various advantages like reduction in greenhouse gas emission, supply security, sustainability (Reijnders, 2006). These biofuels are used in transportation sectors, in automobiles, fuel cells, engines and electricity generations. Thermochemical and biological approaches are ways to change biomass to fluid fuels. Biofuels are ecological, available, sustainable and accessible as well as consistent (Vasudevan, Sharma, & Kumar, 2005).

Biomass and biofuels are attractive in developing and industrialized countries due to these three reasons (Cadenas & Cabezudo, 1998):

- Renewablity
- Have positive environmental factors with content for oxygen level up to 45% compared to petroleum
- Important economic prospective, (replaces fossil fuel) due to increasing price.

Liquid biofuels are categorized as:

- Biodiesels and vegetable oil,
- Bio-crude and synthetic oils and
- Alcohols

Figure 2.1 shows main sources for the liquid biofuels for transportation consumption.

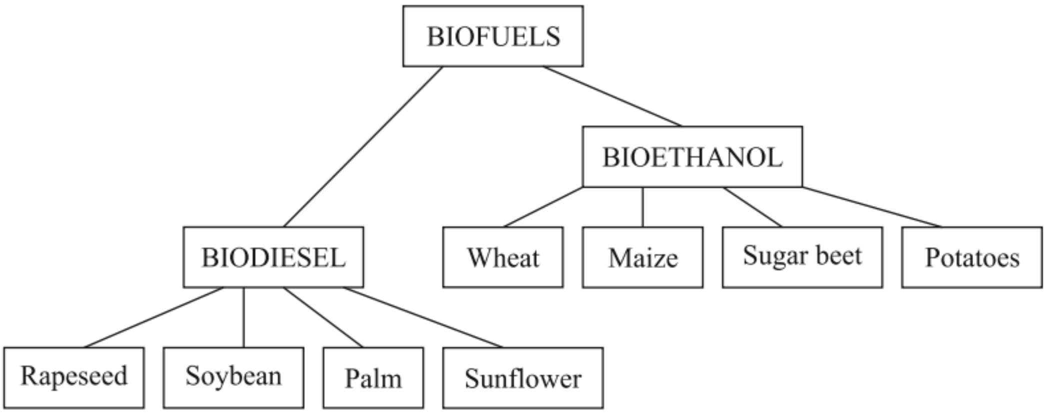

Figure 2.1: Main liquid biofuel sources for automobiles (Demirbas, 2008)

2.2. Historical Development of Biodiesel and Definitions

2.2.1. Development of biodiesel

The first engine that runs by VO (100% peanut oil) was first designed by a German engineer and inventor by Dr. Rudolph Diesel on 10th of August 1893. The first vegetable oil that converted to biodiesel by the transesterification was in 1853 by a group of researchers. A Belgian Scientist G. Chavanne from Brussels University was the first man to be allowed a patent on the theory of biodiesel in 1937 (Demirbas, 2008; Mahmudul et al., 2017). In 1997 the first patent for biodiesel in the industrial process was applied by Brazilian researcher

Expedito Parente. It was in 1979 that South Africa started research on sunflower oil seeking for biodiesel. The first plant of biodiesel was built by an Australian company in 1987 and an industrial scale plant in 1989 in Gaskoks and in 1991 Austria issued first standard for biodiesel (Mekhilef et al., 2011).

2.3. Definitions

Biodiesel is a term coined from the bio of the Greek and diesel of Dr. Rudolph Diesel (inventor of a diesel engine that runs by VO) denotes to the diesel alike processed fuel derivative of renewable bio sources which is produced from biological/ natural fats and oils (Demirbas, 2008).

ASTM defines biodiesel as “a fuel composed of mono-alkyl esters of long-chain fatty acids derived from VOs, animal fats, etc. which are labelled as B100” and adapts the requirements of ASTM D6751 specifications. B100 refers to a 100% biodiesel and 0% petroleum (Demirbas, 2008; Hoekman et al., 2012). ASTM D6751 standard was first published in 2002 (Mekhilef et al., 2011). Biodiesel is made from animal fats or VOs known as triglycerides (TAGs) or simply triglycerides and the chemical process of producing biodiesel is called transesterification (Hoekman et al., 2012). Significant characteristics of biodiesel is that it is mixed with other fuels like petroleum to form a blend which we usually called it as “biodiesel blends”. Pure biodiesel as stated by ASTM D6751 standard was B100, which is 100% pure diesel and 0% petroleum-based diesel fuels. The most widely and regularly used blend is a B20 because of its cheap value, cold weather properties, emissions, and compatibility.

2.4. Characteristics of Vegetable Oils as Fuel

High viscosity property of vegetable oils (due to huge molecular configuration) lowers the volatility of the oils as a fuel which affects the atomization and injection process in CI engine if used directly. Vegetable oils have a flash point of above 220°C compared to 76°C for diesel. As a result vegetable oils have lower values for the cetane number and heating values than those of diesel due to the existence of bound oxygen in the molecular structure. Properties for some of the common boidiesel fedstock compared with petrodiesel is given in Table 2.1.

Table 2.1: Vegetable oil property in comparison to diesel (Kayode & Hart, 2017)

Vegetable oil	Density (kg/L)	kinematic viscosity @ 40 °C (mm^2/s)	Cetane No. (°C)	Heating value (MJ/kg	Cloud point (°C)	Pour point (°C)	Flash point (°C)
Palm	0.9180	39.6	42.0	39.3	31.0	-	267
Sunflower	0.9161	33.9	37.9	39.6	7.2	-15.0	274
Peanut	0.9026	39.6	41.8	39.8	12.8	-6.7	271
Cottonseed	0.9148	33.5	41.8	39.5	1.7	-15.5	234
Soybean	0.9138	32.6	37.9	39.6	-3.9	-12.2	254
Corn	0.9095	34.9	37.6	39.5	-1.1	-40.0	277
Diesel	0.855	3.06	50	43.8	-	-16	76

The problem with the raw oils that prevent us from using them directly is that they are highly viscous fluids, low volatile and have polyunsaturated characters. There are methods in which these oils can be turned to a usable form of fuels by changing their chemical and fluid properties and make suitable for use for engines.

2.5. Production Methods of Biodiesel

Biodiesel can be processed from VOs, waste cooking oil, fats from animals, fungi, algae's. The greatest outcome would be gained from vegetable oils. Usually, the primary step in producing biodiesel is a selection of feedstock. There are more than 350 favorable plant feedstock's known as a possible source for biodiesel processing worldwide. Availability of the feedstock is the main essential factor for production of biodiesels (Atabani et al., 2012; Atadashi, Aroua, & Aziz, 2010; Janaun & Ellis, 2010; Mishra & Goswami, 2018; Shahid & Jamal, 2011). Low cost of processing and high level of production are the two main requirements for the feedstock's biodiesel production. Level of production and obtainability of the feedstock depends on weather condition, topological locations, soil quality, local practices of agriculture and situations (A & R., 2000; Atabani et al., 2012; Balat, 2008, 2010; Demirbas, 2008; Lin, Cunshan, Vittayapadung, Xiangqian, & Mingdong, 2011).
Feedstock's for biodiesels are classified into four main classes:

- Edible VO: used for human consumption most of the time and extracted from plants. Peanut, sunflower, palm, soybean, coconut oil, corn oil, rapeseed oil. etc. are examples of edible vegetable oils.

- Non-edible oils: petroleum based and others like Karanja, sea mango, jatropha, halophytes, and algae, greases and lubricants, etc
- Used or recycled oil and
- Fats from animals: beef, chicken fat, oil from fish, etc.

Edible vegetable oils are first generation feedstock's that are used in the production of biodiesels at the beginning. Around 95% of total produced biodiesel worldwide is from edible vegetable oils, which is 1% palm oil, 2% soybean oil, 13% from sunflower and 84% from rapeseed oil (Atabani et al., 2012; Gu et al., 2018; Soltani, Rashid, Yunus, & Taufiq-Yap, 2015). Over the last few decades, the need for crops and plants for edible vegetable oil has highly increased due to increase in human consumption, therefore it seems the feasibility of producing biodiesel from edible vegetable oil is in question. Second-generation (non-edible) are also best alternatives. Table 2.2 summarizes feedstock's for biodiesel production

Table 2.2: Common feedstocks for biodiesel production (Atabani et al., 2012; Mishra & Goswami, 2018)

Edible oils	**Non-edible oils**	**Animal fats**
Soybeans (Glycine max)	Jatropha curcas	Pork lard
Rapeseed (Brassica napusL.)	Mahua (Madhuca indica)	Beef tallow
Rice bran oil (Oryza sativum)	Pongamia (Pongamia pinnata)	Poultry fat
Barley	Camelina (Camelina Sativa)	Fish oil
Sesame (Sesamum indicum L.)	Cotton seed (Gossypium hirsutum)	Chicken fat
Groundnut	Karanja or honge (Pongamia pinnata)	
Sorghum	Cumaru	
Wheat	Cynara cardunculus	
Corn	Abutilon muticum	
Coconut	Neem (Azadirachta indica)	
Canola	Jojoba (Simmondsia chinensis)	
Peanut	Passion seed (Passiflora edulis)	
Palm and palm kernel (Elaeis guineensis)	Moringa (Moringa oleifera)	
Sunflower (Helianthus annuus)	Tobacco seed	
	Rubber seed tree (Hevca brasiliensis)	
	Salmon oil	
	Tall (Carnegiea gigantean)	
	Coffee ground (Coffea arabica)	
	Nagchampa (Calophyllum inophyllum)	
	Croton megalocarpus	
	Pachira glabra	
	Aleurites moluccana	
	Terminalia belerica	

Extraction of oils from the feedstocks is the next step in the production processes which can be done by one of these methods, mechanical extraction, enzymatic extraction or solvent extraction.

Among these methods, mechanical extraction is widely used and conventional, where by mechanical presses and expellers were used. The kernels and whole seed or a mixture is used in this method. Mechanical extraction yields about 68- 80% of oil (Atabani et al., 2012).

2.5.1. Direct Use and blending

The suggestion of using vegetable oil (VO) as a fuel was first introduced in 1980. In 1981 Bartholomew discussed the hint of using food as a replacement of fuel, signifying petroleum should be used as alternatives rather than alcohols and vegetable oils and he also suggested that renewable energy sources should take place instead of nonrenewable ones (Ma & Hanna, 1999; Mishra & Goswami, 2018). It was in 1980 in Brazil for the first time that an engine was provided with a 10% blend of VO without any modification of the engine. At the same time, a blend of up to 20% of VO and 80% diesel was successful. A 50/50 blend was experimented that lasted for short.

The first international conference of plants and vegetable oils as a fuel that conversed on fuel cost, a consequence of vegetable oils on engine performance, efficiency durability as well as compatibility, processing of fuels, properties, and blends was discussed in North Dakota (ASAE; 1982). Filtered used cooking oil (95% diesel with 5% VO) was seen powering fleets of a diesel engine. Warming was used heat up because of cold temperature and there were no problems observed on the start of the engine. Lubricating and oil contamination was the only reported problem because of high viscosity value of the VO and thus filtering became the most significant process. Generally, due to a highly viscous fluid and low properties, straight use of VOs for diesel engines are unrealistic and difficult as it may result in gum formation and accumulation during storage and ignition (Ma & Hanna, 1999). The potential reasons and suggested solutions are discussed in the following Table 2.3 below.

Table 2.3: Problems, cause and suggested solutions for using direct pure vegetable oils in Diesel (Harwood, 1984)

Problem	Probable cause	Potential solution
Short-term:		
Cold weather starting	High viscosity, low cetane, and low flash point of vegetable oils	Preheat fuel prior to injection. Chemically alter fuel to an ester
Plugging and gumming of filters, lines and injectors	Natural gums (phosphatides) in vegetable oil. Other ash	Partially refine the oil to remove gums. Filter to 4-micron
Engine knocking	Very low cetane of some oils. Improper injection timing.	Adjust injection timing. Use higher compression engines. Preheat fuel prior to injection. Chemically alter fuel to an ester
Long-term: Coking of injectors on piston and head of engine	High viscosity of vegetable oil, incomplete combustion of fuel. Poor combustion at part load with vegetable oils	Heat fuel prior to injection. Switch engine to diesel fuel when operation at part load. Chemically alter the vegetable oil to an ester
Carbon deposits on piston and head of engine	High viscosity of vegetable oil, incomplete combustion of fuel. Poor combustion at part load with vegetable oils	Heat fuel prior to injection. Switch engine to diesel fuel when operation at part load. Chemically alter the vegetable oil to an ester
Excessive engine wear	High viscosity of vegetable oil, incomplete combustion of fuel. Poor combustion at part load with vegetable oils. Possibly free fatty acids in vegetable oil. Dilution of engine lubricating oil due to blow-by of vegetable oil.	Heat fuel prior to injection. Switch engine to diesel fuel when operation at part load. Chemically alter the vegetable oil to an ester. Increase motor oil changes. Motor oil additives to inhibit oxidation

2.5.2. Pyrolysis (thermal cracking)

Pyrolysis is conversion of a given element by application of heat, without or with the presence of catalysts. It is a breakdown of chemical bonds to a smaller molecule by heating without air involvement (Ma & Hanna, 1999). The pyrolyzed materials could be fats, VOs, fatty acids and more.

Thermal cracking of fats and vegetable oils has been experimented in the last 100 years in areas where petroleum fuels lack. Pyrolysis process can be classified into 3 groups as (Ma & Hanna, 1999).

- Fast pyrolysis
- Flash pyrolysis
- Conventional pyrolysis

2.5.3. Micro-emulsification

The efficient way of solving the high viscous property of vegetable oil is micro-emulsification. It is the act of mixing and dispersion of vegetable oil with a straight chain of alcohol like ethanol, methanol and alike. Technically micro emulsification refers to a transparent and stable diffusion of microstructure of a fluid with sizes ranging from 100-1000 Å (Ångström) or equivalent to (0.01- 0.1) micrometers. Vegetable oils can be diffused with alcohol, cetane improver, surfactant (compounds that lower surface tension between two fluid and liquid layers) with ester as dispersion (co-solvent) agent blended with or without diesel fuels. Microemulsion advances spray property by evaporation of elements in the micelles (Freedman, Pryde, & L., 1984), hence improving viscosity property making suitable the oil for consumption for engines.

2.5.4. Dilution

Dilution is an excellent method to decrease high viscosity and density of vegetable oil. It is accomplished with material like diesel fuels, solvents or ethanol. Brake thermal efficiency, brake power, and brake torque can be increased by just adding 4% of ethanol to diesel but it decreases brake specific fuel consumption.

2.5.5. Transesterification (Alcoholysis)

Transesterification or alcoholysis is the method by which animal fat or vegetable oils are reacted with an alcohol to yield glycerol and ester as shown in Figure 2.2. Transesterification is one of the most used and efficient ways of production of biodiesel. Transesterification can take place with or without the presence of catalysts. Most often catalyst was used to increase the product and speed up the process. Because it is a reversible reaction, more alcohol is usually used to move the balance to the yield side. The most common alcohols used in the production processes are ethanol and methanol alcohols. Methanol is preferable, due its chemical, physical property (polar and short chain alcohol) and low-cost availability. It also reacts rapidly with triglycerides and NaOH. Other alcohols includes butanol, propanol, and amyl alcohol (Ma & Hanna, 1999).

For complete transesterification a 3:1 molar ratio (alcohol to TAGs) is required. Higher ratio shifts the equilibrium to the product side and gives more ester. Theoretically, transesterification can be represented as with or without catalysts.

Triglycerides + Monohydric alcohol ⇄ Glycerin +Mono-alkyl esters

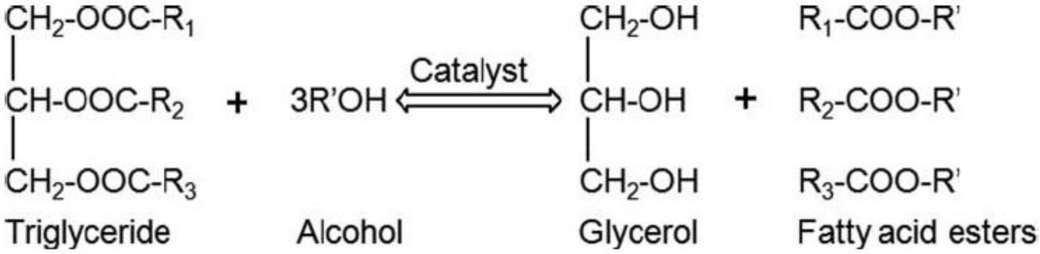

Figure 2.2: Transesterification of triglycerides with alcohol (where R1, R2, R3 are chains of hydrocarbon) (Ma & Hanna, 1999)

Transesterification is a consecutive and reversible process reaction (Jose et al., 1986). Triglyceride is altered to diglyceride and to monoglyceride at the end, as illustrated in the Figure 2.3, a mole of an ester is freed at each stage of the reaction.

$$\text{1. Triglyceride (TG)} + \text{R'OH} \underset{k_4}{\overset{k_1}{\rightleftharpoons}} \text{Diglyceride (DG)} + \text{R'COOR}_1$$

$$\text{2. Diglyceride (DG)} + \text{R'OH} \underset{k_5}{\overset{k_2}{\rightleftharpoons}} \text{Monoglyceride (MG)} + \text{R'COOR}_2$$

$$\text{3. Monoglyceride (MG)} + \text{R'OH} \underset{k_6}{\overset{k_3}{\rightleftharpoons}} \text{Glycerol (GL)} + \text{R'COOR}_3$$

Figure 2.3: Transesterification reactions of vegetable oil with an alcohol to esters and glycerol (Jose et al., 1986)

Depending on the catalyst used in the process, catalytic transesterification can be grouped into:

- Acid-catalyzed transesterification
- Alkali catalytic transesterification
- Diazomethane catalytic transesterification methods

2.5.6. Supercritical transesterification

Supercritical fluids are substances that exhibit properties of liquids and gases because of the fact that they are above their critical pressure and temperature. Their gaseous property enables the fluids a compressibility behavior with a variable density close to liquids and having diffusivity like that of gasses. Small changes in pressure as well as in temperature above the critical temperature also pressure can significantly affect and changes their density-dependent properties like viscosity, diffusivity, (viscosity & diffusivity are both transport properties), specific weight, polarity, and dielectric constants. In a supercritical state, the fluid molecules had high kinetic. At these state, substances will lose about 50-80% of their density than they had in their liquid state (Ngamprasertsith & Sawangkeaw, 2011). Such a change in their property gained acceptance on supercritical fluids as preferred additives and solvents in industries for extraction, increasing the reaction rate, catalysts, and separation. This condition for methanol is shown in Figure 2.4.

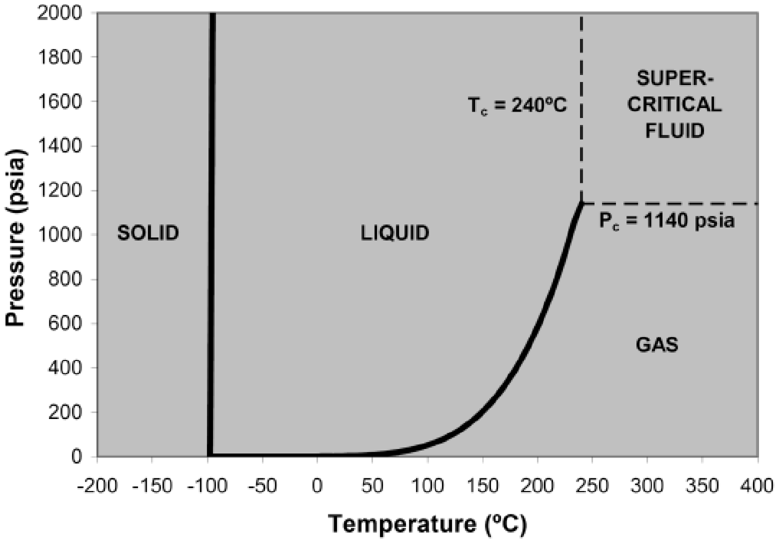

Figure 2.4: Phase diagram for methanol (Babcock, Clausen, Popp, & Schulte, 2014)

The supercritical transesterification method, as shown in Figure 2.5 is one of the processes for the production of biodiesel which is proven to yield maximum product at the end than any other above-mentioned methods (Gumba, Saallah, Misson, Ongkudon, & Anton, 2016). In supercritical transesterification, ethanol and methanol are common alcohols (Table 2.4) that are used for the production process although butanol and propanol were used (Demirbas, 2006). The drawbacks in the aforementioned processes are time-consuming compared to supercritical trasesterification and purification of the catalysts as well as impurities from biodiesel at the end.

Table 2.4: Critical data for commonly used alcohols in supercritical transesterification (Demirbas, 2008)

Alcohols	Mol. weight (g/mol)	Critical temperature (K)	Critical pressure (bar)	Critical density (g/cm^3)
Methanol	32.042	512.58	80.96	0.2720
Ethanol	46.069	516.25	63.84	0.2720

The temperature requirement in supercritical transesterification while using methyl or ethyl alcohols are usually ranges from 525-675K (252-402°C) and a pressure of between 350-600 bars (35-60 MPa). Basically, there are two types of supercritical alcohol transesterification namely, catalytic and non-catalytic supercritical alcohol transesterification. The non-catalytic alcohol transesterification is performed in the absence of catalysts in high-pressure stainless steel cylindrical reactor /autoclave which is filled with the required amount of vegetable oil/animal fat with liquid alcohol and then heat is supplied by an element so that the oil is transesterified by supercritical fluid/alcohol. 3 moles of alcohols and 1 mole of triglyceride is needed to give 3 moles of Fatty Acid Esters and 1 mole of glycerol. To maximize ester production within a short period of time, it's necessary to increase the molar ratio. The catalyzed supercritical alcohol transesterification is done with the addition of catalysts in an autoclave. For example, in catalyzed supercritical methanol transesterification 1-5% of NaOH, CaO or MgO is needed as a catalyst in the process. In this process, the yield rises up to 60-90% at the end of the first minute (Demirbas, 2008).

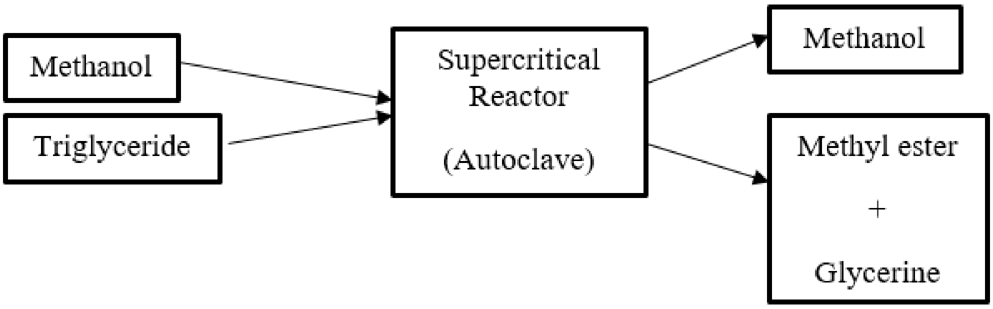

Figure 2.5: Supercritical transesterification process (Demirbas, 2008)

The advantage of supercritical alcohol transesterification:

- Results in maximum yields of product, no experienced soap formation and can be carried out without catalysts
- Takes less time for production with less effort and simpler purification process
- No two-phase nature of alcohol/oil mixture due to the fact that the process is carried out at supercritical state.

The comparison between SCMT with the chemical catalytic method is given below in Table 2.5.

Table 2.5: Comparison between supercritical methanol transesterification (SCMT) with chemical catalytic method (Atabani et al., 2013)

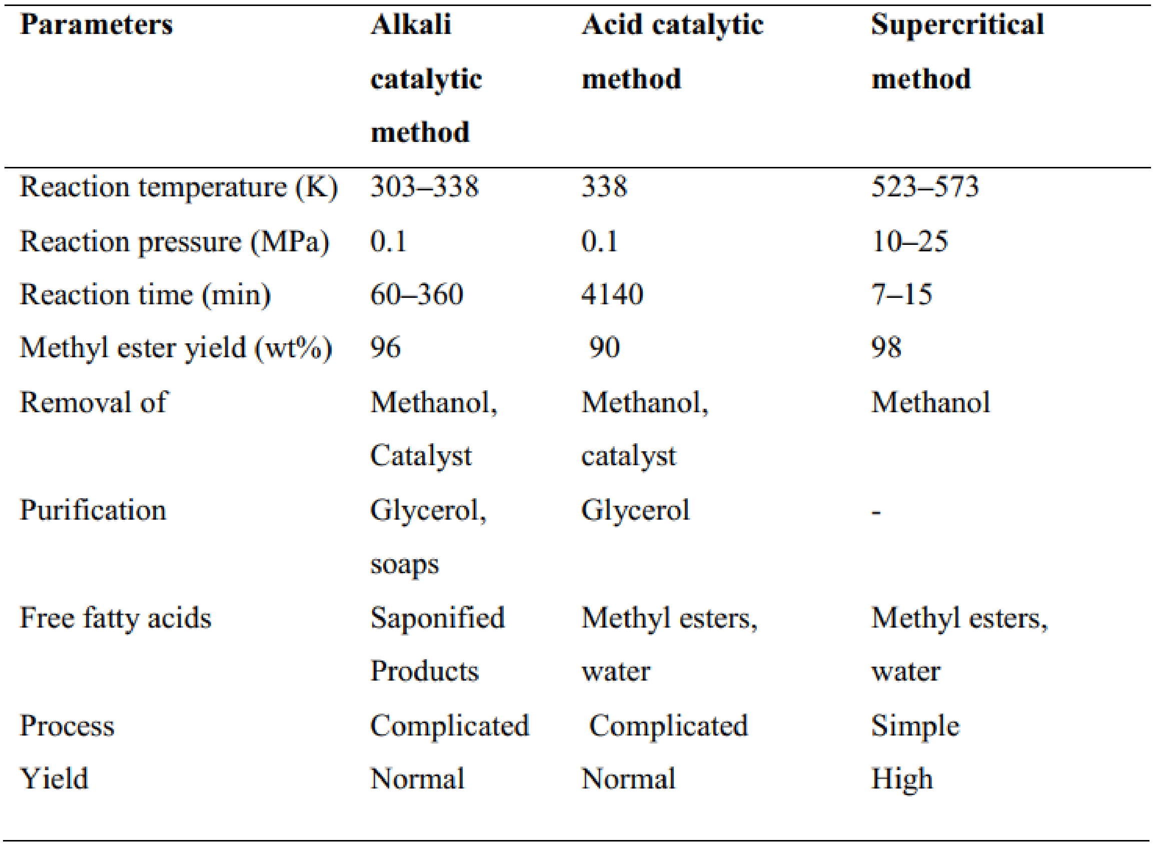

Parameters	Alkali catalytic method	Acid catalytic method	Supercritical method
Reaction temperature (K)	303–338	338	523–573
Reaction pressure (MPa)	0.1	0.1	10–25
Reaction time (min)	60–360	4140	7–15
Methyl ester yield (wt%)	96	90	98
Removal of	Methanol, Catalyst	Methanol, catalyst	Methanol
Purification	Glycerol, soaps	Glycerol	-
Free fatty acids	Saponified Products	Methyl esters, water	Methyl esters, water
Process	Complicated	Complicated	Simple
Yield	Normal	Normal	High

Table 2.6 summarizes, compares and list out the drawbacks of the aforementioned biodiesel production techniques.

Table 2.6: Advantage and difficulties of biodiesel production techniques (Mahmudul et al., 2017)

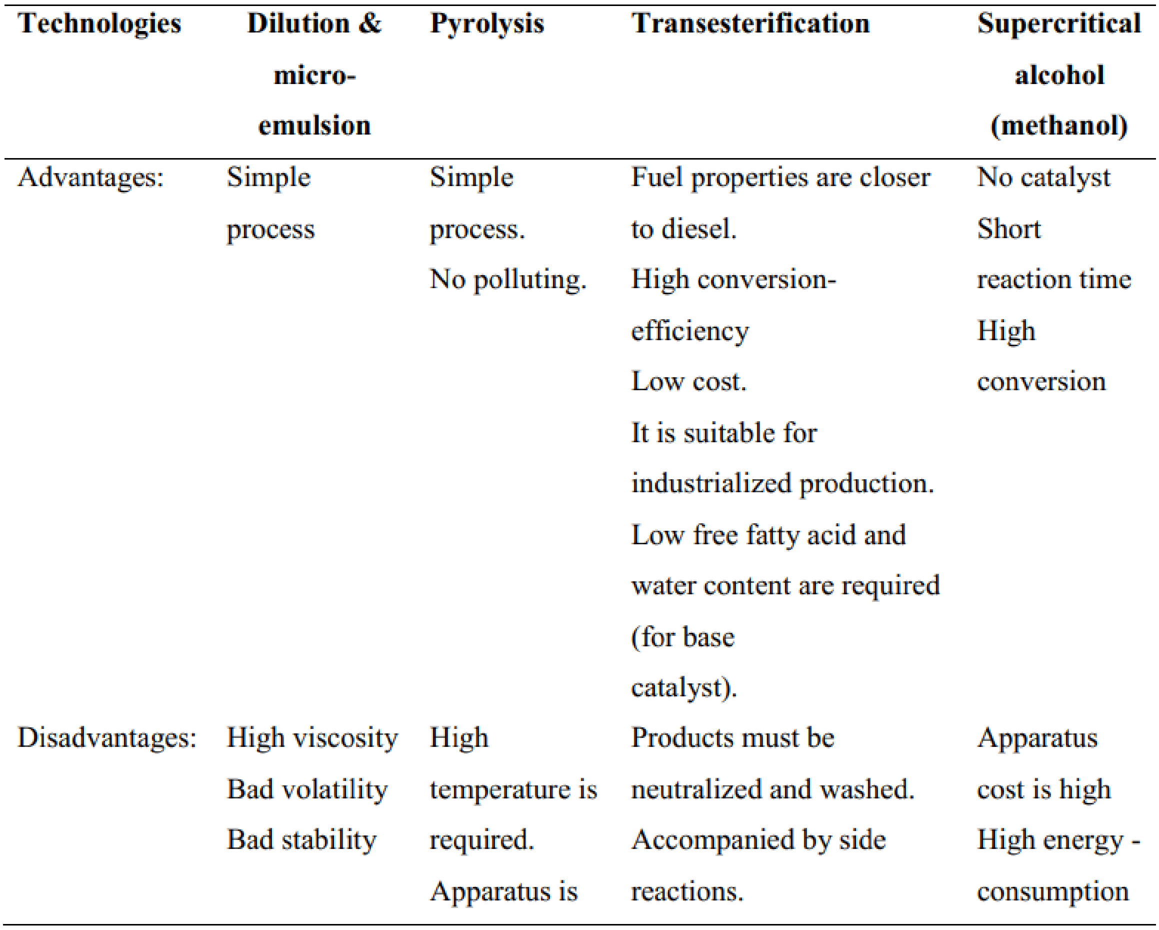

Technologies	Dilution & micro-emulsion	Pyrolysis	Transesterification	Supercritical alcohol (methanol)
Advantages:	Simple process	Simple process. No polluting.	Fuel properties are closer to diesel. High conversion-efficiency Low cost. It is suitable for industrialized production. Low free fatty acid and water content are required (for base catalyst).	No catalyst Short reaction time High conversion
Disadvantages:	High viscosity Bad volatility Bad stability	High temperature is required. Apparatus is	Products must be neutralized and washed. Accompanied by side reactions.	Apparatus cost is high High energy - consumption

Factors affecting transesterification process includes (Atabani et al., 2013):

- Reaction time & temperature,
- free fatty acids,
- moisture and water content.,
- type of alcohol and molar ratio,
- mixing intensity,
- concentration of catalysts,
- organic co-solvents, rate and mode of stirring,
- specific gravity and Purification of the final product.

2.6. Biodiesel Standards and Properties

Advancement in the quality of biodiesel has been done and developed worldwide to keep a merit of the end product, to make sure better standards for production, to gain trust and confidence of end users as well as to keep good and effective trade of biodiesel. The main reason that cause the standard to be set was due to different feedstock's and many kinds of scaled plants with different origins and qualities and with different techniques that may result in quality variation and thus needed to be uniform. The quality of biodiesel fuel can be affected by many factors mainly including feedstock's, production modes, the fatty acid arrangement, refining as well as purification way both before and after production. These reason causes to set a regulation and standard of a fuel quality to assure and confirm applicability on engine performance and intended purpose without difficulties. Some of the physicochemical properties associated with biodiesels as per the standards are explained below.

Density

The ratio for mass per volume of any substance is termed as a density of the substance, mathematically density can be written as:

$$\rho = \frac{m}{V} \qquad (2.1)$$

where: ρ is density (kg/m^3), m is mass (kg) and V is volume (m^3).

Methyl esters are denser than petrochemical diesel that require high injection pressure of the fuel. The following equation which was used for determination of the density of biodiesel was derived after an observation has done on different 158 biodiesel samples from 26 various feedstock's (Giakoumis, 2013).

$$\rho = 869.25 + 9.17n_{DB} \ \text{(kg/m}^3\text{)} \qquad (2.2)$$

where the constant $9.17n_{DB}$ is the number of double bonds in the unsaturated FAME.

Viscosity

Viscosity is a significant flow property of a fluids ability to flow over a given surface and between adjacent molecules. Viscosity in a fuel distresses the operation of spray atomization and fuel injection parts, mostly if the temperature drops there is an escalation in viscosity of a fuel, affecting combustion process. One of the main problem with vegetable oils are their high viscous nature preventing us to use them directly. The higher the viscosity of the fuel, the more the tendency of the fuel to cause engine problem. The kinematic viscosity of biodiesel fuel in a form of methyl ester should be less than that of the parent oil. Kinematic viscosity is already included in almost all biodiesel standards and can be tested and approved in accordance with these standards. The maximum acceptable limit according to ASTM D445 range is 1.9–6.0 mm^2/s and 3.5–5.0 mm^2/s in EN ISO 3104 (Atabani et al., 2013; Knothe & Razon, 2017).

Flashpoint

Flashpoint is the minimum required temperature for the fuel to ignite. Flashpoint is inversely related with volatility which in turn depends on the viscosity of the fuel, meaning that high volatile fluids have less flash point values and vice versa. Flashpoint is the lowest temperature for the fuel to evaporate for ignition to occur. Diesel fuels have a flash point of 55–66°C while pure biodiesel has 150°C.

Flashpoint is measured in accordance with ASTM D93 (93 °C) and EN ISO 3679 (120 °C) (Atabani et al., 2012, 2013).

Cetane number

The measure of fuel ignition/combustion quality is cetane number of the fuels. Higher CN number usually corresponds to a fuel having better ignition quality and is a chief criterion in the selection of methyl esters as biodiesel fuel. It gives information on the time taken /delay/ for fuel to ignite once it is injected to the combustion chamber. Higher CN indicates a short time interval for ignition. Fuels that have minimum CN emits dark smoke due to incomplete combustion and release particulate and gaseous exhaust and unnecessary engine deposits are associated with low CN. Specification of biodiesel by ASTMD613 is 47min. and EN ISO 5165 is 51 min (Atabani et al., 2012, 2013; Hoekman et al., 2012).

Cloud Point

Cloud point test characterizes operability of diesel fuel under low temperature. It is the temperature for the fuels to start making cloud crystals (when the diameter of the crystal is, d ≥ 0.5 μm) upon cooling of the fuel. The cloud point of biodiesel blends is higher than petroleum diesel fuel (Atabani et al., 2012).

Pour Point

Pour point is the lowest temperature that allows the fuel to flow. At this temperature the formed wax starts to form a gel in the fuel. Thus in the characterization of cold flow property cloud point comes first then followed by pour point. Both cloud point (CP) and pour point (PP) are measured based on specification on ASTM D2500, ASTM D97, EN ISO 23015 and standards (Atabani et al., 2012, 2013; M. U. Kaisan, F. O. Anafi, 2017).

Cold filter plugging point

Is the temperature where the wax crystals start to adhere together becoming larger and larger, corresponds to lower working temperature for the vehicle to operate. At this point, the crystals plug into the filter system of the fuel and restrict fuel flow and eventually, the vehicle stops to move. The cold flow mechanism is shown in Figure 2.6.

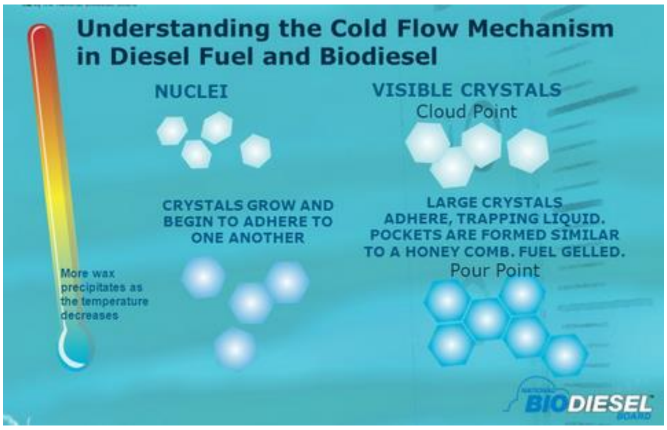

Figure 2.6: The cold flow mechanisms, cold flow and pour point (National biodiesel board)

According to the European biodiesel standard, a biodiesel product must have the specification listed in Table 2.7. There are also other standards that are applied nowadays in USA and others. The properties of diesel and biodiesel were compared in Table 2.8.

Table 2.7: The European biodiesel standard (EN 14214) (Christopher Strong, 2004)

Property	**Test method**	**Limits**		**Unit**
		min	**max**	
Ester content	EN 14103	96.5	-	% (m/m)
Density at 15°C	EN ISO 3675, EN ISO 12185	860	900	kg/m^3
Viscosity at 40°C	EN ISO 3104, ISO 3105	3.5	5.0	mm^2/s
Flash point	EN ISO 3679	120	-	°C
Sulfur content	EN ISO 20846, EN ISO 20884	-	10.0	mg/kg
Carbon residue (in 10% dist. Residue)	EN ISO 10370	-	0.30	% (m/m)
Cetane number	EN ISO 5165	5 1	-	-
Sulfated ash	ISO 3987	-	0.02 %	% (m/m)
Water content	EN ISO 12937	-	500	mg/kg
Total contamination	EN 12662		24	mg/kg
Copper strip corrosion (3 hours, 50°C)	EN ISO 2160	-	1	class
Oxidative stability,110°C	EN 14112	6.0	-	hours
Acid value	EN 14104	-	0.50	mg KOH/g
Iodine value	EN 14111	-	120	g I/100 g
Linolenic acid content	EN 14103	-	12	% (m/m)
Content of FAME with ≥4 double bonds		-	1	% (m/m)
Methanol content	EN 14110	-	0.20	% (m/m)
Monoglyceride content	EN 14105	-	0.80	% (m/m)
Diglyceride content	EN 14105	-	0.20	% (m/m)
Triglyceride content	EN 14105	-	0.20	% (m/m)
Free glycerine	EN 14105, EN 14106	-	0.02	% (m/m)
Total glycerine	EN 14105	-	0.25	% (m/m)
Alkali metals (Na + K)	EN 14108, EN 14109	-	5.0	mg/kg
Earth alkali metals (Ca + Mg)	EN 14538	-	5.0	mg/kg
Phosphorus content	EN 14107	-	10.0	mg/kg

Table 2.8: Comparison of biodiesel property with diesel fuel (Christopher Strong, 2004)

Fuel Property	**Biodiesel**	**Diesel**
Fuel Standard	ASTM PS 121	ASTM D975
Fuel composition	C12-C22 FAME	C10-C21 HC
Lower Heating Value, Btu/gal	117,093	131,295
Kin. Viscosity, @ 40°C	1.9-6.0	1.3-4.1
Specific Gravity kg/l @ 60° F	0.88	0.85
Density, lb/gal @ 15° C	7.328	7.079
Water, ppm by wt.	.05% max	161
Carbon, wt %	77	87
Hydrogen, wt %	12	13
Oxygen, by dif. wt %	11	0
Sulfur, wt %	0.0 - 0.0024	.05 max
Boiling Point (°C)	182-338	188-343
Flash Point (°C)	100-170	60-80
Cloud Point (°C)	-3 to 12	-15 to 5
Pour Point (°C)	-15 to 10	-35 to -15
Cetane Number	48-65	40-55
Stoichiometric Air/Fuel Ratio wt./wt	13.8	15
BOCLE Scuff, grams	>7,000	3,600
HFRR, microns	314	685

2.7. Biodiesel Blends Currently in Use

For improvements in fuel characteristics and various reasons, biodiesel can be blended with various type of other fuels in many kinds of concentrations. Blends of biodiesel can be prepared by mixing with hydrocarbon-based diesel fuels like petroleum diesel. Biodiesel blend mixtures are designated as BXX; B stands for biodiesel while XX represent blend percent. The most widely used biodiesel blends are B2 (2% biodiesel), B5 (5% biodiesel) and B20 (6 to 20% biodiesel) while B100 is a 100% biodiesel.

A B100 has a solvent effect and cleans vehicles fuel system. A B100 must meet the specification of ASTM D6751 in order to be applicable and avoid engine problems. The use of B100 significantly minimizes toxic emissions but increases nitrogen oxides emissions. B100 is uncommon relative to B5 or B20 because of lack of regulatory motivations (Nair & Deepthi, 2013; U.S. Department of Energy, 2018).

B20 (20 percent biodiesel ,80 percent petro diesel) which is widely available diesel blend, is prevalent due to good cost balance, material compatibility, good cold weather properties, emissions and capable of acting as a solvent agent. B20 resolves issues like material compatibility and cold weather performance related to B100. B20 must meet quality standards of ASTM D7467 for applicability. B20 contains a percent or two less energy content than petroleum diesel per gallon while diesel has 8%. Engines running on B20 have similar consumption, torque, horsepower with those use petrodiesel, as a result, there is no report on B20 regarding fuel economy and performance compared to petrodiesel. Engine modification is not required to use B20 and lower blends in the compression ignition engines (Nair & Deepthi, 2013; U.S. Department of Energy, 2018).

B5 blend is a 95% petroleum-based fuel. Being most commonly used biodiesel blend, most vehicle manufacturers optimized their engines and thus approved the use of a B5 blend. ASTM D975 has revised its statement for biodiesel concentrations less than or equal to 5% to be called a diesel fuel.

Biodiesel blending can be done by either of the following methods: Injection mixing (pre-mixing at point of production), Splash mixing (in the truck, one after the other which is least accurate), in line mixing (simultaneous filling on truck tanker) and metered pump filling where the pumps are set to specified volume and percent of each quantity. Table 2.9 shows comparison for B100 versus B20 relative petrodiesel on emission type that was given for heavy-duty engines (Nair & Deepthi, 2013; U.S. Department of Energy, 2018).

Table 2.9: Mean emission of B100 blend and B20 relative to petrodiesel for heavy duty truck (Nair & Deepthi, 2013)

Emission Type	B100	B20
Total Unburnt Hydrocarbons	-67 to -20%	-20 to -2.2%
Carbon Monoxide	-34.50 to 48%	-12 to -6.9%
Particulate Matter	-47% to -32.41%	-12 to -6.4%
Oxides of Nitrogen (NOx)	10 to 13.35%	-2 to +2%

(-ve sign indicates % decrease in emissions of biodiesel blends compared to petrodiesel)

2.8. Advantages and Disadvantages of Biodiesel

2.8.1. Advantages

The following are the main benefits and drawbacks of biodiesel (Atabani et al., 2012; Demirbas, 2008; Hashemzadeh Gargari & Sadrameli, 2018; Innocent, 'donnell, Sylvester, Yahaya, & Isiomanwadike, 2013; Knothe & Gerpen, 2005).

- Biodiesel as a diesel fuel had many advantages like readily available, portability, renewability, lower Sulphur content, biodegradability
- The oxygen content (about 11%) in biodiesel leads to higher combustion efficiency, thus biodiesel is highly combustible fuel.
- Up to B20 blends, Engine modification is not necessary for running, but slight modification and alteration might be necessary for blends over B20.
- Ignition delay can be reduced when using biodiesel because of the high cetane number (60–65) than petroleum diesel (53).
- Produced easily and in a short period.
- Better lubricity property of biodiesel keeps injector units and fuel pump keep lubricated which consequently benefits the engine by reducing wear and tear as well as improving engine efficiency.
- Biodiesel is environmental friendly fuel, produced from leftover edible oils most of the time; nontoxic, non-flammable and less emission of exhaust gasses.

Biodiesel decreases net carbon-dioxide emissions by 78% on a basis of life cycle than typical diesel fuel.

- Drilling, transporting and refining is not needed in case of biodiesel production like that of petroleum fuels enabling almost all country to produce it freely.
- It cuts dependency on pure petroleum and diesel based fuels.

2.8.2. Disadvantages

- Poor cold flow properties (cloud point (CP) & pour point (PP)) associated with biodiesel makes the use of it ineffective in cold weathers and low-temperature areas.
- Even though biodiesel significantly reduces PM emission it is known for increased emission of NO_X (nitrogen oxides) than diesel.
- Has less energy content (<12%) than diesel that leads to increased fuel consumption up to 10% for the same work output in diesel.
- Lower volatilities of biodiesel can cause deposits in engines due to incomplete combustions and need high injecting pressure.
- High viscosity characteristics of biodiesel (11–18 times than diesel) can cause flow problem and gum formation (polymerization).
- As more than 95% of biodiesel is processed from edible oils, it is claimed that this will cause shortage of food consumption and inflation in the price of edible oils that will cause economic instability.

2.9. Jojoba Oil

Jojoba, a plant known by his scientific name as *Simmondsia chinensis* is a distinct and native plant to southern America and northern Mexico, that contains 50% oil by weight in its seed. This is estimated about more than twice as oil content as soybean seed and more than most of the oil crops. Jojoba is known to be drought resistant, long lasting woody shrubs that have a very penetrating root (up to 9-meter depth) and that can live up to 100 to 200 years. The interesting thing about jojoba is that the absence of glycerin makes it not fat but a liquid wax. The oil composed of chains of monoesters in the range containing $C_{20} - C_{22}$ as in many alcohols with double bonds at each end of the ester bond. Jojoba oil has a wide range of application like as chemical processors, cosmetics, lubricants, pharmaceuticals, foods, insulators and many others (Allawzi & Tamimi, 2000; Bilin, Alshanableh, Evcil, & Savas, 2018).

The wax ester in jojoba is heat resistant and tolerant to oxidizing conditions that make it a favorable replacement of synthetic oils that are used in high temperature (with a boiling point of 389 ℃) and pressure lubrication oils. Due to these characteristics, jojoba shrubs are farmed across the arid lands and deserts of the world including across the Middle East and Cyprus (Bilin et al., 2018). World jojoba production is given in Table 2.10.

Table 2.10: Production of jojoba (Ash & Cother, 2005)

Country	**Area (ha)**
Argentina	3,000
USA	2,290
Israel	550
Australia	480
Peru	350
Egypt	240
Mexico	100
Chile	45
Total	7,055

In this work, the jojoba fruits were collected from a test plantation near Nicosia. 15 hectares of jojoba test plantation has been grown since 2004 by the government in near Nicosia. Bilin et al. conducted an experiment to test the details in the oil characteristics of this new oil crop of Mesaoria plain of Cyprus (found between Nicosia and Famagusta) grown under local environments. His work was based on the standard set by IJEC, the International Jojoba Export Council consists of various companies, jojoba growers, traders and processors and academic institutions all around the world. The aim of IJEC was to adopt various physical and chemical standards to test, report and ensure a fine quality of jojoba oil.

A comparison of different chemical properties of Mesaoria plain of Cyprus jojoba oil with the rest of the world is given below in Table 2.11, Table 2.12, Table 2.13, respectively.

Table 2.11: Comparison of fatty acid compositions (%) (Bilin et al., 2018)

Fatty Acid	**Origin of jojoba oil**					**IJEC Standard 1998 – AOCS**
	Mesaoria Plain (Cyprus)	**Negev Desert (Israel)**	**Ismailia Desert (Egypt)**	**JUST (Jordan)**	**Arizona Desert (USA)**	
C16:0 Palmitic acid	1.89	3.0 max.	1.6	0.57	1	≤3.0
C16:1 Palmitoleic acid	0.07	1.0 max.	0.1	0.09	0.4	≤1.0
C18:0 Stearic acid	0.46	5.0 max.	0.9	0.02	0.1	-
C18.1 Oleic acid	12.28	5.0 - 15.0	14.5	4.84	11	5.0 - 15.0
C20:0 Arachidic acid	0.13	3.0 max.	0.2	0.05	0.1	-
C20:1 Eicosenoic acid	71.10	65.0 - 80.0	60.0	37.61	70	65.0 - 80.0
C22:0 Behenic acid	0.18	1.0 max.	0.30	-	0.2	≤1.0
C22:1 Erucic acid	11.69	10.0 - 20.0	11.8	21.68	13	10.0 – 20.0
C24:1 Nervonic acid	1.15	3.0 max.	1.6	0.2	1	≤3.0
Other fatty acids	1.0 max.	3.0 max.	1.0 max.	21.68	1.0 max.	≤3.0

Table 2.12: Comparison of wax esters compositions (%) (Bilin et al., 2018)

Wax ester	**Origin of jojoba oil**				**IJEC Standard 1998 – AOCS**
	Mesaoria Plain (Cyprus)	**Negev Desert (Israel)**	**Ismailia Desert (Egypt)**	**Arizona Desert (USA)**	
C40	28.2	26.0-37.0	30.1	30.5	26.0-34.0
C42	46.3	44.0-56.0	51.1	49.5	44.0-56.0
C44	8.0	8.0-13.0	10	10	8.0-12.0
C46	0.5	3.0 (max)	1.1	1.3	0-3

Table 2.13: Physical and chemical properties of the jojoba oil (Bilin et al., 2018)

Property *[Unit]*	**Origin of jojoba oil**				**IJEC Standard, 1998 – AOCS**
	Mesaoria Plain (Cyprus)	**Negev Desert (Israel)**	**Sonora Desert (Mexico)**	**AJORP (India)**	
Specific Gravity *[g/cm^3]*	0.86 (AOAC 985,16.2016)	0.863-0.873	0.86	0.867	0.86-0.87 (AOCS Cc 10 a)
Refractive Index	1.47 (AOCS Cc 7 25)	1.465-1.467	1.46	-	1.45-1.47 (AOCS Cc 7 25)
Saponification Value *[mg KOH/g]*	92.6 (BS EN ISO 3657)	88.0-98.0	-	86	88-96 (AOCS Cd 3-25)
Viscosity *[mm/s]*	24.55 (at 40 ℃) 6.45 (at 100 ℃) (EN ISO 3104)	-	26.60 (at 40℃)	24.61 (at 40 ℃) 6.40 (at 100 ℃) (ASTM D 445)	-
Acid Value *[mg KOH/g]*	0.5 (EN ISO 660)	1.0 (max)	0.39	0.54	1.0 (max) (AOCS Ci 4-91)
Iodine Value *[gram]*	88.9 /100 (EN ISO 3961)	80.0-90.0	83.11	80 (IP D-84/81)	82-87/ 100 (AOCS Cd 1-25)
Peroxide Value *[$meqO_2/kg$]*	<1 (EN ISO 27107)	2.0 (max)	2	7.2 (ASTM D - 1832 – 99)	2.0 (max) (AOCS Cd 8-53)

CHAPTER 3
EXPERIMENTAL SET- UP AND METHODOLOGY

The current chapter discusses the experimental methods and formulations used in the work as well as the set-ups and steps are discussed in detail.

3.1. Jojoba Oil Extraction

There are many ways to extract jojoba oil from its seed (mechanical extraction via expeller, hydraulic pressing and solvent extractions are known so far), for this specific study the oil was extracted by mechanical extraction via a screw expeller at the laboratory of mechanical engineering department of Near East University. After the fruits of jojoba shrubs were collected from plantation center near Nicosia, seeds were separated, cleaned, washed and dried for processing. The seeds were pressed by worm shaft (stainless steel screw) against the housing and the inner surface of expeller, upon squeezing under high pressure the oil pours through outlet hole found at the bottom outer surface of the housing.

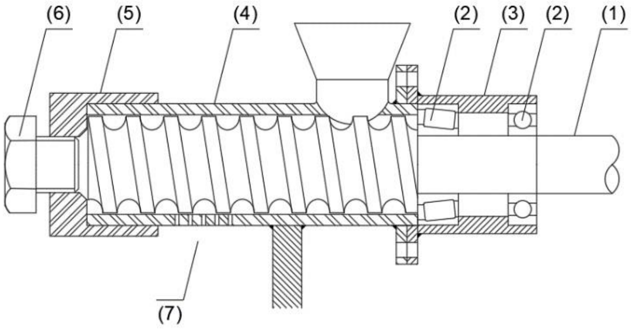

Figure 3.1: Sectional view of the jojoba oil expeller used (Bilin et al., 2018)

Where:

(1) Worm shaft, (2) Bearings, (3) Bearing case, (4) Worm shaft housing, (5) Sediment adjusting nut, (6) Pressure adjusting bolt, (7) Oil outlet hole.

3.2. Thermal Analysis via Cooling Curves

Thermal analysis is a technique for collection of thermo-chemical and physical properties of materials while the material is undergoing a phase change as a result of heat transfer that occurred throughout the process. It is a widely used technique in materials and metallurgical engineering fields to convey information about the thermal characteristics and behaviors like freezing and melting point, specific heat constants, latent heat releases, heat transfer coefficients as well as in the determination of solid fraction evolution in casting and solidification of alloys and metals.

Thermal analysis application in this study was based on the examination of cooling curves of jojoba oil – biodiesel blends. During phase change in the jojoba oil – biodiesel blend the heat transfer mechanisms may take place with one or combination of the following heat transfer mechanisms.

- conduction,
- convection,
- and radiation.

3.2.1. Conduction

Conduction heat transfer occurs due to the interaction of particles whereby heat energy is transferred or flows from more energetic to less energetic particles. One dimensional heat transfer rate or heat flux is given by (Incropera, Dewitt, Bergman., & Lavine, 2000).

$$q = \frac{\dot{Q}}{A} = -k\frac{dT}{dx} \qquad (3.1)$$

Where: q is heat flux per unit area, $\dot{Q}$ is total heat flow rate through the surface , A is the urface area , k is thermal conductivity and $\frac{dT}{dx}$ is temperature gradient (Incropera et al., 2000). The –ve sign indicates that heat transfer takes place in the minimal direction.

3.2.2. Convection

Convection heat transfer takes place when a certain material is exposed to a fluid where the fluid temperature is different from that of the exposed body. If the T_s is surface temperature of the body and T_∞ is the fluid temperature , the heat flux through the surface is given by:

$$q = -\dot{Q} = hA(T_s - T_\infty) \qquad (3.2)$$

Where: A is the surface area and h is convective heat transfer coefficient.

3.2.3. Radiation

In radiation heat transfer the heat energy is carried out by electromagnetic waves. The radiation heat transfer rate is given by:

$$q = \sigma A T^4 \qquad (3.3)$$

in which: $\sigma = 5.67 \times 10^{-8} wm^{-2}K^{-4}$ is Stephan-Boltzman constant , A is surface area and T is the absolute temperature of the body. In a case where the body of temperature T is enclosed by isothermal surface whose temperature is T_{sur} , the heat transfer rate can be expressed as;

$$q_{rad} = \sigma \epsilon A(T^4 - {T_{sur}}^4) \qquad (3.4)$$

Where ϵ is emissivity of the object that ranges from (0-1). In this study (of biodiesel- jojoba thermal analysis) radiation heat transfer may be neglected when compared to conduction and convection heat transfers.

Thermal analysis can be carried out by one of the following methods or techniques. Differential Thermal Analysis (DTA), Differential Scanning Calorimetry (DSC) and the Cooling Curve Analyses (CCA) are useful techniques in the determination of solidification of alloys and metals (Erbaş, 2014). The DTA is based on the temperature difference between the sample and the reference material in the same heat treatment. DSC uses the same principle with DTA but with the inclusion of heat source to balance temperatures of the sample and the reference.

The Computer Aided Cooling Curve Analysis (CA-CCA) is the most applicable, practical and low-cost method compared to Differential Scanning Calorimetry (DSC) and Differential Thermal Analysis (DTA) (Naghdali, Jafari, & Malekan, 2018). It is based on the analysis of the temperature upon cooling small volume of sample. It monitors temperature change that takes place as the sample cools down. The solidus or eutectic and liquidus temperature2018, phase transition point, solid fraction, latent heat…etc. can be obtained using the CA-CCA. Depending on the heat flow model used, the CA-CCA uses either Fourier or Newtonian thermal analysis method. Even though more accurate prediction of latent heat is obtained by the Fourier analysis, it is complicated than the Newtonian method. The current work is based on CA-CCA in which Newtonian thermal analysis is used.

3.3. Newtonian Thermal Analysis (NTA)

In CA-CCA in which NTA is used, the cooling curve analysis is based on the consecutive recordings of temperature versus time data collected during the phase change process. The recording process is carried out by putting the suitable thermocouple in the melt, recording the temperature and corresponding time as the melt cools down and solidifies (Dehnavi, 2015; Evcil, Al-Shanableh, & Savas, 2018). Usually, the cooling curve only does not provide enough information on the sample, for this case the first and second order of first derivatives of the cooling curves as well as the zero curves are implemented to fully interpret the phase change. The use of the derivative and zero curves assist and improves the accuracy of extracting information's which cannot be done by examining the cooling curve only.

Newtonian Thermal Analysis (NTA) is based on the following assumptions:

- Is based on Newtonian cooling of the sample that takes the thermal gradient through the sample to be zero (homogeneous temperature distribution and thus assumes high conductivity) in which the lumped heat capacity model is assumed. In this case *Biot number*, $Bi = \frac{h}{k} L_C << 0.1$, where h is convective heat transfer coefficient, k is the conductivity of material and L_C is the characteristic length defined as the ratio of volume to surface area.

- Heat transmission modes from the sample to surrounding are represented by a particular formulation and the bath temperature throughout the process is constant (for calculation of zero curves).
- The sensible specific heat in the no phase change region is assumed as constant.

For a given sample of material under phase transformation, the heat equation can be written as:

$$\dot{Q}_{net} = \dot{Q}_{loss} + \dot{Q}_{PT} + \dot{Q}_{in} \tag{3.5}$$

Where: $\dot{Q}_{net}$ is net heat rate of a given volume, $\dot{Q}_{loss}$ is rate of the heat lost and $\dot{Q}_{PT}$ is heat rate generated during phase transformation and $\dot{Q}_{in}$ is heat rate supplied. Since there is no supplied and generated heat, equation (3.5) in combination with convective heat transfer (3.2) can be rewritten as;

$$\dot{Q} = \frac{dQ_{loss}}{dt} = V\rho C_p \frac{dT}{dt} = -hA(T - T_{\infty}) \tag{3.6}$$

This is Newton's law of cooling (NLC), which states that the rate of heat loss is proportional to the temperature difference between the sample and ambient temperatures where T is uniformly distributed instantaneous temperature, and A, T_{∞}, h, C_p, V, Q_L, ρ, T, and t are surface area, ambient temperature, heat transfer coefficient, specific heat of the sample, volume of the sample, latent heat of solidification, density of the sample, temperature, and time, respectively. The left hand side term in the equation is the heat generated by phase transformation, the second term is heat lost by the sample and the right hand side of the equation is heat transferred to the mold (bath in our case).

Rearranging equation (3.6) gives:

$$\frac{dT}{dt}_{\mathrm{cc}} = \frac{1}{\mathrm{V\rho C_p}}\left[\frac{dQ_L}{dt} - hA(T - T_{\infty})\right] \tag{3.7}$$

This is the equation representing the cooling curve. In the absence of phase transformation equation (3.6) reduces to what’s known as zero curve equation

$$\frac{dT}{dt}_{zc} = \frac{-hA}{\mathrm{V\rho C_p}}(T - T_{\infty}) \tag{3.8}$$

Rewriting equation (3.7) and solving for the rate of heat released during phase transformation, one can get the following equation:

$$\frac{dQ_L}{dt} = V\rho C_p \left[\frac{dT}{dt}_{\mathrm{cc}} + \frac{hA}{\mathrm{V\rho C_p}}(T - T_\infty)\right] = \mathrm{V\rho C_p}\left[\frac{dT}{dt}_{\mathrm{cc}} - \frac{dT}{dt}_{zc})\right] \qquad (3.9)$$

Integrating equation (3.9) from *0* to $\mathrm{t_s}$, where $\mathrm{t_s}$ is solidification time and noting subscripts ***cc*** and ***zc*** for cooling and zero curve;

$$Q_L = V\rho C_p \int_0^{\mathrm{t_s}} \left[\frac{dT}{dt}_{\mathrm{cc}} - \frac{dT}{dt}_{zc}\right] \mathrm{dt} \qquad (3.10)$$

Or, alternatively;

$$\frac{Q_L}{\mathrm{V\rho}} = L = C_p(area\ under\ cc\ derivative - \\ area\ under\ zc\ derivatives) \qquad (3.11)$$

Where L is latent heat. Equation (3.11) gives the numerical integration of latent heat. The solid fraction evolved during solidification can be determined from equation (3.12) as the ratio of the cumulative area under the derivative curve to the total area under the derivative curve which is also calculated by numerical calculation.

$$F_s = \frac{\left(\int_0^{\mathrm{t}}\left[\frac{dT}{dt}_{\mathrm{cc}} - \frac{dT}{dt}_{zc}\right]\mathrm{dt}\right)}{\left(\int_0^{t_s}\left[\frac{dT}{dt}_{cc} - \frac{dT}{dt}_{zc}\right]dt\right)} = \frac{\mathrm{C_p}}{\mathrm{L}} \int_0^{\mathrm{t}} \left[\frac{dT}{dt}_{\mathrm{cc}} - \frac{dT}{dt}_{zc}\right] \mathrm{dt} \qquad (3.12)$$

3.4. Derivation of Newtonian Zero Curve Equation

Application of energy balance to the sample that is under phase change can be written as:

$$\sum E_{in} = \sum E_{out}\ or\ \Delta E = \sum \mathrm{E_{in}} + \sum E_{gen} - \sum E_{out} \qquad (3.13)$$

Where; $\sum E_{in}$ is total energy supplied, $\sum E_{gen}$ is energy generated during solidification and $\sum \mathrm{E_{out}}$ energy lost, it follows that during the CA-CCA analysis, the power balance is:

$$\frac{\partial \mathrm{E}}{\partial \mathrm{t}} = \frac{\partial(\sum \mathrm{E_{in}})}{\partial \mathrm{t}} + \frac{\partial(\sum \mathrm{E_{gen}})}{\partial \mathrm{t}} - \frac{\partial(\sum \mathrm{E_{out}})}{\partial \mathrm{t}} \quad \text{or} \quad \dot{E}_{net} = \dot{E}_{in} + \dot{E}_{gen} - \dot{E}_{out} \qquad (3.14)$$

Since there is no energy input and generated energy during the CA-CCA equation (3.14) reduces to;

$$\frac{\partial E}{\partial t} = \dot{E}_{out} = -UA(T - T_{\infty}) \tag{3.15}$$

Where; U is overall heat transfer coefficient, A is sample surface area, T & T_{∞} are sample and ambient temperatures. Rate of change of energy can also be written in terms of mass of the sample and specific internal energy as:

$$\frac{\partial E}{\partial t} = \frac{\partial (mu)}{\partial t} \tag{3.16}$$

$$\frac{\partial E}{\partial t} = m\frac{\partial u}{\partial t} = m\frac{\partial \mathrm{u}}{\partial \mathrm{T}}\frac{\partial \mathrm{T}}{\partial \mathrm{t}} = mC_p\frac{\partial \mathrm{T}}{\partial \mathrm{t}} \tag{3.17}$$

Where C_p is sample specific heat value. Equating equation (3.15) and (3.17) results in the following type of equation.

$$mC_p\frac{\partial T}{\partial t} = -UA(T - T_{\infty}) \tag{3.18}$$

Up on rearranging:

$$z_N = \frac{\partial \mathrm{T}}{\partial \mathrm{t}} = -\frac{UA}{mC_p}(T - T_{\infty}) \tag{3.19}$$

Equation (3.19) is known as the Newtonian Zero Curve (Z_N) equation. Now considering;

$\frac{\partial T}{\partial t} \approx - \Delta T = T(t) - T_{\infty}$ (final temperature difference) where the minus sign indicates change in temperature is decreasing and $\Delta T_0 = T_{int} - T_{\infty}$ (initial temperature difference) and assuming T_{∞} as constant and rearranging ;

$\frac{\partial T}{\Delta \mathrm{T}} = -\frac{UA}{\mathrm{mC_p}}\partial t$ but $\partial T = \partial(T(t) - T_{\infty}) = \partial(\Delta \mathrm{T})$ since T_{∞} is constant, therefore the above equation can be rewritten as;

$$\frac{\partial(\Delta \mathrm{T})}{\Delta \mathrm{T}} = -\frac{UA}{mC_p}\partial t \tag{3.20}$$

taking the parameter $\frac{UA}{mC_p}$ as a constant, that is distinct in liquid and solid phases the above equation can be integrated as;

$$\int_{\Delta T_0}^{\Delta T}\left[\frac{\partial(\Delta T)}{\Delta T}\right] = -\frac{UA}{mC_p}\int_0^t \partial t \tag{3.21}$$

Upon integration of equation (3.21);

$$\Delta T = (\Delta T_0)\, exp^{-\frac{UA}{mC_p}t} \tag{3.22}$$

back substitution and rearranging gives;

$$T(t) = T_\infty + (T_{int} - T_\infty)\, exp^{-\frac{UA}{mC_P}t} \tag{3.23}$$

the first time derivative of equation (3.23), assuming T_∞ as a constant gives,

$$z_N = \frac{dT(t)}{dt} = -\frac{UA}{mC_P}(T_{intl} - T_\infty)\, exp^{-\frac{UA}{mC_P}t} \tag{3.24}$$

Equation (3.24) is the Newtonian Zero Curve equation and it is important to note that equation (3.22) and (3.24) can be used for both liquid and solid phases independently by substituting the initial conditions and necessary constants.

3.5. Cooling Curve Analysis (CCA) Setup

This was the system where the necessary data was recorded. The sample temperature with respect to time was recorded as it cools down and solidifies. The liquid and solid fractions, as well as cold flow properties, can be examined from the data of this experiment. The Cooling Curve Analysis setup was composed of the following subunits.

3.5.1. The data collection part

This was the specific part of the setup used to record primary data particularly sample and cooling bath temperature versus time. This part contains data logger connected to a computer. The data logger shown in Figure 3.2 is used in the study. It was designed with 5 channels to be connected with different types of thermocouples. Two channels were used in this experiment to record data, one records the sample temperature while the other is recording the cooling bath temperature at the same time.

Figure 3.2: Data Logger, ODEL UDL 100

A computer connected and installed with specific software (Dali 08 Data Acquisition and Logging Interface) in this case was used which interprets the signal of the logger, record and display the data. The complete schematic illustration is shown in Figure 3.3.

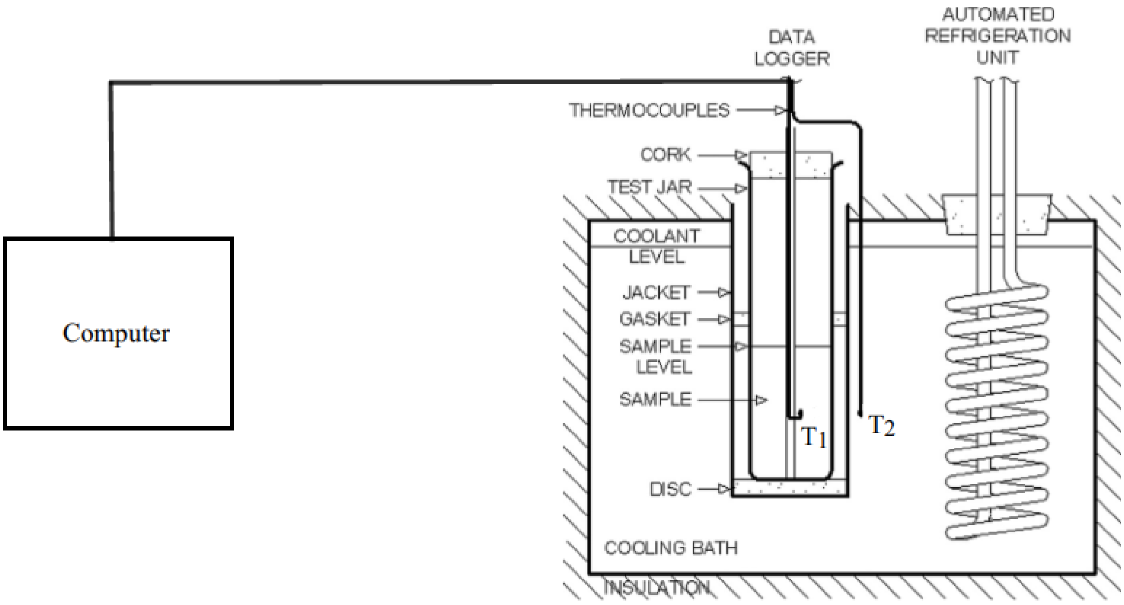

Figure 3.3: Schematic illustration of CA-CCA setup

The readings of the thermocouples after interpretation is displayed by the interface as shown in Figure 3.4. Options are provided for data selection for capturing throughout the experiment. The data is originally recorded within a second interval but later on, it can be saved as one's preference every 15 secs, 30 secs, 45 secs and 60 secs and more. A successive reading at each second of the thermocouple is shown in the black panel at the bottom of the interface. The recorded data is exported to Microsoft Excel or other suitable software to be analyzed.

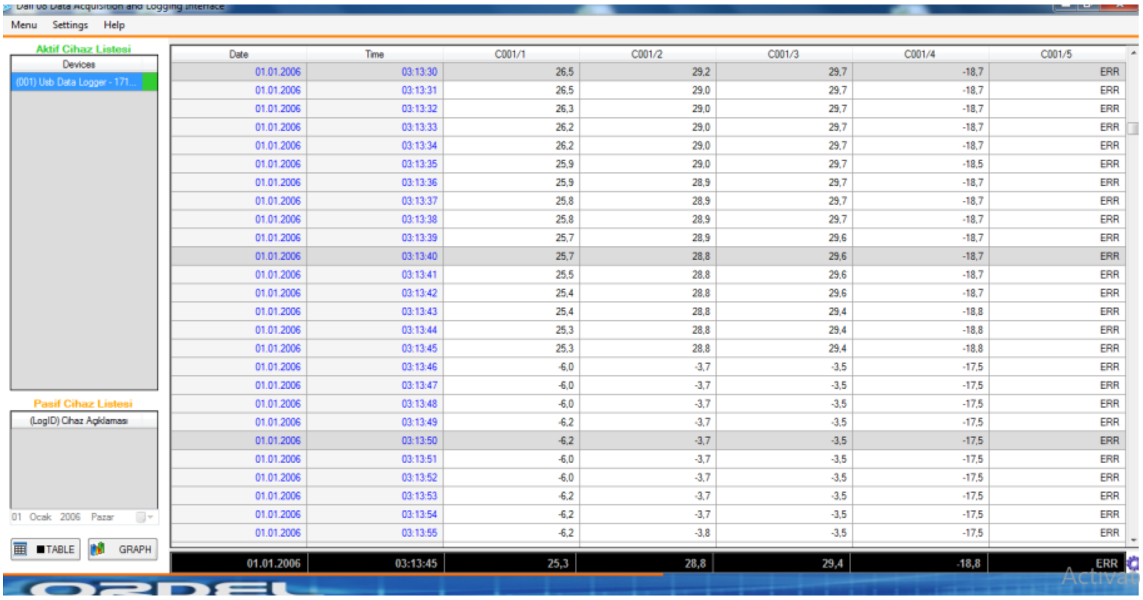

Date	Time	C001/1	C001/2	C001/3	C001/4	C001/5
01.01.2006	03:13:30	26,5	29,2	29,7	-18,7	ERR
01.01.2006	03:13:31	26,5	29,0	29,7	-18,7	ERR
01.01.2006	03:13:32	26,3	29,0	29,7	-18,7	ERR
01.01.2006	03:13:33	26,2	29,0	29,7	-18,7	ERR
01.01.2006	03:13:34	26,2	29,0	29,7	-18,7	ERR
01.01.2006	03:13:35	25,9	29,0	29,7	-18,5	ERR
01.01.2006	03:13:36	25,9	28,9	29,7	-18,7	ERR
01.01.2006	03:13:37	25,8	28,9	29,7	-18,7	ERR
01.01.2006	03:13:38	25,8	28,9	29,7	-18,7	ERR
01.01.2006	03:13:39	25,7	28,9	29,6	-18,7	ERR
01.01.2006	03:13:40	25,7	28,8	29,6	-18,7	ERR
01.01.2006	03:13:41	25,5	28,8	29,6	-18,7	ERR
01.01.2006	03:13:42	25,4	28,8	29,6	-18,7	ERR
01.01.2006	03:13:43	25,4	28,8	29,4	-18,8	ERR
01.01.2006	03:13:44	25,3	28,8	29,4	-18,8	ERR
01.01.2006	03:13:45	25,3	28,8	29,4	-18,8	ERR
01.01.2006	03:13:46	-6,0	-3,7	-3,5	-17,5	ERR
01.01.2006	03:13:47	-6,0	-3,7	-3,5	-17,5	ERR
01.01.2006	03:13:48	-6,0	-3,7	-3,5	-17,5	ERR
01.01.2006	03:13:49	-6,2	-3,7	-3,5	-17,5	ERR
01.01.2006	03:13:50	-6,2	-3,7	-3,5	-17,5	ERR
01.01.2006	03:13:51	-6,0	-3,7	-3,5	-17,5	ERR
01.01.2006	03:13:52	-6,0	-3,7	-3,5	-17,5	ERR
01.01.2006	03:13:53	-6,2	-3,7	-3,5	-17,5	ERR
01.01.2006	03:13:54	-6,2	-3,7	-3,5	-17,5	ERR
01.01.2006	03:13:55	-6,2	-3,8	-3,5	-17,5	ERR

01.01.2006	03:13:45	25,3	28,8	29,4	-18,8	ERR

Figure 3.4: Recorded data by Data Logger Interface

3.5.2. The cooling bath part

The cooling bath system was the part where the sample cools down. After the required amount of sample is measured, it is immersed to the bath tank which is made from thick glass. The glass is a good insulator of heat and thus maintains an internal temperature of the coolant and it is sealed with silicone to prevent the coolant escaping from the bath tank.

The coolant used was ethyl alcohol. Ethyl alcohol was selected because of its low freezing point which was -114.1 °C. The whole body of the bath tank was insulated with Styrofoam (which is a good insulator of heat) that prevents heat transfer between the ethyl alcohol (coolant) and the room temperature. There is a coil in which the refrigeration gas is carried through and circulated between the heat exchanger and cooling bath. It removes heat from ethyl alcohol to keep the temperature of the alcohol as low as possible and reject it to the surrounding.

Two T-type thermocouples were used in this experiment; one is used to measure sample temperature which is mounted on the stand in the bath while the other reads the cooling bath temperature. There was also a thermostat wire inserted to the bath so that the thermostat reads the bath temperature to keep on cooling up to the pre-set value. By default, the bath temperature was monitored by both the thermocouple and the thermostat. The cooling bath system is shown in Figure 3.5.

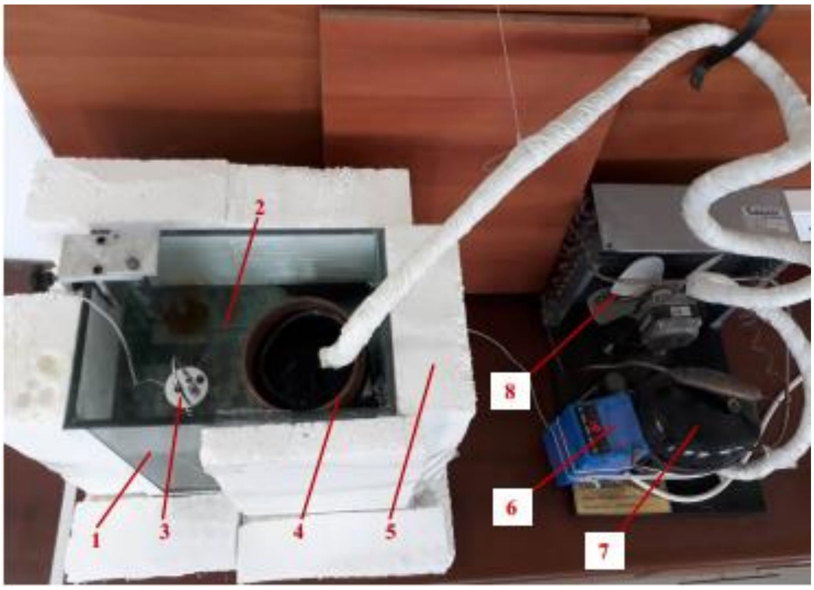

Figure 3.5: The cooling bath system

Where, 1 is Cooling bath reservoir, 2- Alcohol (ethyl alcohol), 3- Test jar containing the sample/viscometer holder, 4 - Coil, 5- Insulator (Styrofoam), 6 - Thermostat, 7- Compressor, 8 - Cooling fan.

3.5.3. The compression unit

The compression unit consisted of the compressor and temperature display and control unit as shown in Figure 3.6. The refrigerator gas is cooled down by the compressor which in turn cools the coolant alcohol in the bath. The control unit is adjusted to the required temperature and needs a minimum of two hours to reach the pre-set value to proceed to our experiment. The optimum working temperature is usually ≈ -20°C for the bath and it takes 2-3 hours to reach this temperature depending on the ambient temperature.

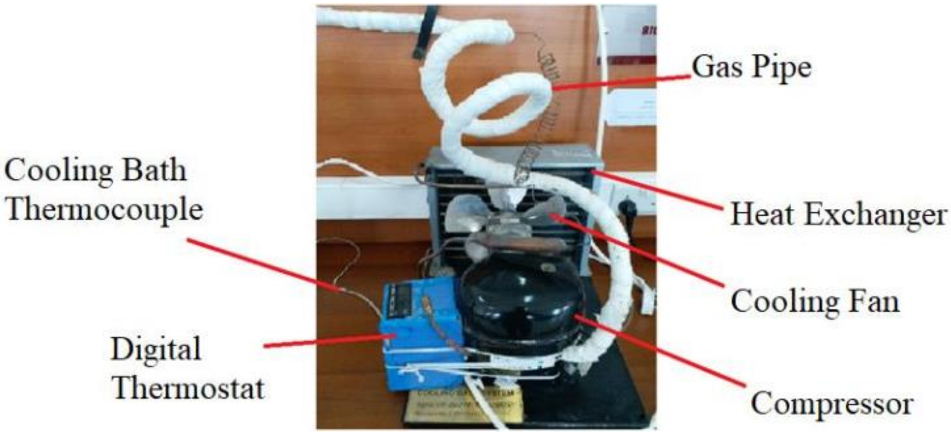

Figure 3.6: The compression unit

3.6. General Steps Involved in Performing CA-CCA

Generally, the following procedures were used for the data collection of the blend samples for cooling curve analysis.

1. Switch on the digital thermostat and set it to the required temperature, wait for about 2-3 hours until the set temperature reads on the display.
2. Measure and prepare the sample (Biodiesel –Jojoba oil blend by volume ratio) as the bath gets ready for experimentation and cooled down to adjusted temperature (≈-20°C).
3. Once the cooling bath was ready, heat the sample to 60°C max. The heating was done by electromagnetic stirrer and heater by first heating a half filled water in 5000 ml beaker and then heating the sample in the hot water, the temperature can be measured by a hand thermometer.

Figure 3.7: Electromagnetic stirrer and heater

4. Open the data acquisition software on the computer and the gently adjust the test jar (cylinder) containing the sample, insert the thermocouple wire and fix it to the stand support which is immersed to the cooling alcohol bath. Make sure that the other thermocouple and thermostat wires are inserted in the cooling alcohol bath at the same time.
5. Cover the top of the alcohol bath by styrofoam and ensure the thermocouple is reading both sample and cooling bath temperatures.
6. Wait for about 3 hours or more until the sample completely solidifies and the difference in temperature of the sample and bath $(T - T_{\infty})$ becomes as low as possible.
7. Capture and save the recorded data for different time intervals i.e. 15 secs, 30 secs, 45 secs, 60 secs…. etc. as a preference. This can be used later for comparison whilst the CCA is done. By default, the data is recorded within a second interval by the software. averaged temperature reports are an optimized output for analysis.
8. Remove the test jar from the cooling bath and heat it up to re-melt and preserve it for further experiment.
9. Repeat steps 1-8 until all blend samples are tested on a similar process.

3.7. The Cooling Curve and Phase Diagram

In the determination of phase diagrams, the data's are obtained from a various range of measurements, many of which are conducted primarily for reasons other than the purpose of constructing phase diagrams. Construction of an accurate phase diagram just using one method of an experiment is impossible as well as no phase diagram can be fully considered as accurate without justifying the data with at least one other method. In the construction of accurate phase diagram knowledge of the chemical composition of the samples and individual phases are very important (ASM, 1992).

3.7.1. Cooling curve

Thermal analysis is one of the widely used way of determining phase boundaries. The sample temperature is allowed to cool down usually from the liquid phase, from an elevated temperature. The cooling of an element takes place at the instantaneous rate that's dependent on its heat capacity. If no phase change is observed as in amorphous (non-crystalline) materials such as glass, the shape of the cooling curve for temperature versus time results in a smooth and monotonically decreasing curve as shown in Figure 3.8.

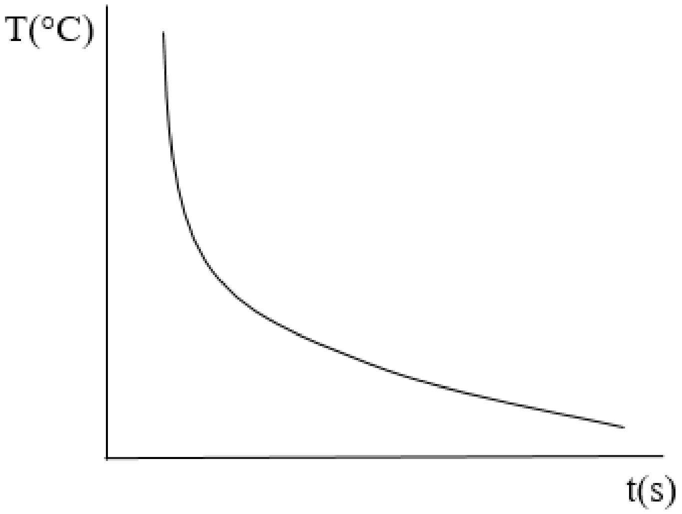

Figure 3.8: Ideal cooling curve for a pure non-crystalline (amorphous) substance that do not undergo a phase transformation (ASM, 1992)

If, however, when a crystalline material is cooled through its freezing temperature, its temperature is maintained near that temperature of a freezing point until the freezing ends and the curve experiences a discontinuity at which phase transformation starts as shown in Figure 3.9. The reasons for such phenomenon are that first, the new phase has a different heat capacity that is different from the old phase, second and significantly when phase transforms heat is given off. When heat is given off upon phase transformation, the cooling rate dramatically decreases. Therefore, a sudden change in the slope of the cooling curve always alerts that phase change has started. After phase change ends the normal cooling rate resumes. Due to slight cooling rates, it becomes difficult to detect a phase transformation by thermal analysis that gives off heat in a very small amount.

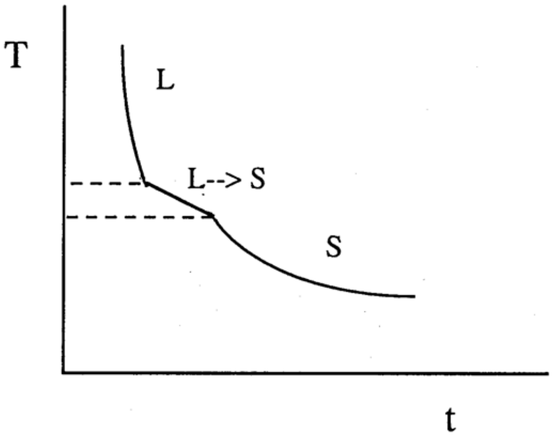

Figure 3.9: Cooling curve of a crystalline material that's undergoing an L → S phase transformation (Prince, 1966)

During transformation, the rate of cooling decreased and upon completion, the cooling rate resumes at a faster rate, it is observed that the rate of cooling for liquid and solid is different because of difference in heat capacity of both phases (liquid and solid).

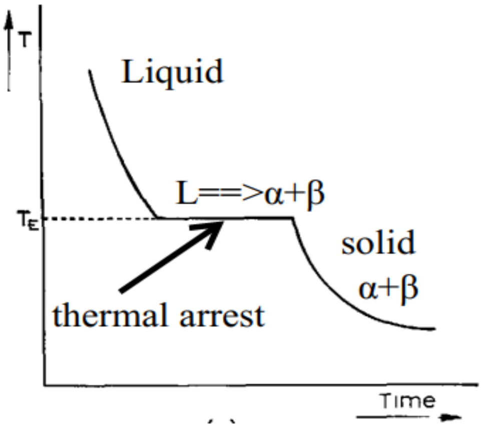

Figure 3.10: Cooling curve of a crystalline material under the eutectic phase transformation (Prince, 1966)

The other condition is that where cooling rate entirely stops under phase transformation which results in a thermal arrest of the cooling curve as shown in the Figure 3.10. Cooling curve for an alloy of a given composition will specify the solidus, liquidus, eutectic and other transformations on the curve. A phase diagram having unique eutectic temperature (T_E) can be prepared by having several cooling curves of such type for various compositions as in Figure 3.11.

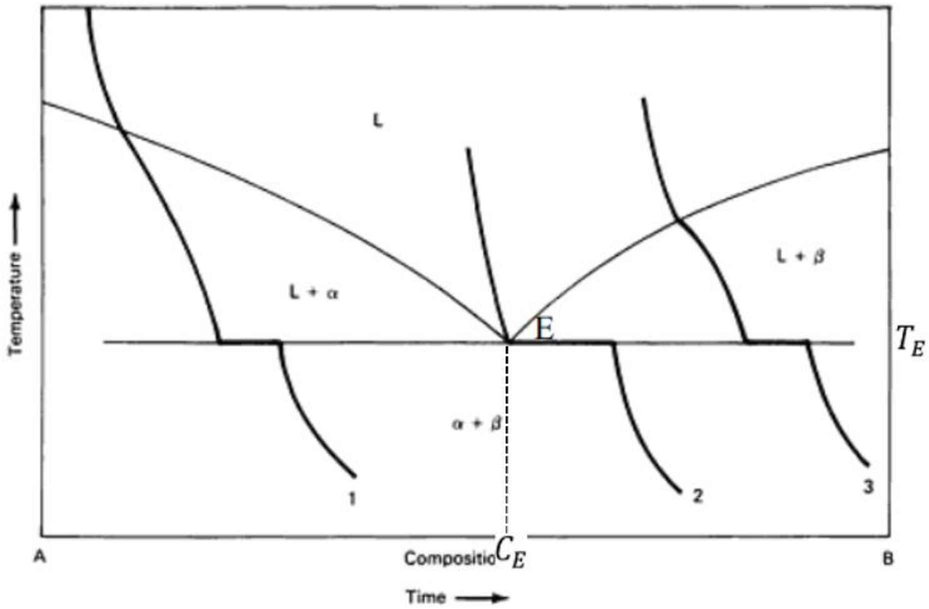

Figure 3.11: Superimposition of (1) a hypo-eutectic alloy, (2) a eutectic alloy, and (3) a hyper-eutectic alloy cooling curves in eutectic type phase diagram (ASM, 1992; Prince, 1966)

Point E in Figure 3.11 is where two solid phases and a liquid one co-exist at equilibrium which is known as the eutectic or invariant point at corresponding eutectic composition C_E and eutectic temperature T_E (indicated by a solidus horizontal isotherm line). Eutectic reaction takes place at corresponding eutectic composition and eutectic temperature**,** where a mixture of two solid phases evolved from the liquid phase**,** considering that eutectic reaction may be expressed as;

$$\text{Liquid} \underset{\text{Heating}}{\overset{\text{Cooling}}{\rightleftarrows}} \underbrace{\text{Solid}_1 + \text{Solid}_2}_{\text{Eutectic mixture}}$$

A good example of such a phase diagram construction is from Ag-Cu cooling curves of different compositions. In the figure given below, the area from the top to point *a* on the cooling curve represents cooling of the liquid, the liquids keep cooling in the region *a* to *b* at a lower rate since a new solid phase is crystallizing and heat of fusion is given off. The eutectic thermal arrest takes place from *b* to *c* until every drop of the liquid solidifies, shorter or longer depending upon the concentration of liquid left when the liquid phase reaches the eutectic point. The last portion on the cooling curve, below point *c* to the end of the curve the mixture is all solid and keeps on cooling to room temperature at a slower rate than that of the liquid phase because of difference in heat capacity. The collective information of these curves leads to the construction of the eutectic type of phase diagrams as shown in Figure 3.11 or Figure 3.12.

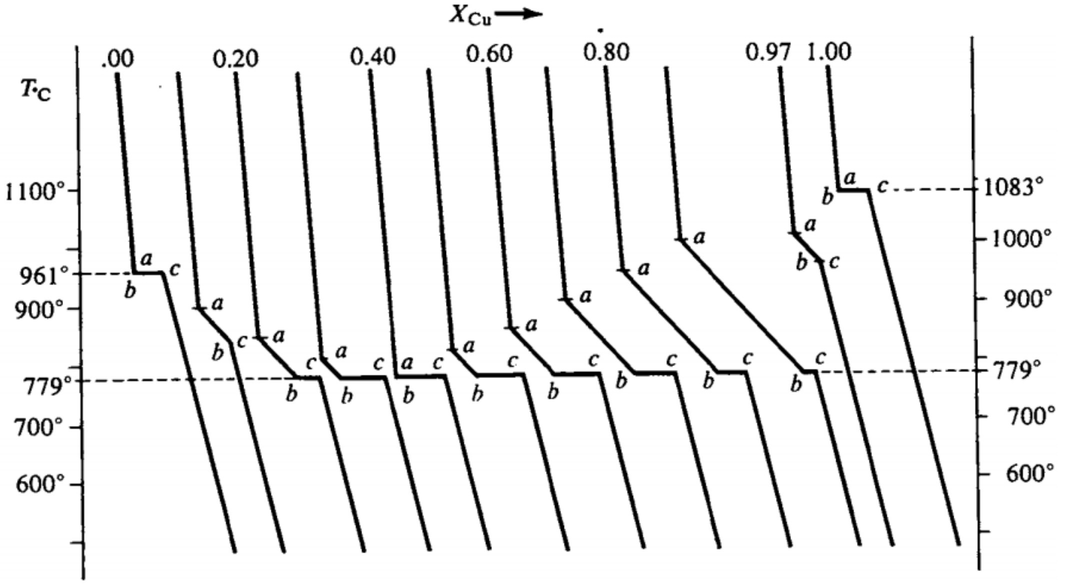

Figure 3.12: Ag-Cu cooling curves of different compositions for typical eutectic type phase diagram construction (Dickerson, 1969).

Other techniques like chemical analysis, x-ray diffraction, physical properties, metallographic methods, and thermodynamic modeling can be used to determine the phase diagram of substances (ASM, 1992)

3.8. The Gibbs Phase Rule

Gibbs phase rule is a thermodynamic principle that expresses the number of degrees of freedom in terms of phases present and number of a chemical constituent in the system which was deducted by *J. W. Gibbs* in 1878. It also represents a criterion for the number of possible phases that will co-exist within a closed system at equilibrium. The Gibbs phase rule is useful in construction and analysis of phase diagram. It is expressed by the following generalized and simple relation (William & Rethwisch, 2009).

$$P + F = C + N \tag{3.25}$$

Where; P is number of phase exits, F is degrees of freedom (number of intensive variables or independent of the quantity of material used to define the system like temperature, pressure, composition), C is number of constituents and N is number of non-compositional elements (e.g., pressure and temperature).

Another important expression in phase diagram analysis is the lever rule in which compositions and relative amounts of phases are determined. This can be seen later on the next chapter up on the construction of Biodiesel-Jojoba oil blend phase diagram.

CHAPTER 4

RESULTS AND DISCUSSION

The current chapter discusses the results and the outcome of the experiments. A total of 18 samples of JO-BD blends were tested. Percent compositions were varied from 0 -100 %. The start and end of the solid phases were identified for all of the samples. Prior to the experimentation both of the thermocouples were calibrated with reference to the standard thermometer. Calibration curves of the thermocouples are shown in the Figure 4.1.

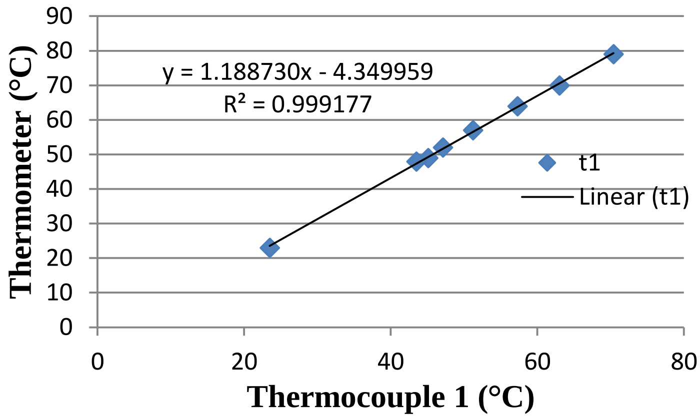

(a)

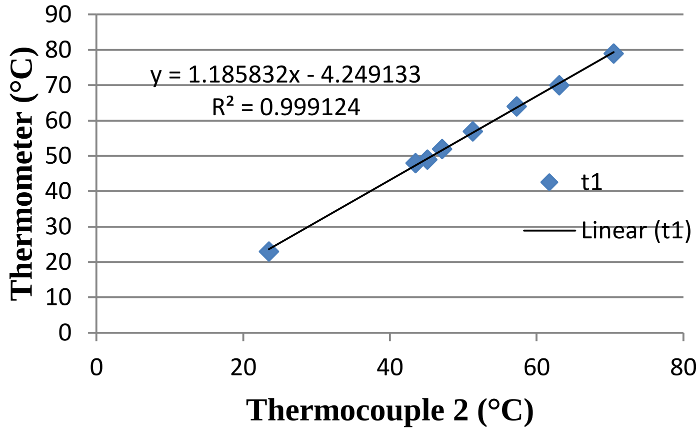

(b)

Figure 4.1: Calibration of **(a)** Thermocouple-1, **(b)** Thermocouple-2 with a standard thermometer

The difference in temperature of the thermocouples (thermocouple-1 ± thermocouple-2) were found to be ± 0.1°C and, the difference in temperature reading of the thermometer versus thermocouples were found to be $\varDelta T = (T - t_1) = 2.9\,°\mathrm{C}$ and $\varDelta T = (T - t_2) = 2.9\,°\mathrm{C}$, where: T, t_1 and t_2 were readings of thermometer, thermocouple-1 and thermocouple-2, respectively.

4.1. Numerical Approach and Determination of Constants

The samples were cooled down from an average temperature of 55°C in an ethyl alcohol cooling bath that was set to -20°C on average. It was suggested to start the cooling process from ≈ 60°C to get enough data for the determination of the term $\frac{UA}{MC_P}$ in the liquid phase (Evcil et al., 2018) and, to cool down as possible as the cooling system permits to get sufficient data for evaluation of same the constant ($\frac{UA}{MC_P}$) separately in the solid phase.

This study is based on the work done by (Evcil et al., 2018). In addition to the cooling curve, the rate of change of temperature with respect to time T'_n and the corresponding instantaneous time $t_{T'_n}$ were calculated using first and second order approaches which are given by the following equations.

$$T^{1st} = \left(\frac{dT}{dt}\right)_n = \frac{T_{n+1} - T_n}{t_{n+1} - t_n}, \quad (t_{T'})_n = \frac{t_n + t_{n+1}}{2} \tag{4.1}$$

$$T^{2nd} = \left(\frac{dT}{dt}\right)_n = \frac{T_{n+1} - T_{n-1}}{t_{n+1} - t_{n-1}}, \quad (t_{T'})_n = \frac{t_{n-1} + t_{n+1}}{2} \tag{4.2}$$

The cooling curve (temperature versus time) and their rate of changes with respect to time from equation (4.1) and (4.2) are plotted for sample B10J90 with its averaged time interval in Figure 4.2 and Figure 4.3, respectively. Different time interval data are plotted for comparison in addition to derivative curves which are also inspected for a better result. It is obvious that second-order numerical differentiation gives more accurate result than the first order in the determination of rate plot $\left(\frac{dT}{dt}\right)$.

Therefore, it can be concluded that for the rest of the samples, second order plots are used in each necessary occasions for interpretation.

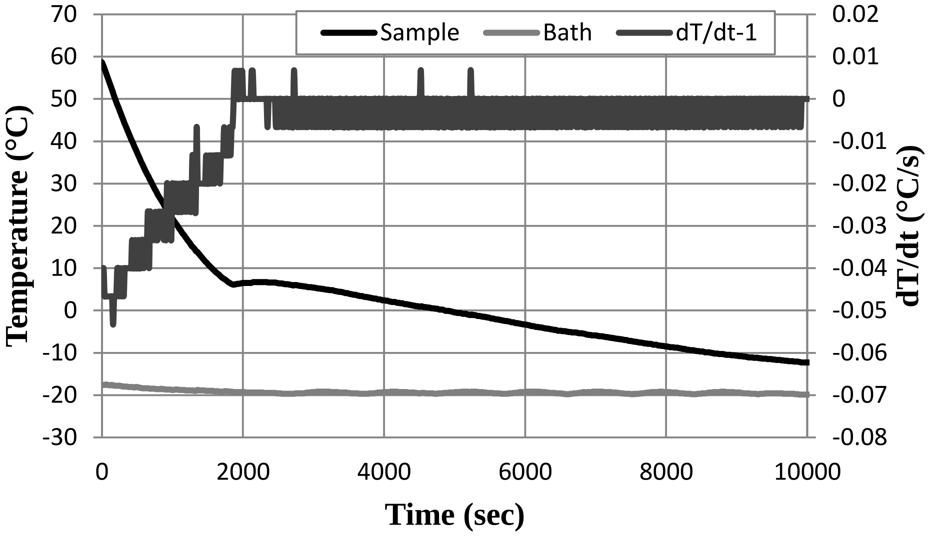

Figure 4.2: B10J90 cooling and first order $\left(\frac{dT}{dt}\right)$ curve for 15 sec. interval

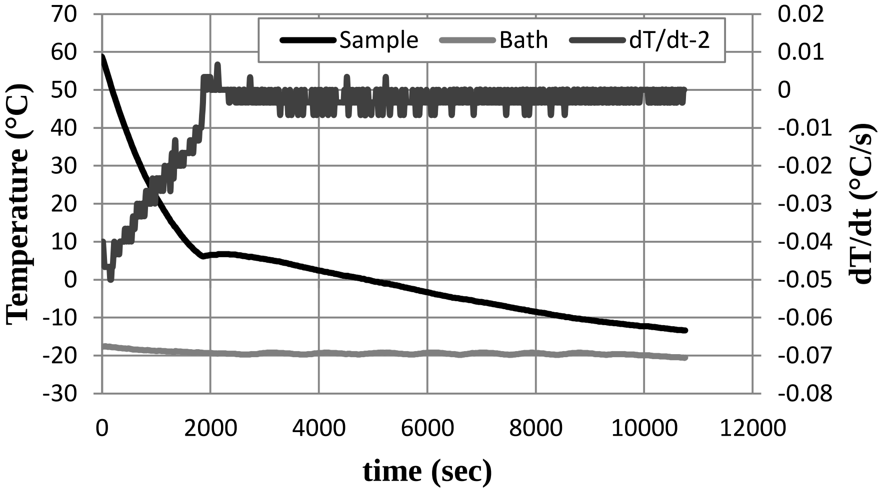

Figure 4.3: B10J90 cooling and second order $\left(\frac{dT}{dt}\right)$ curve for 15 sec. interval

The other point is to identify the plot for the different time intervals for which the plots are clear and easy for manipulations and observations. The cooling curve, as well as second order curve plots, are compared for 15 sec. (Figure 4.3), 30 sec. (Figure 4.4), 45sec. (Figure 4.5), and 60 sec. (Figure 4.6), time interval, respectively.

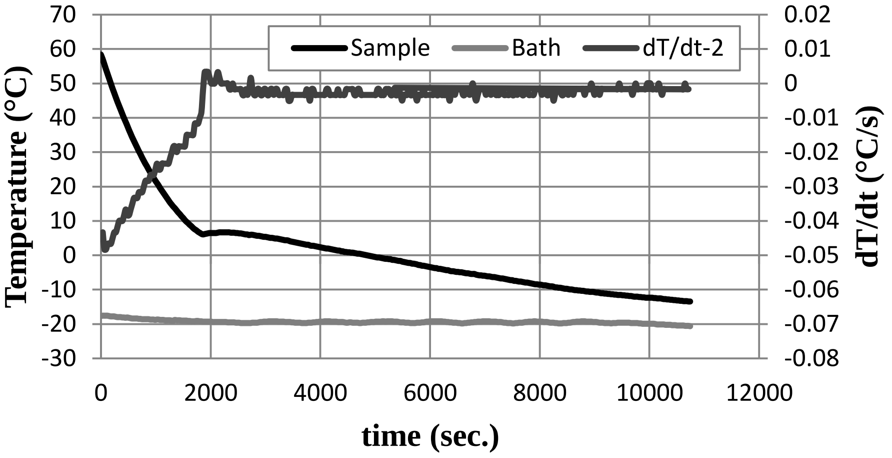

Figure 4.4: B10J90 cooling and second order $\left(\frac{dT}{dt}\right)$ curve for 30 sec. interval

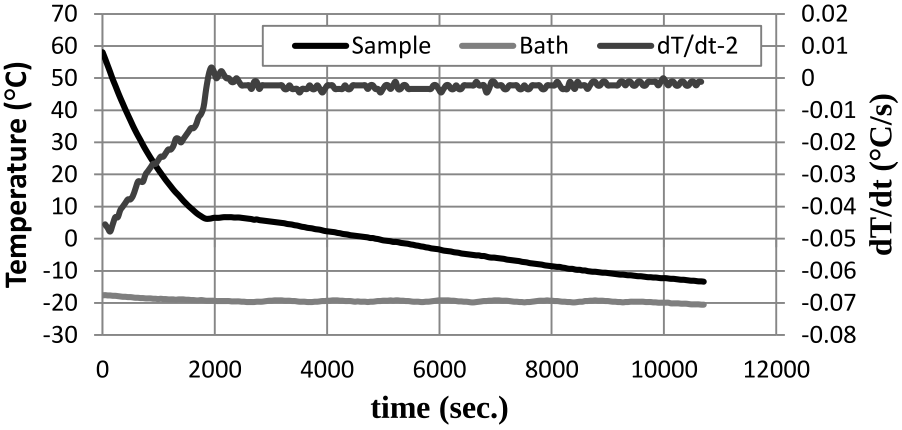

Figure 4.5: B10J90 cooling and second order $\left(\frac{dT}{dt}\right)$ curve for 45 sec. interval

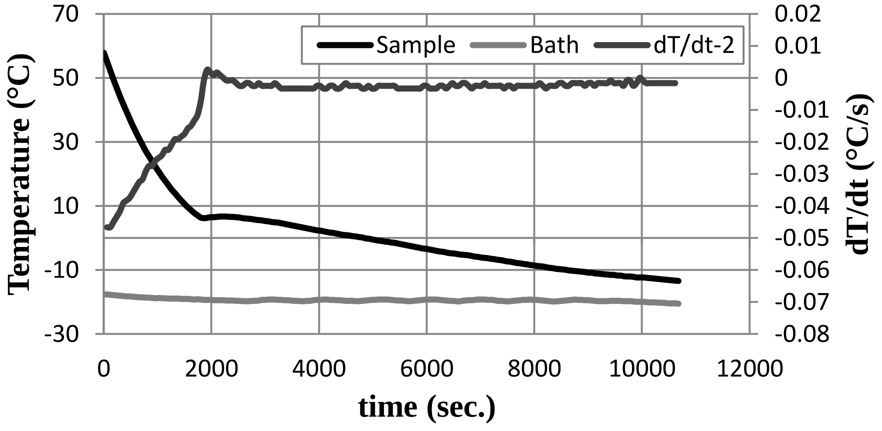

Figure 4.6: B10J90 cooling and second order $\left(\frac{dT}{dt}\right)$ curve for 60 sec. interval

Generally, it is observed that from the given plots, second order and 60 sec. interval numerical data provide the best plots for determinations of unknowns. For this reason, it's recommended to use 60 sec. interval data and 2^{nd} order data for all of the samples.

4.1.1. Determination of $\frac{UA}{mC_P}$

The value for the term $\frac{UA}{mC_P}$ can be determined from, rate the of change of temperature $\left(\frac{dT}{dt}\right)$ versus $(T_s - T_\infty)$ plot for all of the samples for liquid and solid phases independently. The rate of change of temperature that was calculated from the experimental data as well as from equation (3.19) versus the difference in temperature of the sample and the bath $(T_s - T_\infty)$ for liquid, solid and mixed phases are given collectively in Figure 4.7. This can be helpful to identify the possible end point of the liquid phase and start of the solid that are plotted individually for the determination of $\frac{UA}{mC_P}$ for both cases.

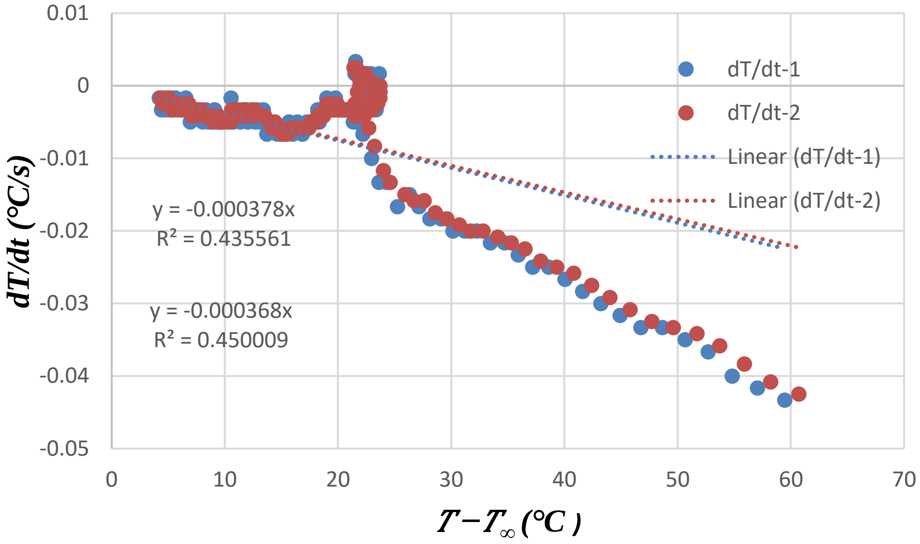

Figure 4.7: Plot of the rate of change of temperature versus the difference in temperature for J100

Second order numerical differentiation is applied in the calculation of $\frac{dT}{dt}$ and $\frac{UA}{mC_P}$. Change in $\frac{UA}{mC_P}$ (coefficient of cooling rate with respect to the temperature difference of sample and bath) value in the liquid, and solid states depends on the composition of fatty acid methyl esters and their crystallization (Evcil et al., 2018). It is observed that the liquid phase seems to end where the temperature difference is around ≈ 25.9°C and the solid phase exists for a difference of ≤ 12.8°C while the transition region i.e. liquid solid mixture, covers between 12.8°C to 25.9°C.

Examining the liquid and solid regions separately gives a cooling rate coefficient with respect to a temperature difference of sample and bath $\left(\frac{UA}{mC_P}\right)$ as shown in Figure 4.8 and Figure 4.9.

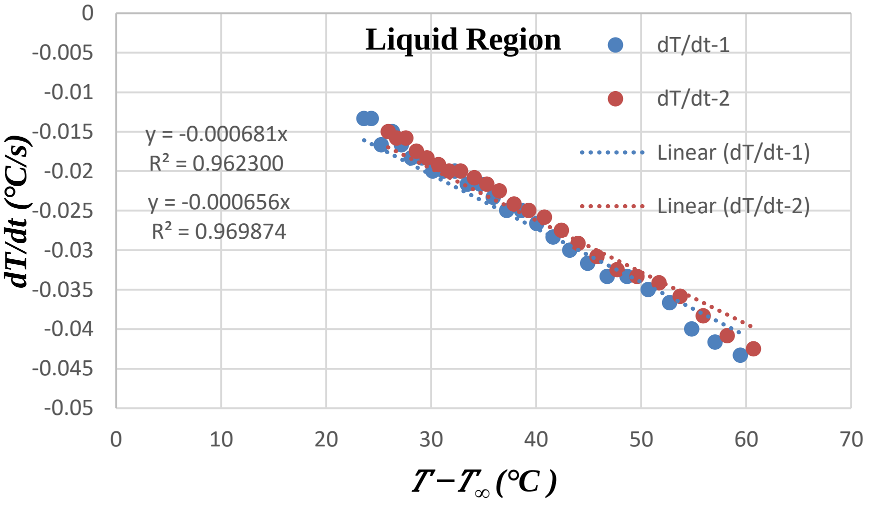

Figure 4.8: Liquid region for J100 just before freezing starts

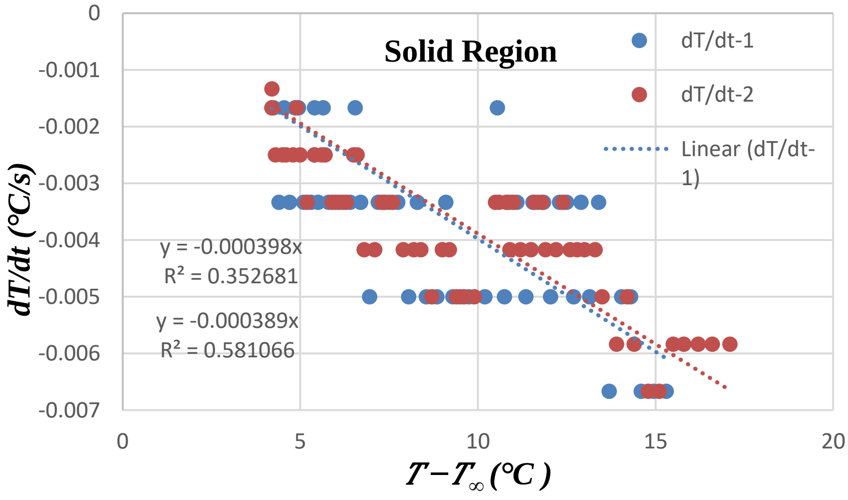

Figure 4.9: Solid region for J100 after the end of the liquid phase and region of freezing

In Figure 4.8 and 4.9 liquid and solid phases are given where numerical differentiation of the first and second order was applied. Accordingly, for the liquid phase, the value can be determined as 6.81×10^{-4} ($R^2 = 0.962300$) using first order differentiation and 6.56×10^{-4} ($R^2 = 0.969874$) using second-order differentiation. Similarly, in the solid phase, the value can be determined as 3.98×10^{-4} ($R^2 = 0.352681$) using first order differentiation and 3.89×10^{-4} ($R^2 = 0.581066$) using second-order differentiation. Smoother plots and second-order differentiation results in higher R^2 values. The lower temperature difference between the sample and the bath that ranges from (4 to 15 °C) resulted in scattered and dispersed data in the solid region which in turn resulted in the rate of change of temperature of the sample from -0.001 to -0.007 $\frac{°C}{s}$. In the liquid phase, the difference in temperature is 24 to 60°C and the rate of change of temperature is -0.013 to -0.0425 $\frac{°C}{s}$.

The liquid and solid phase Newtonian Zero Curve plot is given in Figure 4.10 based on Equation (3.23) and (3.24) along with the rate curve on rate versus temperature difference graph.

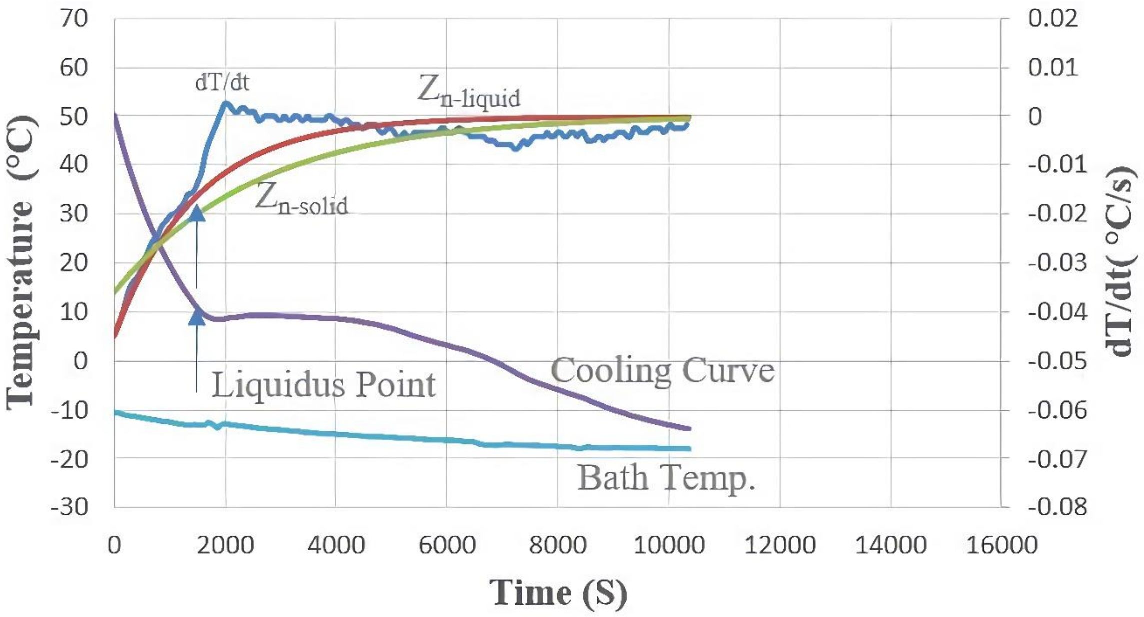

Figure 4.10: Newtonian Zero Curve based on liquid and solid phase given with the cooling curve and rate curve for J100

In Figure 4.10, the time at which the rate curve deviates from the Newtonian Zero Curve based on the liquid $(Z_n\ liquid)$ is the time at which freezing starts and the corresponding temperature is taken as the start of freezing temperature (liquidus temperature in the phase diagram). Similarly, the time at which the rate curve deviates from the Newtonian Zero Curve based on solid is the time at which freezing ends and the corresponding temperature can be taken as the temperature at which the freezing ends (solidus temperature in the phase diagram). From Figure 4.10 it is observed that the liquid phase ends at 1500 sec. which corresponds to 10.8 °C and the solid phase ends at 7260 sec. where the corresponding temperature is – 2.5 °C. This can be verified with reasonable accuracy from Figure 4.7 (Plot of rate of change of temperature versus difference in temperature for J100) that the start of freezing temperature (temperature where liquid phase ends) is (25.9 – 15.5 °C) = 10.4 °C and the solid phase ends at (12.8 – 15.5 °C) = – 2.7 °C.

Similarly, the plot of the rate of change of temperature $\frac{dT}{dt}$ versus the temperature difference between the sample and bath $(T - T_\infty)$ for B100 is given in Figure 4.11.

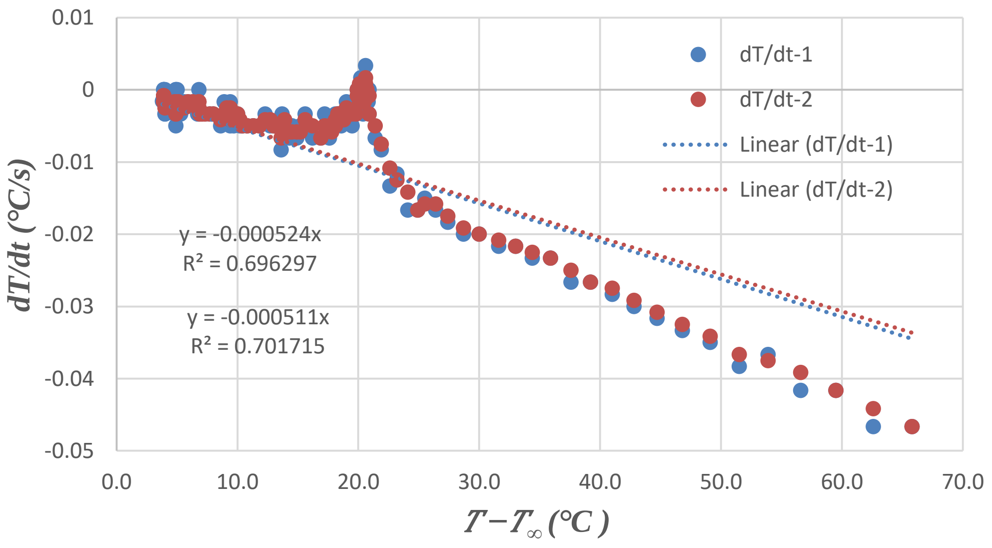

Figure 4.11: Plot of the rate of change of temperature versus the difference in temperature for B100

From Figure 4.11 the liquid phase ends for the difference in sample and bath temperature of 24.1 °C and the freezing temperature would be (24.1 – 16.2) = 7.9 °C. The transition region covers from 24.1 °C to 15.6 °C while the solid phase starts at the difference of 15.6 °C and a temperature of (15.6 – 16.2) = – 0.6 °C. The liquid and solid based, rate vs temperature difference is given in Figure 4.12 and Figure 4.13, respectively to determine the unknown term $\frac{UA}{mC_P}$ (cooling rate coefficient) for both cases.

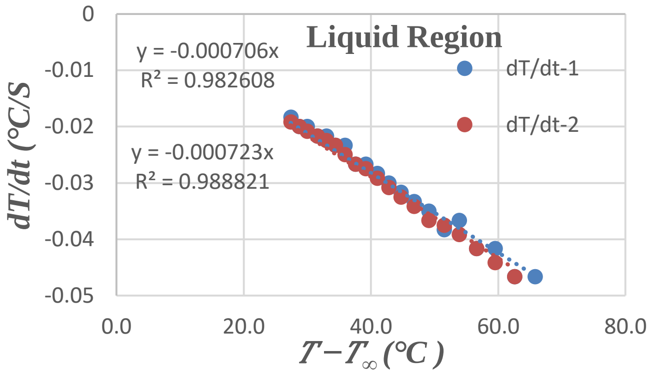

Figure 4.12: Liquid region for B100 just before freezing starts

From Figure 4.12 application of first-order numerical differentiation gives the term $\frac{UA}{mC_P}$ to be , 7.06×10^{-4} (R² = 0.982608) and using second order the value can be 7.23×10^{-4} (R² = 0.988821). The rate of change of temperature in the sample ranges from 0.019 to 0.046 $\frac{°C}{S}$ while the temperature difference ranges from 27.4°C to 65.8°C for first and second order data respectively.

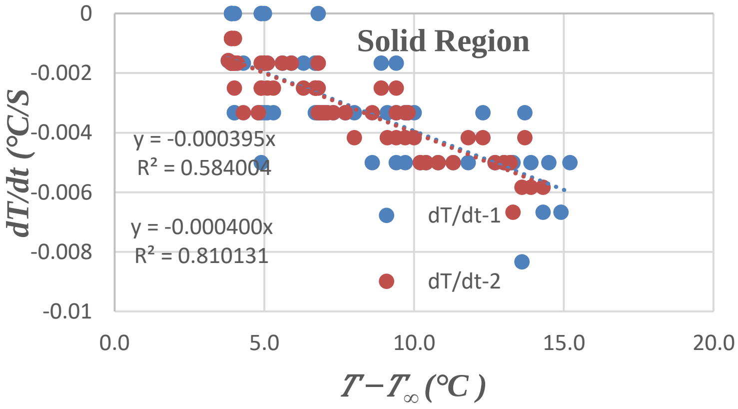

Figure 4.13: Solid region for B100 after the end of the liquid phase and region of freezing

The value of $\frac{UA}{mC_P}$ in the solid region is determined as 3.95×10^{-4} (R^2 = 0.584004) using first order numerical differentiation and 4.00×10^{-4} (R^2 = 0.810131) using second order differentiation (Figure 4.13). The rate of change of the temperature in the sample ranges from 0.00083 to 0.00583 $\frac{°C}{S}$ for the second order data and the difference in temperature runs from 3.9 °C to 14.3 °C. This lower temperature difference resulted in the scatter of the data of the solid region.

Cooling curve, the bath temperature curve, as well as the Newtonian Zero Curve based on liquid and solid phases, are given with the rate curve for B100 in Figure 4.14 below. The start and end of a freezing temperature can be determined.

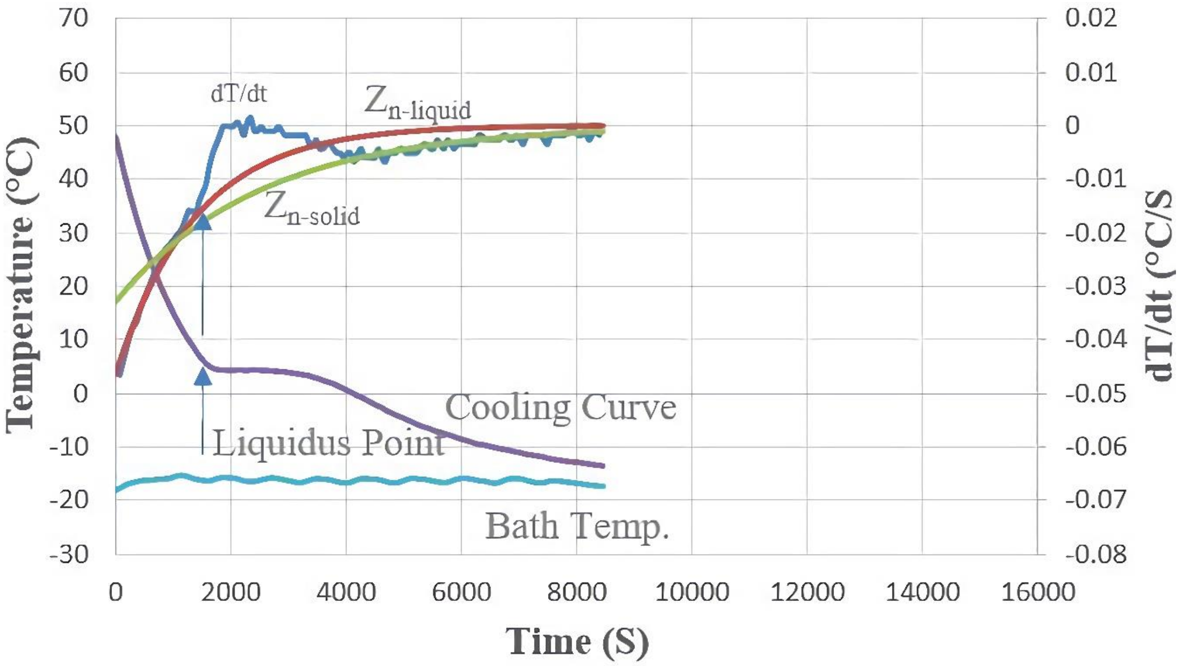

Figure 4.14: Newtonian Zero Curve based on liquid and solid phase given with the cooling curve and rate curve for B100

The time at which second order rate curve deviates from the liquid based Newtonian Zero Curve is the time at which freezing starts and the corresponding temperature is freezing temperature (for the cooling process) or melting temperature (for melting process). It can be seen that from the graph, the freezing time is 1440 sec. that corresponds to 7.2 °C. This is the liquidus temperature in the phase diagram. The time at which freezing ends is 4200 sec. for which – 0.4 °C is the representing temperature.

In a similar way, the values of $\frac{UA}{mC_P}$ for each of the samples were found for both the liquid and solid phases. The graphs are shown in appendix section and the values are in Table 4.1.

Table 4.1: Values for cooling rate coefficient $\frac{UA}{mC_P}$ determined

Samples	$\boldsymbol{\frac{UA}{mC_P}}$ **(Liquid Phase)**		$\boldsymbol{\frac{UA}{mC_P}}$ **(Solid Phase)**	
	$\boldsymbol{1^{st} order}$	$\boldsymbol{2^{nd} order}$	$\boldsymbol{1^{st} order}$	$\boldsymbol{2^{nd} order}$
B100	7.06×10^{-4} $R^2 = 0.982608$	7.23×10^{-4} $R^2 = 0.988821$	3.95×10^{-4} $R^2 = 0.584004$	4.00×10^{-4} $R^2 = 0.810131$
B95J5	7.56×10^{-4} $R^2 = 0.956508$	7.15×10^{-4} $R^2 = 0.963566$	2.60×10^{-4} $R^2 = 0.532923$	2.78×10^{-4} $R^2 = 0.740647$
B90J10	7.66×10^{-4} $R^2 = 0.980900$	7.67×10^{-4} $R^2 = 0.983480$	2.94×10^{-4} $R^2 = 0.259407$	3.04×10^{-4} $R^2 = 0.781048$
B80J20	7.27×10^{-4} $R^2 = 0.955552$	7.27×10^{-4} $R^2 = 0.964896$	2.20×10^{-4} $R^2 = 0.512588$	2.48×10^{-4} $R^2 = 0.608846$
B70J30	6.36×10^{-4} $R^2 = 0.852457$	6.56×10^{-4} $R^2 = 0.975725$	2.19×10^{-4} $R^2 = 0.413541$	2.32×10^{-4} $R^2 = 0.709024$
B62J38	7.25×10^{-4} $R^2 = 0.857224$	7.07×10^{-4} $R^2 = 0.960921$	2.54×10^{-4} $R^2 = 0.357031$	2.56×10^{-4} $R^2 = 0.614228$
B60J40	6.51×10^{-4} $R^2 = 0.963235$	6.53×10^{-4} $R^2 = 0.974331$	2.24×10^{-4} $R^2 = -0.177599$	2.38×10^{-4} $R^2 = 0.636077$
B58J42	6.91×10^{-4} $R^2 = 0.980927$	6.65×10^{-4} $R^2 = 0.987654$	2.46×10^{-4} $R^2 = 0.505427$	2.42×10^{-4} $R^2 = 0.742327$
B56J44	6.95×10^{-4} $R^2 = 0.985442$	6.62×10^{-4} $R^2 = 0.983230$	2.40×10^{-4} $R^2 = 0.386628$	3.39×10^{-4} $R^2 = 0.676322$
B54J46	6.51×10^{-4} $R^2 = 0.963485$	6.31×10^{-4} $R^2 = 0.986008$	2.36×10^{-4} $R^2 = 0.222383$	2.44×10^{-4} $R^2 = 0.727835$
B52J48	6.74×10^{-4} $R^2 = 0.979119$	6.48×10^{-4} $R^2 = 0.984022$	2.33×10^{-4} $R^2 = 0.424087$	2.33×10^{-4} $R^2 = 0.654316$
B50J50	6.64×10^{-4} $R^2 = 0.968268$	6.39×10^{-4} $R^2 = 0.980252$	2.03×10^{-4} $R^2 = 0.327537$	2.01×10^{-4} $R^2 = 0.651138$
B40J60	6.05×10^{-4} $R^2 = 0.917479$	6.18×10^{-4} $R^2 = 0.958129$	1.47×10^{-4} $R^2 = 0.266987$	1.53×10^{-4} $R^2 = 0.610471$
B30J70	6.41×10^{-4} $R^2 = 0.958727$	6.47×10^{-4} $R^2 = 0.974964$	1.77×10^{-4} $R^2 = 0.205093$	1.89×10^{-4} $R^2 = 0.528773$
B20J80	6.24×10^{-4} $R^2 = 0.941336$	6.35×10^{-4} $R^2 = 0.967937$	2.71×10^{-4} $R^2 = 0.391730$	2.04×10^{-4} $R^2 = 0.660685$

B10J90	6.50×10^{-4} $R^2 = 0.977490$	6.26×10^{-4} $R^2 = 0.984407$	1.99×10^{-4} $R^2 = 0.182390$	1.96×10^{-4} $R^2 = 0.514920$
B5J95	6.58×10^{-4} $R^2 = 0.974956$	6.36×10^{-4} $R^2 = 0.979027$	2.24×10^{-4} $R^2 = 0.321234$	2.46×10^{-4} $R^2 = 0.745604$
J100	6.81×10^{-4} $R^2 = 0.962300$	6.56×10^{-4} $R^2 = 0.969874$	3.98×10^{-4} $R^2 = 0.352681$	3.89×10^{-4} $R^2 = 0.581066$

The values were taken to six significant digits for both liquid and solid phase based on the first and second order numerical differentiation.

Similarly, the liquidus (start of freezing temperature) and solidus (end of freezing) temperatures were also determined as shown in Table 4.2.

Table 4.2: Liquidus (start of freezing) and solidus (end of freezing) temperatures determined

%B	**%J**	T_L (°C)	T_S (°C)
100	0	7.2	-0.4
95	5	6.5	1.7
90	10	5.8	-0.6
80	20	5.2	-6.7
70	30	3.7	-4.6
62	38	2.5	-3.2
60	40	1.7	-1.4
58	42	0.5	-0.5
56	44	1.6	-1.8
54	46	2.3	-1.9
52	48	3	-2.2
50	50	3.3	-0.5
40	60	5.1	-1.5
30	70	6	-2.3
20	80	7.4	-3.5
10	90	8.3	-1.7
5	95	9.4	-2..8
0	100	10.8	-2.5

The biodiesel sample used in this experiment was composed of the following free fatty acids as given in Table 4.3. Various properties of the biodiesel sample used were tested as per EN, ASTM and ISO standards and were listed in Table 4.4. From the data given in Table 4.2, the constructed Phase diagram of a pseudo eutectic binary phase system representing the compositions and temperatures is shown in Figure 4.15.

Table 4.3: Fatty acid methyl ester composition of the biodiesel used in the current work (bought from market with specification)

Common Name	Lipid Number	Composition (%)
Lauric acid	C 12.0	0.1
Myristic acid	C 14.0	0.7
Palmitic acid	C 16.0	24.8
Palmitoleic acid	C 16.1	1.0
Hexadecadienoic acid	C 16.2	0.2
Margaric acid	C 17.0	0.1
Stearic acid	C 18.0	5.1
Oleic acid	C 18.1	41.6
Linoleic acid	C 18.2	22.3
Linolenic acid	C 18.3	2.9
Arachidic acid	C 20.0	0.4
Gondoic acid	C 20.1	0.4
Behenic acid	C 22.0	0.1
Unknowns	-	0.3
Total		100

Table 4.4: Tested properties of the sample biodiesel in accordance with the international Standards (bought from market with specification)

Property	**Test method**	**Limits**		**Unit**	**Test result**
		min	**max**		
FAME content	EN 14103	96.5	-	mass %	99.0
Density at 15°C	ISO 12185	860.0	900.0	kg/m^3	879.4
Viscosity at 40°C	EN ISO 3104	3.5	5.0	mm^2/s	4.42
Flash point	ISO 3679	101	-	°C	>140
Sulfur content (S)	EN ISO 20846	-	10.0	mg/kg	6.5
Cetane number	EN 15195	51	-	-	59.5
Sulfated ash	ISO 3987	-	0.02	mass %	<0.005
Water karl fischer	EN ISO 12937	-	300	mg/kg	300
Total contamination	EN 12662:1998	-	24	mg/kg	<6
Copper strip corrosion (3 hours / 50°C)	EN ISO 2160	-	class 1	-	1A
Oxidation stability (110°C)	EN 14112	8.0	-	hours	>11
Acid number	EN 14104	-	0.50	mg KOH/g	0.35
Iodine value	EN 14111	-	120	g I2/100 g	82
Linolenic acid content	EN 14103	-	12.0	mass %	2.9
Content of FAME with ≥4 double bonds	EN15779	-	1.0	mass %	<0.10
Methanol content	EN 14110	-	0.20	mass %	0.03
Mono-glyceride content	EN 14105	-	0.70	mass %	0.33
Di-glyceride content	EN 14105	-	0.20	mass %	0.07
Tri-glyceride content	EN 14105	-	0.20	mass %	0.05
Free glycerol	EN 14105	-	0.02	mass %	<0.010
Total glycerol	EN 14105	-	0.25	mass %	0.106
Group I (Alkali) metals (Na + K)	EN 14538	-	5.0	mg/kg	< 2.0
Earth alkali metals (Group II) (Ca + Mg)	EN 14538	-	5.0	mg/kg	< 2.0
Phosphorus content	EN 14107	-	4.0	mg/kg	< 4.0
Cold Filter Plugging Point	EN116	-	-	°C	+2
Melting Point of Organic Chemicals	ISO 6321	-	-	°C	+7
Kinematic Viscosity at 20°C	ASTM D 445	-	-	mm^2/s	7.2
Temperature by viscosity of 50 mPass	Calculated	-	-	°C	+8

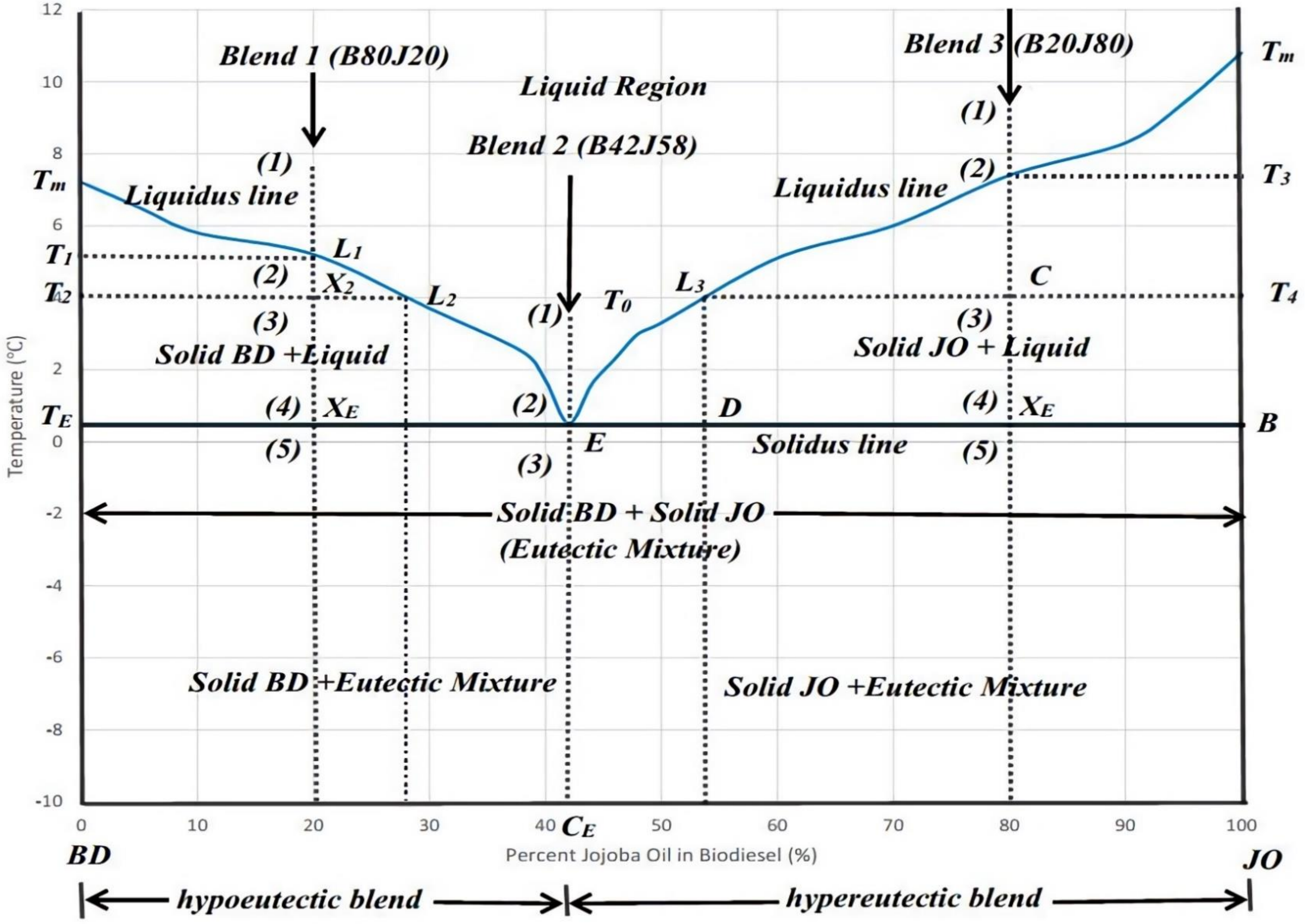

Figure 4.15: The pseudo eutectic binary BD-JO phase diagram constructed from the data of the samples

4.2. The Lever's Rule and Gibb's Phase Rule

4.2.1. Blend 1

From Figure 4.15, 80BD-20JO a hypoeutectic blend composed of 80% biodiesel and 20% jojoba oil, which is a homogenous liquid solution as shown at (1) until the liquidus temperature (T_1) is reached. At this point the liquid solution (L_1) is saturated in BD, and as the temperature is slightly decreasing, the excess BD must solidify ($L_1 \longrightarrow BD(Solid)$) which is just below T_1 at point (2) and leaves the remaining liquid solution richer in JO. It can be seen that at temperature (T_2), solid is pure BD and the liquid solution composition L_2 is 72BD-28JO. The amount of BD and L_2 can be calculated using the Lever's rule as:

$$\% \, BD = \frac{X_2L_2}{T_2L_2} \times 100 = \frac{8}{28} \times 100 = 28.58\%$$

$$\% \, L_2 = \frac{X_2T_2}{T_2L_2} \times 100 = \frac{20}{28} \times 100 = 71.42\%$$

As solidification progresses the amount of pure BD gradually increases by precipitating from the liquid, at (3) and the JO content in the liquid composition gets richer and richer as the liquidus line gradually decreases to the right towards the eutectic point. At the meantime the amount of liquid is getting low and low and gets minimum at the eutectic point E. When the blend reaches the composition (X_E), the eutectic line, the liquid is at point E. Hence the eutectic reaction can be written as below in which the liquid dissociates in to two solids (BD and JO) simultaneously at T_E.

$$Liquid \ \rightarrow BD + JO \tag{4.3}$$

The properties just a fraction of degrees above T_E for the blend 1 is given (from Lever rule) as given in Table 4.5 below (at point (4) on the diagram).

Table 4.5: Composition and relative amounts for blend 1 just one degree above T_E in the hypoeutectic region

Phase	Liquid (BD + JO)	Solid BD
Composition	58BD - 42JO	100BD
Relative Amounts	$\frac{X_ET_E}{T_EE}\times 100$ $= \frac{20}{42} \times 100 = 47.62\%$	$\frac{X_EE}{T_EE}\times 100$ $= \frac{22}{42} \times 100 = 52.38\%$

The remaining 47.62% liquid mixture, once reached the eutectic point, it solidifies to an identical mixture of BD-JO as in that of the eutectic composition. When solidification came to an end the blend contains 52.38% of pure primary BD or pro-eutectic BD which was solidified between T_1 and T_E (before eutectic reaction) and 47.62% of eutectic (BD + JO) mixture as shown at (5) on the diagram.

Every sample to the left of the eutectic point E, upon solidification, will contain primary (pro-eutectic) BD and the solid phases of the eutectic mixture.

4.2.2. Blend 2

Blend 2 is a eutectic composition of 58BD - 42JO. It's cooled down from T_0 and remain liquid solution until it reaches the eutectic point E on the horizontal constant temperature line. Since point E is the intersection of two liquidus and solidus line, the eutectic liquid sample starts to solidify and the temperature remains constant until every drop of the sample turned to solid according to $Eutectic\ Liquid\ \rightarrow BD + JO$. The resulting solid is, a solid mixture of two phases (assuming that the solid mixtures are completely insoluble to each other). These phases are the one that are found at either end of the horizontal isotherm line i.e. pure BD (vertical temperature axis at left end) and pure JO at the other end side.

In the diagram, at point (1) the sample is in the liquid state and (2) where the sample starts to solidify. At point (2) small amount of BD sample begins to solidify that leaves the remaining liquid richer in JO. As a result, the liquid composition will slightly shift to the right and to restore the liquid composition equilibrium, JO starts to solidify too. If, too much JO is solidified the liquid composition will shift to the right demanding BD to solidify to maintain equilibrium on the same principle. Thus, at a constant temperature, the resulting solid is pure BD and pure JO making eutectic mixture shown at point (3) on the phase diagram, i.e. Figure 4.15.

The change in phase of this liquid mixture composition of E into two solids at constant temperature is known as eutectic reaction. It can be written in general form as:

$$Liquid\ mixure\ \rightleftarrows Solid\ BD + Solid\ JO$$

4.2.3. Blend 3

Blend 3, a hypereutectic blend is a 20BD-80JO composition which undergoes the same cooling process as blend 1, the cooling process starts from (1), but when the liquidus line at a temperature T_3 is reached, crystals of pure JO starts to be formed from the liquid solution ($Liquid\ mixture\ \longrightarrow JO\ (Solid)$) instead of BD as shown at point (2) in the diagram. More and more of JO crystals will be formed as the temperature gradually decreases, leaving the remaining liquid solution richer in BD. The relative amount of liquid and composition gradually decreases as the temperature drops to the left along the liquidus curve until point E is reached. The remaining liquid solidifies to the eutectic mixture (BD + JO) as shown at (5) according to $Liquid\ mixture\ \longrightarrow JO\ (Solid) + BD\ (Solid)$.

At T_4 solid is pure JO and the liquid solution composition L_3 is 46BD-54JO. The amount of BD and L_3, at point (3) can be calculated using the Lever's rule as:

$$\%\ JO = \frac{CL_3}{T_4L_3} \times 100 = \frac{26}{46} \times 100 = 56.52\%\ \text{(volume percent)}$$

$$\%\ L_3 = \frac{CT_4}{T_4L_3} \times 100 = \frac{20}{46} \times 100 = 43.48\%\ \text{(volume percent)}$$

As solidification progresses the amount of pure JO gradually increases by precipitating from the liquid, and the BD content in the liquid composition gets richer and richer as the liquidus line gradually decreases to the left towards the eutectic point. At meantime the amount of liquid is getting low and low and gets minimum at the eutectic point E. When the blend reaches the composition (X_E), on the eutectic line, the liquid is at point E.

Table 4.6: Composition and relative amounts for blend 3 just one degree above T_E in the hypereutectic region

Phase	**Liquid (BD + JO)**	**Solid JO**
Composition	58BD - 42JO	100JO
Relative Amounts	$\frac{\boldsymbol{X_E B}}{\boldsymbol{BE}}\times 100$	$\frac{\boldsymbol{X_E E}}{\boldsymbol{BE}}\times 100$
	$= \frac{20}{58} \times 100 = 34.49\%$	$= \frac{38}{58} \times 100 = 65.51\%$

Once the remaining liquid reaches eutectic temperature and hence composition, it completely solidifies to make 34.49% of the solid eutectic mixture (BD + JO) and 65.51%

of the amount will be a pro-eutectic (pure) JO which was solidified between T_3 and T_E (before eutectic reaction).

Every sample to the right of the eutectic point E upon solidification will contain primary (pro-eutectic) JO and the eutectic mixture of BD + JO solid phases.

In a multi-component binary or ternary equilibrium system, a description of relation between number of phases (P), number of components (C), number of non-compositional variables (temperature and pressure most of the time) (N) and degrees of freedom (F) can be expressed by the *Gibb's phase rule* as indicated by Equation (3.25). Rewriting Equation (3.25) and knowing that N = 2 (non-compositional variables), the degrees of freedom (F) can be expressed as:

$$F = C - P + 2 \tag{4.3}$$

In the BD-JO, there are two components: BD and JO, thus C = 2, at fixed atmospheric pressure equation (4.3) reduces to the form $F = C - P + 1$ and in the liquid region P = 1, therefore, $F = 2 - 1 + 1 = 2$. The pressure is constant throughout the process, letting temperature and composition change freely in the liquid region.

At the liquidus curve, $C = P = 2$ thus, $F = C - P + 1 = 2 - 2 + 1 = 1$. Therefore, if the pressure is constant, either composition or temperature can change freely, but not both. At point E (eutectic point), three phases co-exist i.e. crystals (solid) of BD, crystals of JO, and liquid mixture ($P = 3$), number of constituents ($C = 2$), thus $F = 0$. At this point, the pressure is fixed and neither the temperature nor the composition change freely. Therefore, the eutectic point is the only invariant point where two solids (solid JO and solid BD) and liquid phases can co-exist at equilibrium.

CHAPTER 5
CONCLUSION AND RECOMMENDATION

5.1. Conclusion

Biodiesel is a processed fuel derivative of biological sources, such as vegetable oils, waste cooking oils, animal fats. Biodiesel is eco-friendly, easily available, cost-effective. These fuels can be blended with conventional petroleum-based diesel fuels without modifying the engine operating system. A biodiesel blend of less than 20% can be used as an equivalent diesel fuel substitute. Among the production method, supercritical alcohol transesterification is known for the maximum (up to 95%) yield. The high viscosity characteristics of vegetable oils remain the main challenge of using them as a direct fuel.

In this investigation, the eutectic behavior of BD-JO blend samples were studied. A total of 18 samples were tested based on a volume percentage. The jojoba oil required for the experiment was extracted from its local seed at the laboratory of Mechanical Engineering of NEU. Since thermal analysis is one of the widely used ways of determining phase boundaries, the Newtonian Thermal Analysis (NTA) of the cooling curve was the method of the study.

The samples were cooled down from an average temperature of 55°C in an ethyl alcohol cooling bath that was set to -20°C. The value for $\frac{UA}{MC_P}$ (Ratio of a temperature difference to heat transfer rate) was determined for both liquid and solid phases. The rate of change of temperature with respect to time and the corresponding instantaneous time were calculated using first and second order approach. It is observed that the second order approach and 60 sec. interval numerical data provides the best and optimized plots for determinations of unknowns and constants. The heat transmission modes from the sample to surrounding was represented by a particular and a unique formulation and the bath temperature throughout the process was assumed to be constant. The Newtonian Zero Curve (Z_N) based on liquid and solid phases along with the rate and cooling curve is plotted and used to locate the liquidus and solidus temperature. The resulting binary pseudo eutectic phase diagram was constructed based on the liquidus temperature collected from the samples and was analyzed.

5.2. Recommendation and Future Work

Fourier thermal analysis has been claimed to be more accurate than the Newtonian thermal analysis in prediction of latent heat and constants, this would improve the quality of the data's, resulting in the accuracy of the phase diagram. Therefore, it's recommended to repeat the same procedure using Fourier thermal analysis and compare the results. It is also recommended to cool the samples cold enough more than the current value which is about (-14 to -18 °C), so that the value of $\frac{UA}{mC_P}$ in the solid region of the samples can be improved.

The fact that biodiesel is a combination of more than 10 fatty acid methyl esters, makes the determination of solidus temperature and the actual eutectic temperature difficult. The eutectic point in this study was assumed where the two liquidus curves intercept each other and it is also the minimum temperature of all of the samples which is 0.5°C, at the composition of 58BD-42JO.

In order to rely on the accuracy of the constructed phase diagram, it's necessary to verify the phase boundaries (solidus and liquidus temperatures) of the samples using alternative techniques other than CA-CCA such as DSC (Differential scanning calorimetry), microscopic examinations, chemical analysis, x-ray diffraction, physical properties, metallographic methods, and thermodynamic modeling.

REFERENCES

A, S., & R., P. (2000). Triglycerides-based diesel fuels. *Renewable & Sustainable Energy Reviews*, *4*, 111–133.

Allawzi, M. A., & Tamimi, A. (2000). Extraction of Jojoba oil by pressing and leaching Extraction of jojoba oil by pressing and leaching, *8947*(November 2017). https://doi.org/10.1016/S1385-8947(99)00119-9

Antolın, G., Tinaut, F., & Briceno, Y. (2002). Optimisation of biodiesel production by sunflower oil transesterification. *Bioresource …*, *83*(2), 111–114. https://doi.org/10.1016/S0960-8524(01)00200-0

Ash, G., & Cother, E. J. (2005). Aspects of Jojoba Agronomy and Management, *2113*(December). https://doi.org/10.1016/S0065-2113(04)85007-7

ASM. (1992). *ASM Handbook Volume 3 - Alloy Phase Diagrams*. *ASM Handbook*. https://doi.org/10.1007/BF02869318

Atabani, A. E., Silitonga, A. S., Badruddin, I. A., Mahlia, T. M. I., Masjuki, H. H., & Mekhilef, S. (2012). A comprehensive review on biodiesel as an alternative energy resource and its characteristics. *Renewable and Sustainable Energy Reviews*, *16*(4), 2070–2093. https://doi.org/10.1016/j.rser.2012.01.003

Atabani, A. E., Silitonga, A. S., Ong, H. C., Mahlia, T. M. I., Masjuki, H. H., Badruddin, I. A., & Fayaz, H. (2013). Non-edible vegetable oils: A critical evaluation of oil extraction, fatty acid compositions, biodiesel production, characteristics, engine performance and emissions production. *Renewable and Sustainable Energy Reviews*, *18*, 211–245. https://doi.org/10.1016/j.rser.2012.10.013

Atadashi, I. M., Aroua, M. K., & Aziz, A. A. (2010). High quality biodiesel and its diesel engine application: A review. *Renewable and Sustainable Energy Reviews*, *14*(7), 1999–2008. https://doi.org/10.1016/j.rser.2010.03.020

Azam, M. M., Waris, A., & Nahar, N. M. (2005). Prospects and potential of fatty acid methyl esters of some non-traditional seed oils for use as biodiesel in India. *Biomass and Bioenergy*, *29*(4), 293–302. https://doi.org/10.1016/j.biombioe.2005.05.001

Babcock, R. E., Clausen, P. I. E. C., Popp, M. P., & Schulte, B. I. W. (2014). Yield characteristics of biodiesel produced from chiken Fat-Tall Oil Blended Feedstocks. *ResearchGate*, (August 2016).

Balat, M., & Balat, H. (2008). A critical review of bio-diesel as a vehicular fuel. *Energy Conversion and Management*, *49*(10), 2727–2741. https://doi.org/10.1016/j.enconman.2008.03.016

Balat, M., & Balat, H. (2010). Progress in biodiesel processing. *Applied Energy*, *87*(6), 1815–1835. https://doi.org/10.1016/j.apenergy.2010.01.012

Bilin, M., Alshanableh, F., Evcil, A., & Savas, M. A. (2018). A Comparative Examination of the Quality of Jojoba Seed Oil Harvested on the Mesaoria Plain of Cyprus Island. In *ISMSIT 2018 - 2nd International Symposium on Multidisciplinary Studies and Innovative Technologies, Proceedings* (pp. 1–5). Ankara, Turkey. https://doi.org/10.1109/ISMSIT.2018.8567052

Cadenas, A., & Cabezudo, S. (1998). Biofuels as Sustainable Technologies: Perspectives for Less Developed Countries. *Technological Forecasting and Social Change*, *58*(1–2), 83–103. https://doi.org/10.1016/s0040-1625(97)00083-8

Christopher Strong, C. E. and D. S. (2004). Evaluation of Biodiesel Fuel : Literature Review by Western Transportation Institute College of Engineering Montana State University – Bozeman Prepared for the Montana Department of Transportation Research Section 2701 Prospect Avenue Helena , MT 59620-10, (January).

Dehnavi, M. (2015). Cooling curve analysis in binary Al-Cu alloys: Part II- Effect of Cooling Rate and Grain Refinement on The Thermal and Thermodynamic Characteristics.

Demirbas, A. (2005a). “ Biodiesel Production from Vegetable Oils .” *Journal of Scientific & Industrial Research*, *64*(November), 858–865.

Demirbas, A. (2005b). Biodiesel production from vegetable oils via catalytic and non-catalytic supercritical methanol transesterification methods. *Progress in Energy and Combustion Science*, *31*(5–6), 466–487. https://doi.org/10.1016/j.pecs.2005.09.001

Demirbas, A. (2006). Biodiesel production via non-catalytic SCF method and biodiesel fuel characteristics. *Energy Conversion and Management*, *47*(15–16), 2271–2282. https://doi.org/10.1016/j.enconman.2005.11.019

Demirbas, A. (2008). *Biodiesel a Realistic Fuel Alternative for Diesel Engines*.

Demirbaş, A., & Arin, G. (2002). An overview of biomass pyrolysis. *Energy Sources*, *24*(5), 471–482. https://doi.org/10.1080/00908310252889979

Dickerson, R. E. (1969). *MOLECULAR THERMODYNAMICS*. W. A. Benjamin, Inc.

Erbaş, K. C. (2014). On the Newtonian Thermal Analysis of Casting : a Critical Aproach.

Beykent University Journal of Science and Engineering, *7*(2), 47–60.

Evcil, A., Al-Shanableh, F., & Savas, M. A. (2018). Variation of solid fraction with cold flow properties of biodiesel produced from waste frying oil. *Fuel*, *215*(December 2017), 522–527. https://doi.org/10.1016/j.fuel.2017.11.055

Freedman, B., Pryde, E. H., & L., M. T. (1984). Variables affecting the yield of fatty esters from Transesterification vegetable oils. *J. Am. Oil Chem. Soc.*, *10*(61), 1638–1643.

Fukuda, H., Kond, A., & Noda, H. (2009). Biodiesel Fuel Production by Transesterification. *Biotechnology Advances*, *92*(5). https://doi.org/10.1016/j.biotechadv.2008.10.008

Giakoumis, E. G. (2013). A statistical investigation of biodiesel physical and chemical properties, and their correlation with the degree of unsaturation. *Renewable Energy*, *50*, 858–878. https://doi.org/10.1016/j.renene.2012.07.040

Gu, J., Gao, Y., Xu, X., Wu, J., Yu, L., Xin, Z., & Sun, S. (2018). Biodiesel production from palm oil and mixed dimethyl/diethyl carbonate with controllable cold flow properties. *Fuel*, *216*(September 2017), 781–786. https://doi.org/10.1016/j.fuel.2017.09.081

Gumba, R. E., Saallah, S., Misson, M., Ongkudon, C. M., & Anton, A. (2016). Green biodiesel production: a review on feedstock, catalyst, monolithic reactor, and supercritical fluid technology. *Biofuel Research Journal*, *3*(3), 431–447. https://doi.org/10.18331/BRJ2016.3.3.3

Han, H., Cao, W., & Zhang, J. (2005). Preparation of biodiesel from soybean oil using supercritical methanol and CO2 as co-solvent. *Process Biochemistry*, *40*(9), 3148–3151. https://doi.org/10.1016/j.procbio.2005.03.014

Harwood, H. J. (1984). Oleochemicals as a fuel: Mechanical and economic feasibility. *Journal of the American Oil Chemists' Society*, *61*(2), 315–324. https://doi.org/10.1007/BF02678788

Hashemzadeh Gargari, M., & Sadrameli, S. M. (2018). Investigating continuous biodiesel production from linseed oil in the presence of a Co-solvent and a heterogeneous based catalyst in a packed bed reactor. *Energy*, *148*, 888–895. https://doi.org/10.1016/j.energy.2018.01.105

Hoekman, S. K., Broch, A., Robbins, C., Ceniceros, E., & Natarajan, M. (2012). Review of biodiesel composition, properties, and specifications. *Renewable and Sustainable Energy Reviews*, *16*(1), 143–169. https://doi.org/10.1016/j.rser.2011.07.143

Incropera, F. P. D., Dewitt, D. P., Bergman., T. L., & Lavine, A. S. (2000). *Fundamentals* *of Heat and Mass Transfer*. *JOHN WILEY & SONS*.

Innocent, D. S., ’donnell, O., Sylvester, P., Yahaya, M. F., & Isiomanwadike, L. N. O. (2013). Comparative Analysis of Biodiesel and Petroleum Diesel. *International Journal of Education and Research*, *1*(8), 1–8.

Iso, M., Chen, B., Eguchi, M., Kudo, T., & Shrestha, S. (2001). Production of biodiesel fuel from triglycerides and alcohol using immobilized lipase. *Journal of Molecular Catalysis - B Enzymatic*, *16*(1), 53–58. https://doi.org/10.1016/S1381-1177(01)00045-5

Janaun, J., & Ellis, N. (2010). Perspectives on biodiesel as a sustainable fuel. *Renewable and Sustainable Energy Reviews*, *14*(4), 1312–1320. https://doi.org/10.1016/j.rser.2009.12.011

Jose, S., Coustille, J. L., Perrin, J. L., Prevot, A., Timms, R. E., Freedman, B., & Regional, N. (1986). Transesterification Kinetics of Soybean Oil1, *63*(10).

Kayode, B., & Hart, A. (2017). An overview of transesterification methods for producing biodiesel from waste vegetable oils. *Biofuels*, *7269*, 1–19. https://doi.org/10.1080/17597269.2017.1306683

Knothe, G., & Gerpen, J. Van. (2005). *The Biodiesel Handbook*. https://doi.org/10.1201/9781439822357

Knothe, G., & Razon, L. F. (2017). Biodiesel fuels. *Progress in Energy and Combustion Science*, *58*, 36–59. https://doi.org/10.1016/j.pecs.2016.08.001

Lin, L., Cunshan, Z., Vittayapadung, S., Xiangqian, S., & Mingdong, D. (2011). Opportunities and challenges for biodiesel fuel. *Applied Energy*, *88*(4), 1020–1031. https://doi.org/10.1016/j.apenergy.2010.09.029

M. U. Kaisan, F. O. Anafi, S. U. D. M. K. and J. N. (2017). Fuel Properties of Biodiesel From Neem , Cotton and Jatropha Binary and Multi-. *Researchgate*, (May).

Ma, F., & Hanna, M. A. (1999). Biodiesel production : a review. *Bioresour Technol*, *70*, 1–15. https://doi.org/10.1016/S0960-8524(99)00025-5

Mahmudul, H. M., Hagos, F. Y., Mamat, R., Adam, A. A., Ishak, W. F. W., & Alenezi, R. (2017). Production, characterization and performance of biodiesel as an alternative fuel in diesel engines – A review. *Renewable and Sustainable Energy Reviews*, *72*(January), 497–509. https://doi.org/10.1016/j.rser.2017.01.001

Mekhilef, S., Silitonga, A. S., Mahlia, T. M. I., Badruddin, I. A., Masjuki, H. H., & Atabani,

A. E. (2011). A review on prospect of Jatropha curcas for biodiesel in Indonesia. *Renewable and Sustainable Energy Reviews, 15*(8), 3733–3756. https://doi.org/10.1016/j.rser.2011.07.011

Mishra, V. K., & Goswami, R. (2018). A review of production, properties and advantages of biodiesel. *Biofuels*, *9*(2), 273–289. https://doi.org/10.1080/17597269.2017.1336350

Murugesan, A., Umarani, C., Chinnusamy, T. R., Krishnan, M., Subramanian, R., & Neduzchezhain, N. (2009). Production and analysis of bio-diesel from non-edible oils-A review. *Renewable and Sustainable Energy Reviews, 13*(4), 825–834. https://doi.org/10.1016/j.rser.2008.02.003

Naghdali, S., Jafari, H., & Malekan, M. (2018). Cooling curve thermal analysis and microstructure characterization of Mg-5Zn-1Y-xCa (0–1 wt%) alloys. *Thermochimica Acta*, *667*(July), 50–58. https://doi.org/10.1016/j.tca.2018.07.011

Nair, J. N., & Deepthi, J. (2013). Study of Biodiesel Blends and Emission Characteristics of biodiesel. *International Journal of Innovative Research in Science, Engineering and Technology (IJIRSET)*, *2*(8), 3710–3715.

Nelson, L. A., Foglia, T. A., & Marmer, W. N. (1996). Lipase-catalyzed production of biodiesel. *JAOCS, Journal of the American Oil Chemists' Society*, *73*(9), 1191–1195. https://doi.org/10.1007/BF02523383

Ngamprasertsith, S., & Sawangkeaw, R. (2011). Transesterification in Supercritical Conditions. *Biodiesel - Feedstocks and Processing Technologies*. https://doi.org/10.5772/26239

Nie, K., Xie, F., Wang, F., & Tan, T. (2006). Lipase catalyzed methanolysis to produce biodiesel: Optimization of the biodiesel production. *Journal of Molecular Catalysis B: Enzymatic*, *43*(1–4), 142–147. https://doi.org/10.1016/j.molcatb.2006.07.016

Prince, A. (1966). *Alloy phase equilibria*. New York: Elsevier publishing company.

Reijnders, L. (2006). Conditions for the sustainability of biomass based fuel use. *Energy Policy*, *34*(7), 863–876. https://doi.org/10.1016/j.enpol.2004.09.001

Shahid, E. M., & Jamal, Y. (2011). Production of biodiesel: A technical review. *Renewable and Sustainable Energy Reviews, 15*(9), 4732–4745. https://doi.org/10.1016/j.rser.2011.07.079

Sheehan, T, D., J, B., & PG., R. (1998). A look back at the U. S. Department of Energy's aquatic species program: biodiesel from algae. *National Renewable Energy*

Laboratory, *328*, 291 p. https://doi.org/10.2172/15003040

Shimada, Y. (2002). Enzymatic alcoholysis for biodiesel fuel production and Enzymatic alcoholysis for biodiesel fuel production and. *Journal of Molecular Catalysis B: Enzymatic*, *17*(3–5), 133–142.

Soltani, S., Rashid, U., Yunus, R., & Taufiq-Yap, Y. H. (2015). Synthesis of Biodiesel through Catalytic Transesterification of Various Feedstocks using Fast Solvothermal Technology: A Critical Review. *Catalysis Reviews - Science and Engineering*, *57*(4), 407–435. https://doi.org/10.1080/01614940.2015.1066640

Vasudevan, P., Sharma, S., & Kumar, A. (2005). Liquid fuel from biomass: An overview. *Journal of Scientific and Industrial Research*, *64*(11), 822–831. https://doi.org/10.1016/S1381-1169(97)00038-1

William, D. C., & Rethwisch, D. G. (2009). *Materials Science and Engineering: An Introduction, 8th Edition*.

Zhang, Y., Dubé, M. A., McLean, D. D., & Kates, M. (2003). Biodiesel production from waste cooking oil: 1. Process design and technological assessment. *Bioresource Technology*, *89*(1), 1–16. https://doi.org/10.1016/S0960-8524(03)00040-3

APPENDIX

Newtonian Zero Curve based on liquid and solid phases given with the cooling curve and rate curve

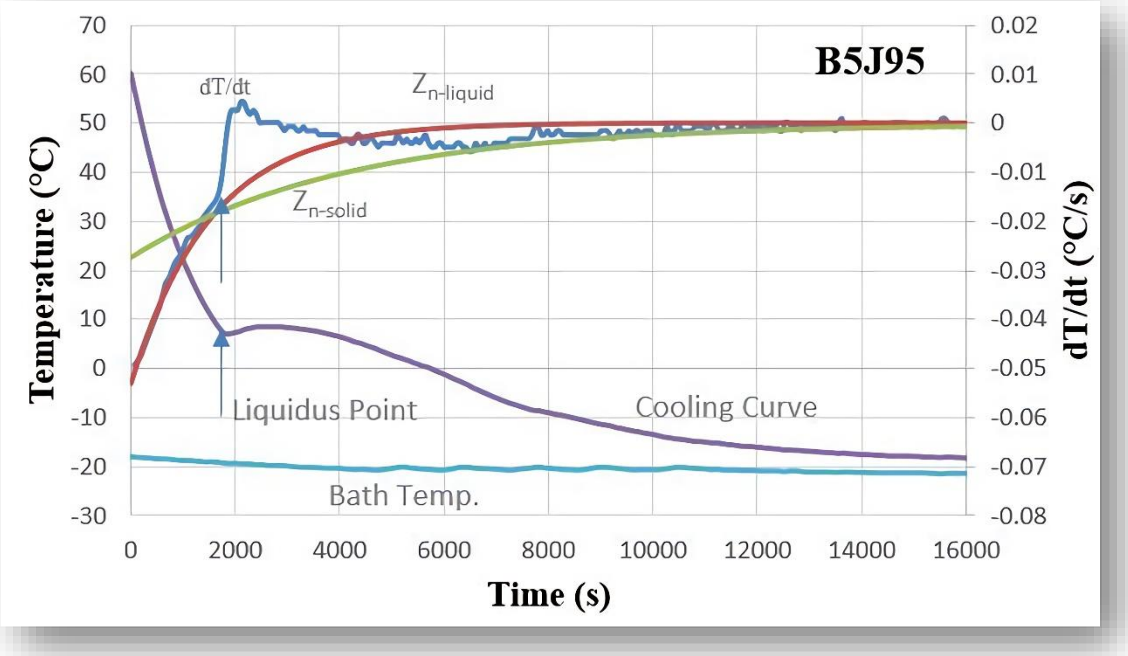

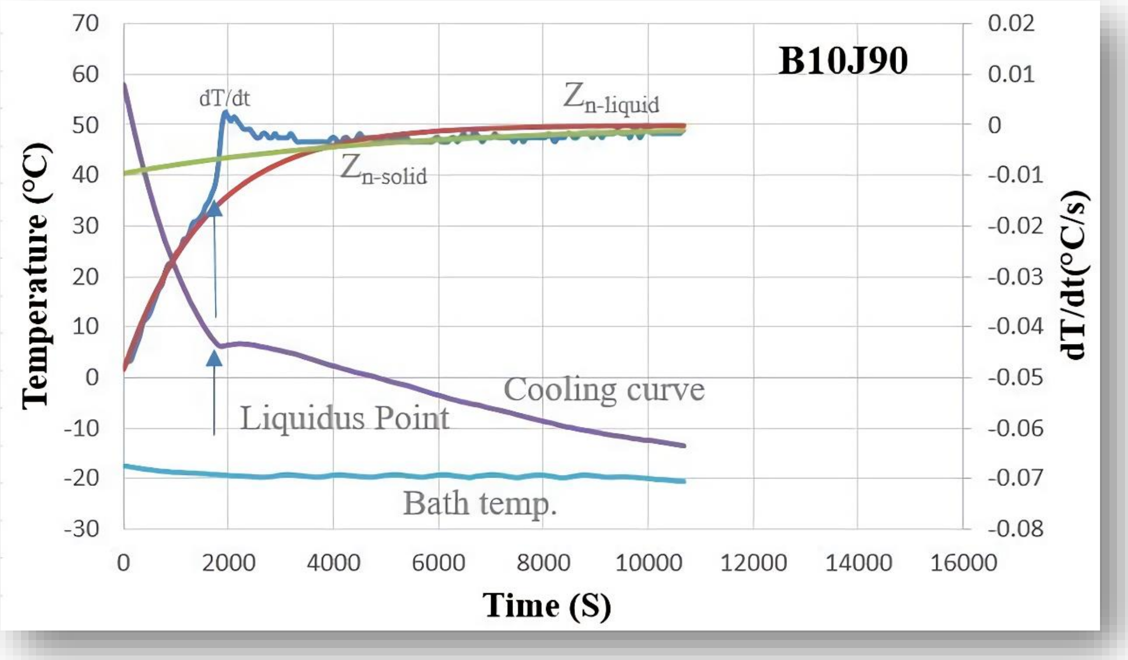

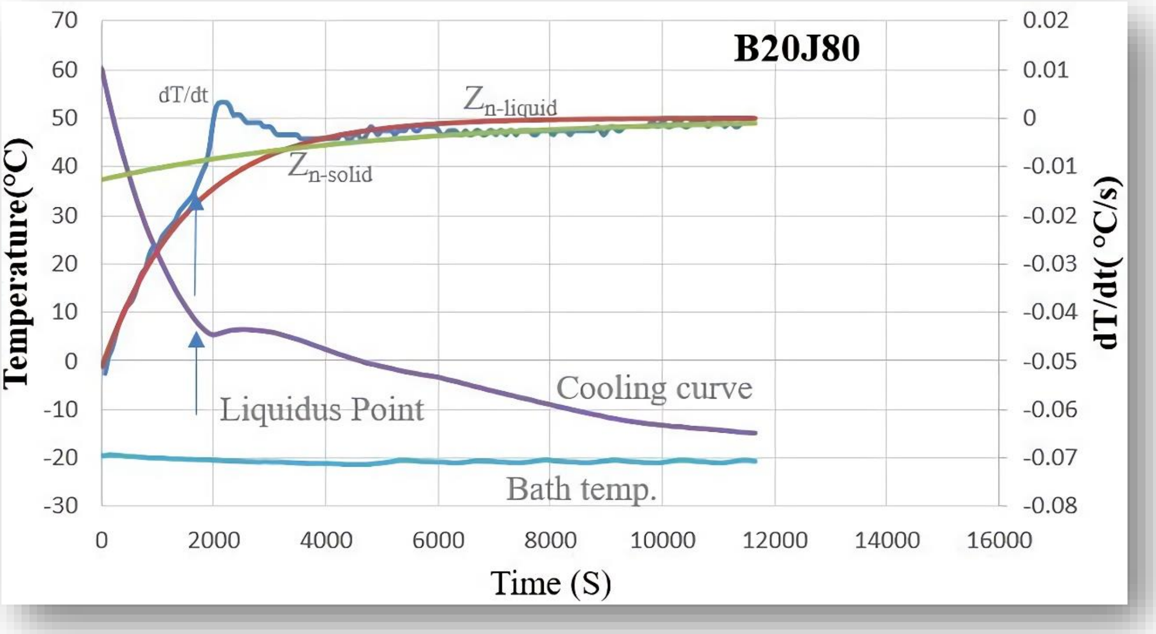

B20J80
Temperature(°C)
dT/dt(°C/s)
70
60
50
40
30
20
10
0
-10
-20
-30
0.02
0.01
0
-0.01
-0.02
-0.03
-0.04
-0.05
-0.06
-0.07
-0.08
0
2000
4000
6000
8000
10000
12000
14000
16000
Time (S)
dT/dt
$Z_{n\text{-liquid}}$
$Z_{n\text{-solid}}$
Liquidus Point
Cooling curve
Bath temp.

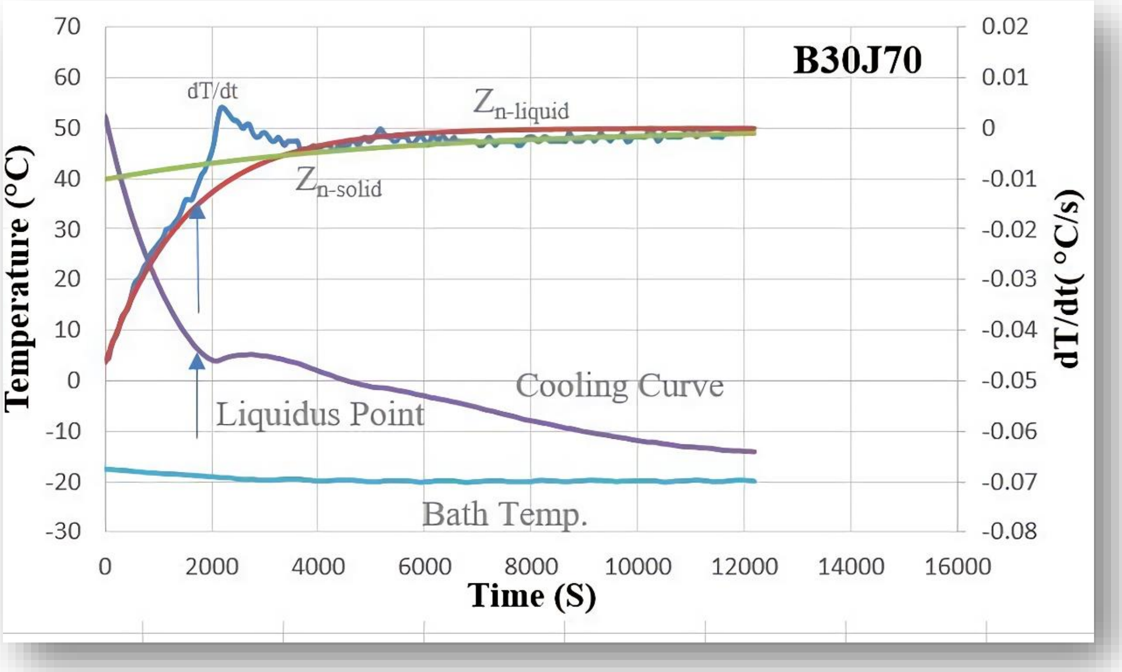

B30J70
Temperature (°C)
dT/dt(°C/s)
70
60
50
40
30
20
10
0
-10
-20
-30
0.02
0.01
0
-0.01
-0.02
-0.03
-0.04
-0.05
-0.06
-0.07
-0.08
0
2000
4000
6000
8000
10000
12000
14000
16000
Time (S)
dT/dt
$Z_{n\text{-liquid}}$
$Z_{n\text{-solid}}$
Liquidus Point
Cooling Curve
Bath Temp.

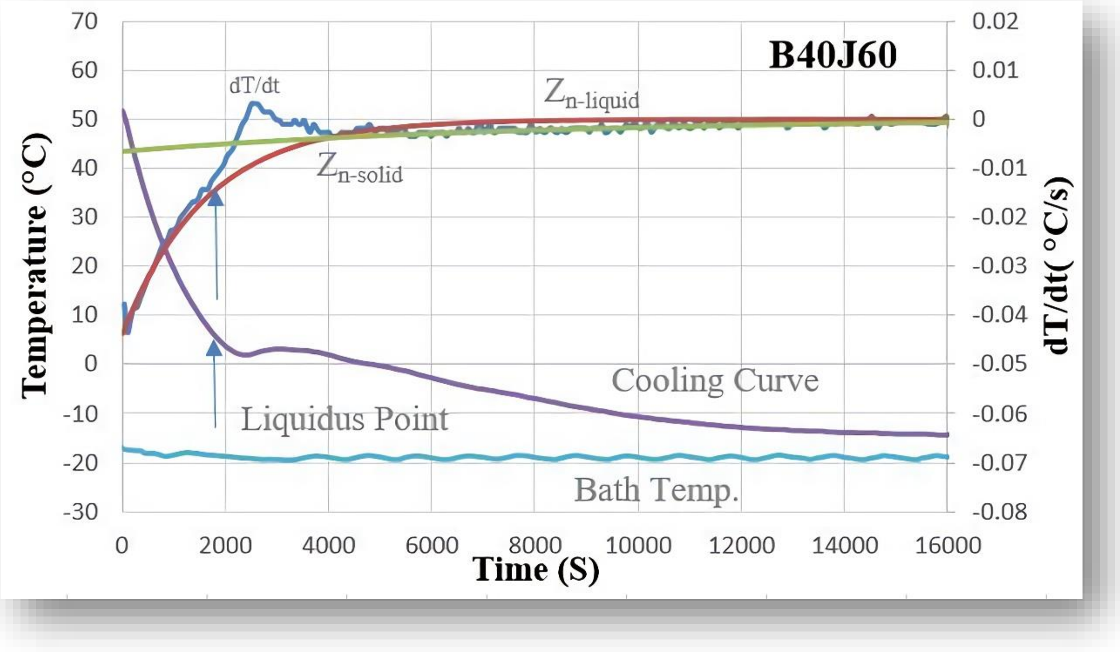
B40J60
Temperature (°C)
dT/dt(°C/s)
Time (S)
dT/dt
$Z_{n\text{-liquid}}$
$Z_{n\text{-solid}}$
Cooling Curve
Liquidus Point
Bath Temp.
70
60
50
40
30
20
10
0
-10
-20
-30
0.02
0.01
0
-0.01
-0.02
-0.03
-0.04
-0.05
-0.06
-0.07
-0.08
0
2000
4000
6000
8000
10000
12000
14000
16000

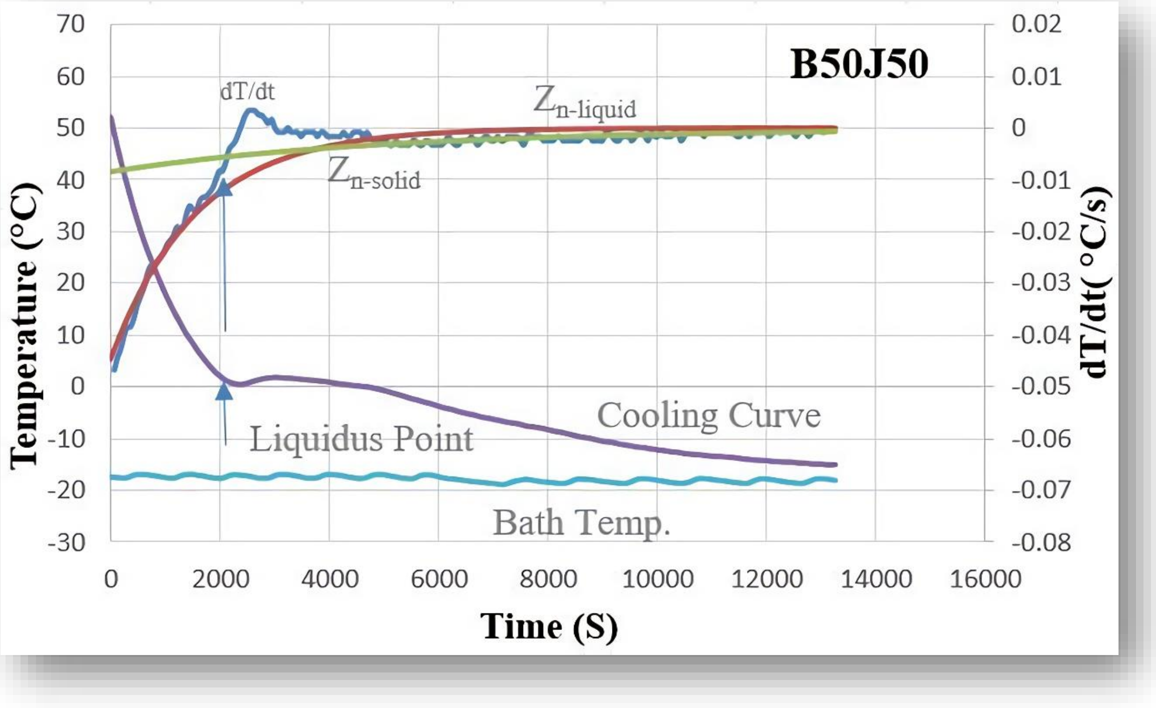
B50J50
Temperature (°C)
dT/dt(°C/s)
Time (S)
dT/dt
$Z_{n\text{-liquid}}$
$Z_{n\text{-solid}}$
Cooling Curve
Liquidus Point
Bath Temp.
70
60
50
40
30
20
10
0
-10
-20
-30
0.02
0.01
0
-0.01
-0.02
-0.03
-0.04
-0.05
-0.06
-0.07
-0.08
0
2000
4000
6000
8000
10000
12000
14000
16000

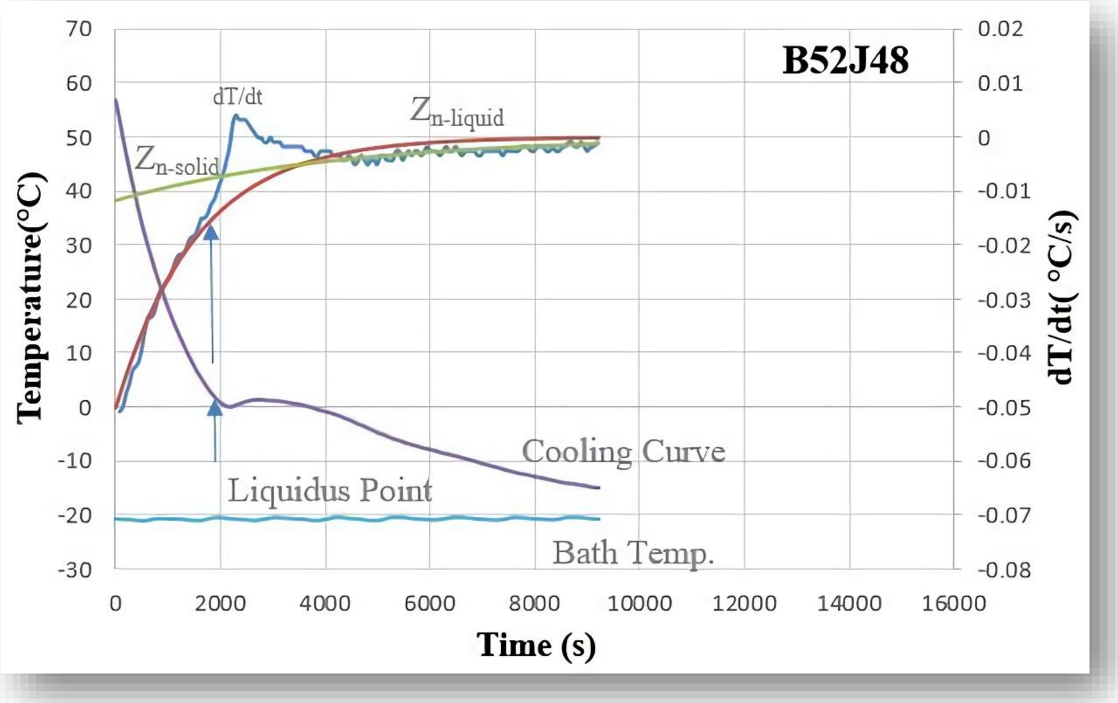
B52J48
Temperature(°C)
dT/dt(°C/s)
Time (s)
70
60
50
40
30
20
10
0
-10
-20
-30
0.02
0.01
0
-0.01
-0.02
-0.03
-0.04
-0.05
-0.06
-0.07
-0.08
0
2000
4000
6000
8000
10000
12000
14000
16000
dT/dt
Zn-liquid
Zn-solid
Cooling Curve
Liquidus Point
Bath Temp.

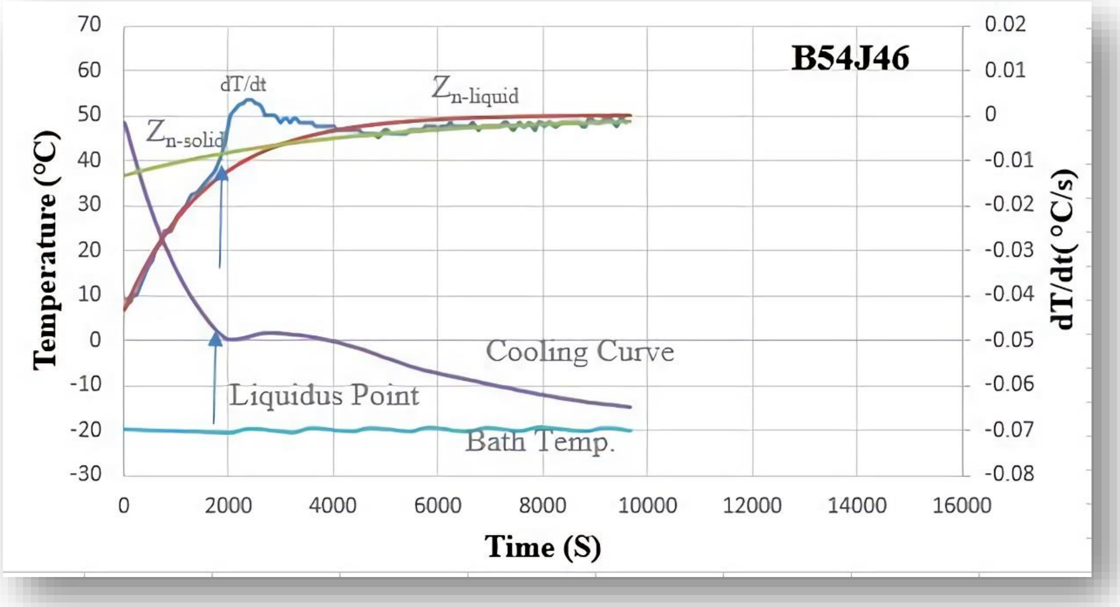
B54J46
Temperature (°C)
dT/dt(°C/s)
Time (S)
70
60
50
40
30
20
10
0
-10
-20
-30
0.02
0.01
0
-0.01
-0.02
-0.03
-0.04
-0.05
-0.06
-0.07
-0.08
0
2000
4000
6000
8000
10000
12000
14000
16000
dT/dt
Zn-liquid
Zn-solid
Cooling Curve
Liquidus Point
Bath Temp.

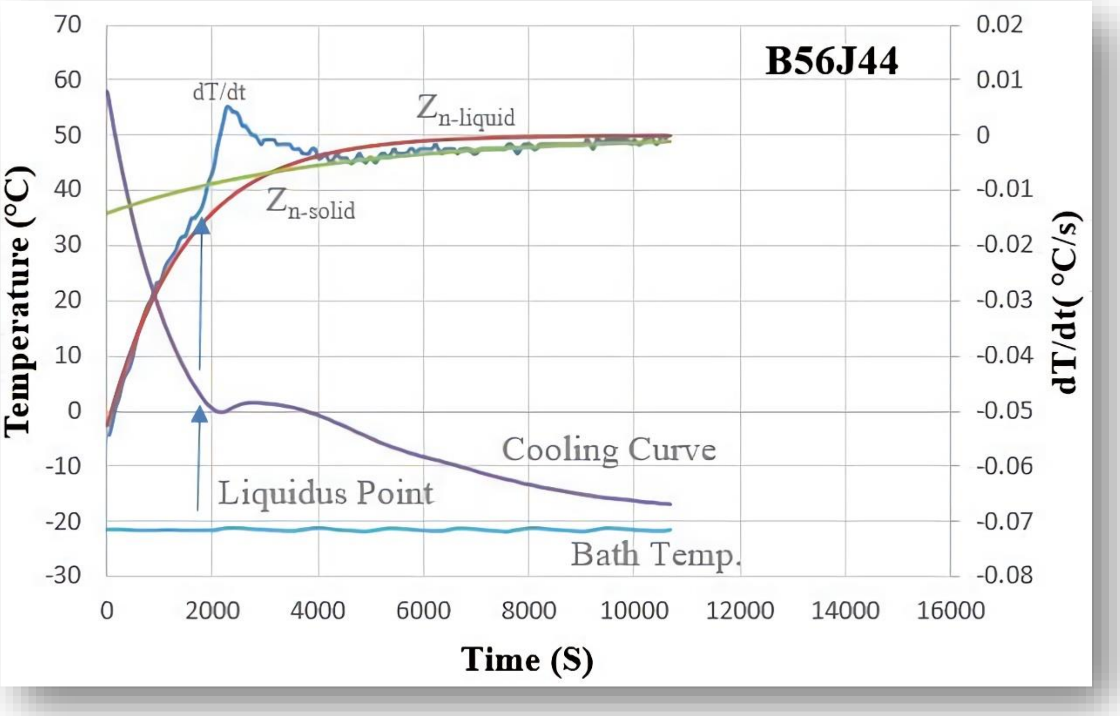
B56J44
Temperature (°C)
dT/dt(°C/s)
Time (S)
dT/dt
Zn-liquid
Zn-solid
Cooling Curve
Liquidus Point
Bath Temp.
70
60
50
40
30
20
10
0
-10
-20
-30
0.02
0.01
0
-0.01
-0.02
-0.03
-0.04
-0.05
-0.06
-0.07
-0.08
0
2000
4000
6000
8000
10000
12000
14000
16000

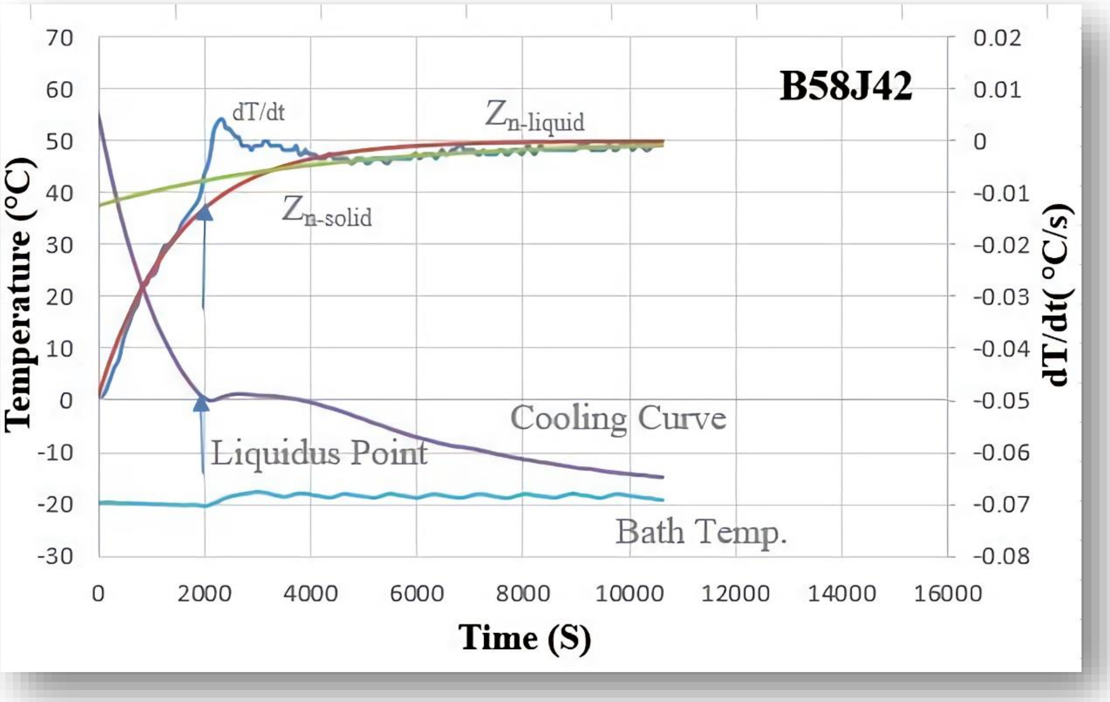
B58J42
Temperature (°C)
dT/dt(°C/s)
Time (S)
dT/dt
Zn-liquid
Zn-solid
Cooling Curve
Liquidus Point
Bath Temp.
70
60
50
40
30
20
10
0
-10
-20
-30
0.02
0.01
0
-0.01
-0.02
-0.03
-0.04
-0.05
-0.06
-0.07
-0.08
0
2000
4000
6000
8000
10000
12000
14000
16000

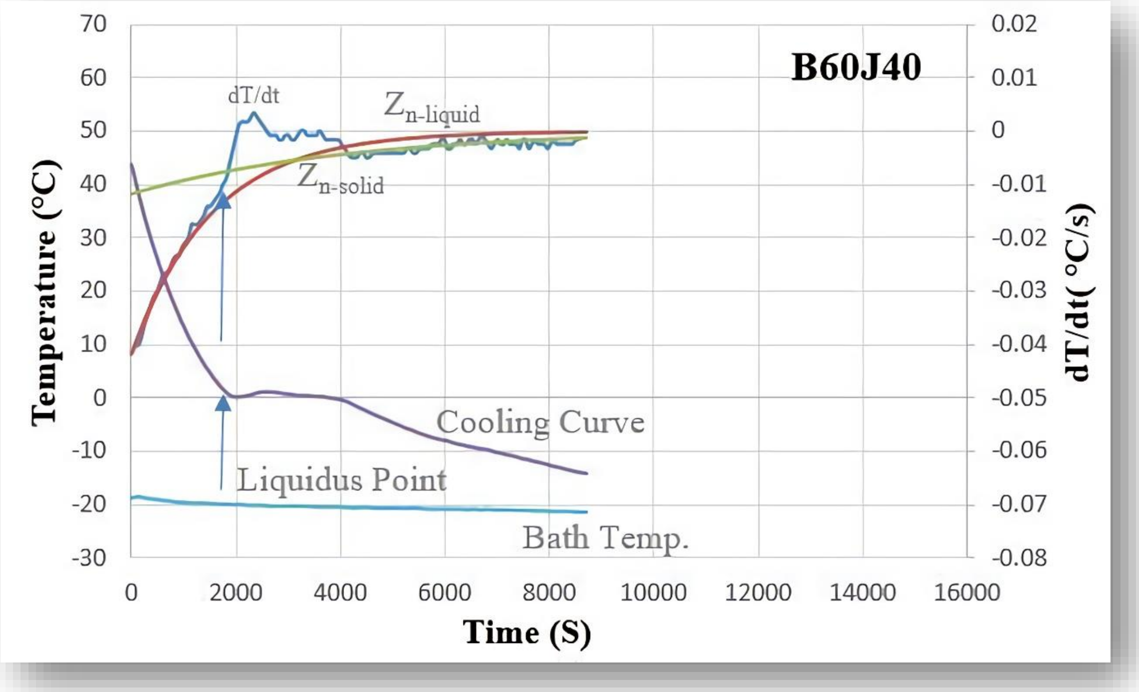
B60J40
Temperature (°C)
70
60
50
40
30
20
10
0
-10
-20
-30
dT/dt(°C/s)
0.02
0.01
0
-0.01
-0.02
-0.03
-0.04
-0.05
-0.06
-0.07
-0.08
Time (S)
0
2000
4000
6000
8000
10000
12000
14000
16000
dT/dt
Zn-liquid
Zn-solid
Cooling Curve
Liquidus Point
Bath Temp.

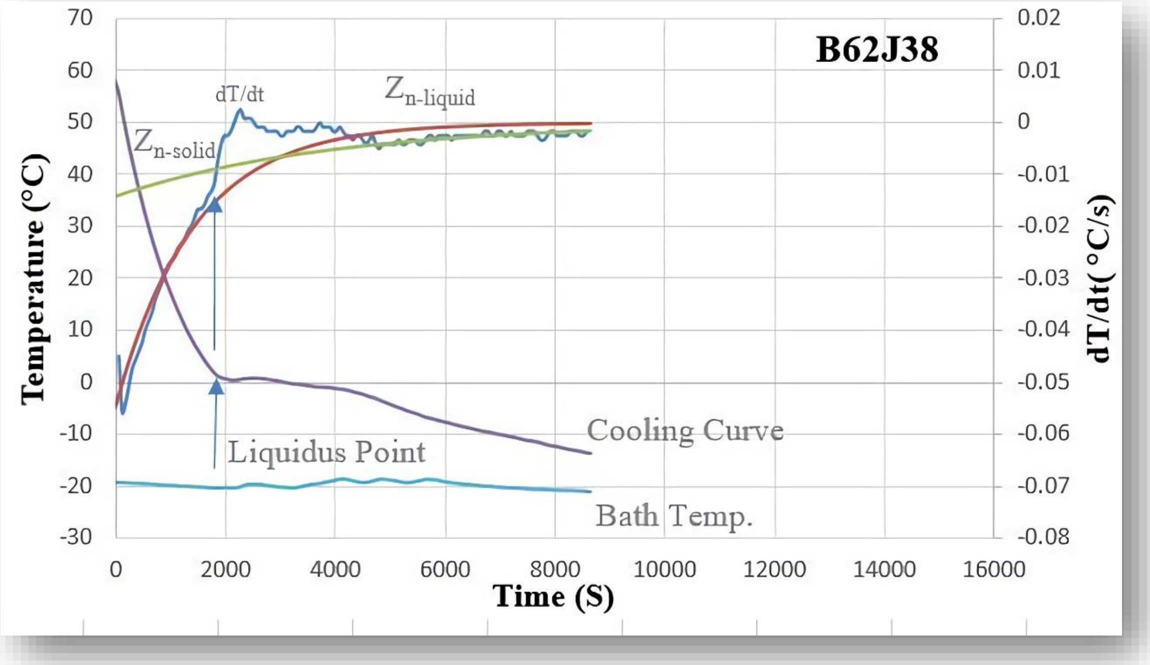
B62J38
Temperature (°C)
70
60
50
40
30
20
10
0
-10
-20
-30
dT/dt(°C/s)
0.02
0.01
0
-0.01
-0.02
-0.03
-0.04
-0.05
-0.06
-0.07
-0.08
Time (S)
0
2000
4000
6000
8000
10000
12000
14000
16000
dT/dt
Zn-liquid
Zn-solid
Cooling Curve
Liquidus Point
Bath Temp.

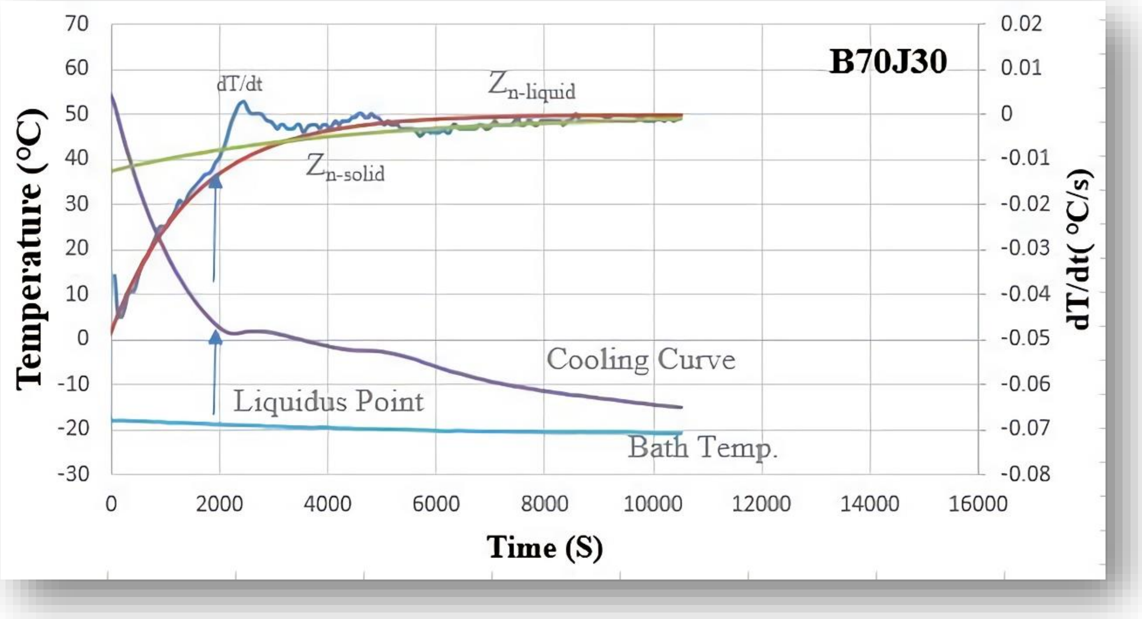
B70J30
Temperature (°C)
dT/dt(°C/s)
Time (S)
dT/dt
Zn-liquid
Zn-solid
Cooling Curve
Liquidus Point
Bath Temp.
70
60
50
40
30
20
10
0
-10
-20
-30
0.02
0.01
0
-0.01
-0.02
-0.03
-0.04
-0.05
-0.06
-0.07
-0.08
0
2000
4000
6000
8000
10000
12000
14000
16000

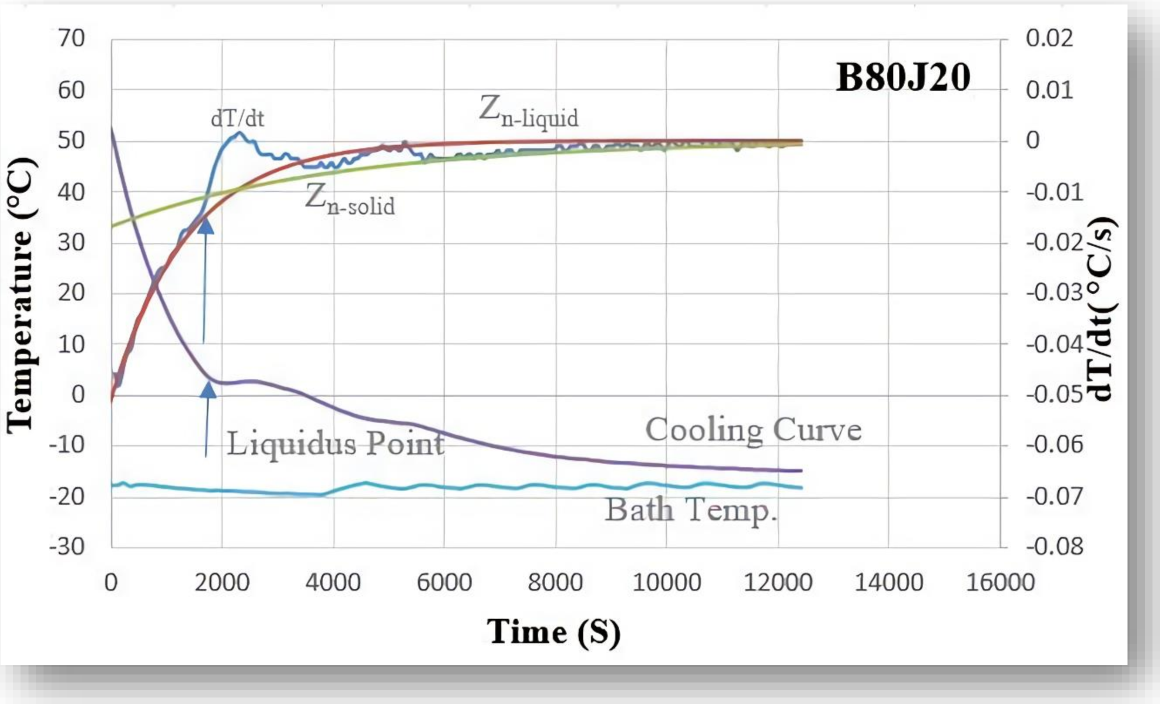
B80J20
Temperature (°C)
dT/dt(°C/s)
Time (S)
dT/dt
Zn-liquid
Zn-solid
Cooling Curve
Liquidus Point
Bath Temp.
70
60
50
40
30
20
10
0
-10
-20
-30
0.02
0.01
0
-0.01
-0.02
-0.03
-0.04
-0.05
-0.06
-0.07
-0.08
0
2000
4000
6000
8000
10000
12000
14000
16000

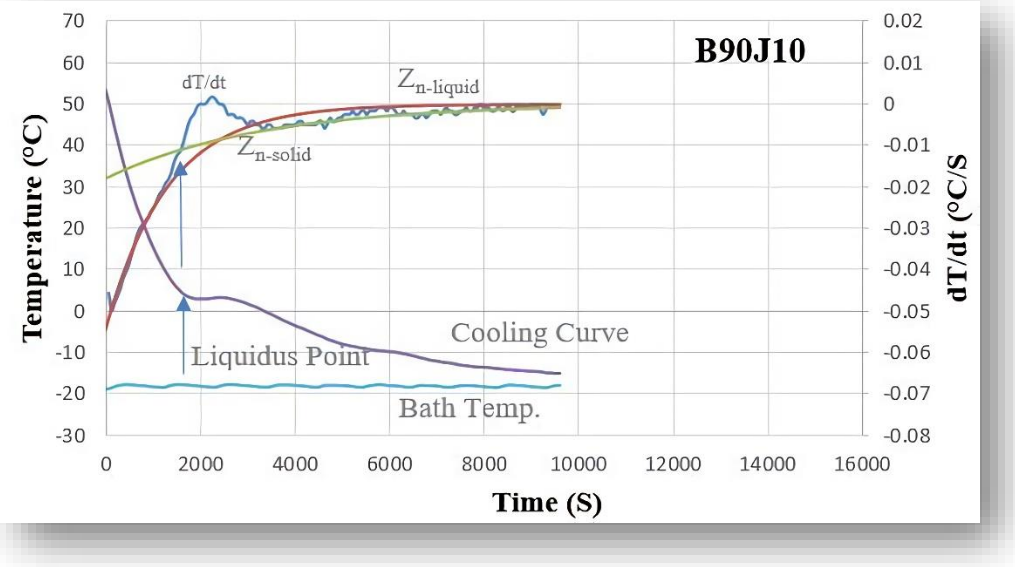
B90J10
Temperature (°C)
dT/dt (°C/S
Time (S)
dT/dt
$Z_{n\text{-liquid}}$
$Z_{n\text{-solid}}$
Liquidus Point
Cooling Curve
Bath Temp.
70
60
50
40
30
20
10
0
-10
-20
-30
0.02
0.01
0
-0.01
-0.02
-0.03
-0.04
-0.05
-0.06
-0.07
-0.08
0
2000
4000
6000
8000
10000
12000
14000
16000

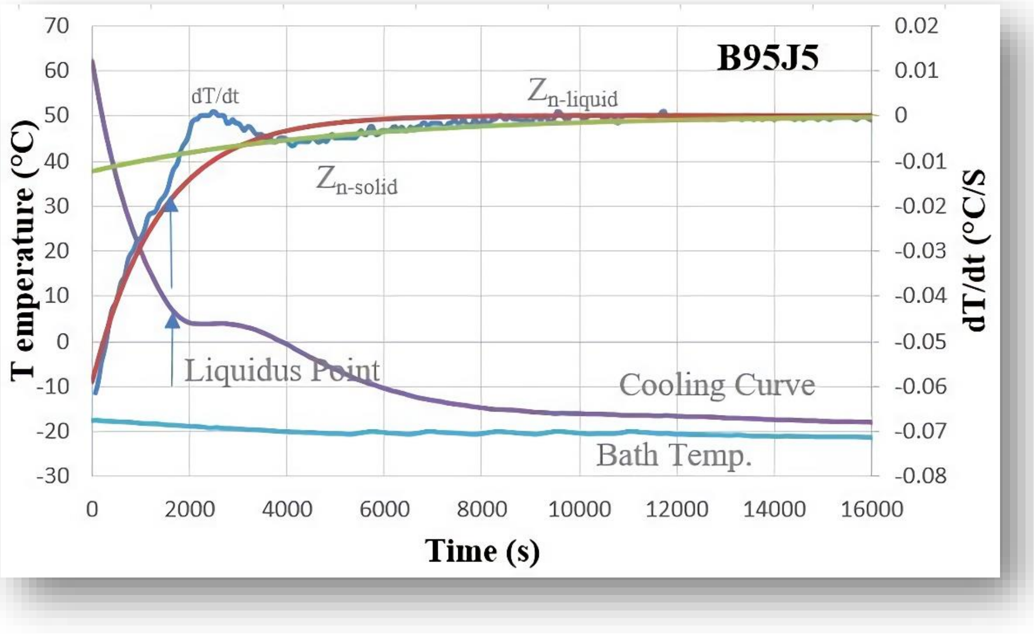
B95J5
T emperature (°C)
dT/dt (°C/S
Time (s)
dT/dt
$Z_{n\text{-liquid}}$
$Z_{n\text{-solid}}$
Liquidus Point
Cooling Curve
Bath Temp.
70
60
50
40
30
20
10
0
-10
-20
-30
0.02
0.01
0
-0.01
-0.02
-0.03
-0.04
-0.05
-0.06
-0.07
-0.08
0
2000
4000
6000
8000
10000
12000
14000
16000